CENTRO DE INVESTIGACIÓN Y DE ESTUDIOS AVANZADOS
DEL INSTITUTO POLITÉCNICO NACIONAL

UNIDAD ZACATENCO
DEPARTAMENTO DE FÍSICA

"Guías Ópticas: Analogías Clásico-Cuánticas"

Tesis que presenta

Alejandro Alberto Romero Osnaya

para obtener el Grado de

Doctor en Ciencias

en la Especialidad de

Física

Director de tesis: Dr. José Oscar Rosas Ortiz

Ciudad de México Noviembre, 2021

CENTER FOR RESEARCH AND ADVANCED STUDIES OF THE NATIONAL POLYTECHNIC INSTITUTE

PHYSICS DEPARTMENT

"Optical Waveguides: Quantum-Classical Analogies"

by

Alejandro Alberto Romero Osnaya

In order to obtain the

Doctor of Science

degree, speciality in

Physics

Advisor: Ph. D. José Oscar Rosas Ortiz

Mexico City November, 2021

El presente trabajo ha sido posible gracias al apoyo económico del Consejo Nacional de Ciencia y Tecnología (CONACyT) a través de la beca 424582 y de los proyectos de investigación A1-S-24569 y CF19-304307. También se reconoce el apoyo brindado por el Centro de Investigación y de Estudios Avanzados (Cinvestav).

Agradecimientos

Aprovecho este espacio para expresar mi profundo y más sincero agradecimiento a todas las personas que han contribuido a la realización y finalización de este trabajo. En primer lugar agradezco a mi asesor, el Dr. Oscar Rosas Ortiz. Sus sugerencias y cuestionamientos sirvieron de guía a lo largo de cada desafío enfrentado. Agradezco también a la Dra. Sara Guadalupe Cruz y Cruz, por su asistencia en la etapa final de este trabajo. Agradezco a mis sinodales Dr. Alfonso Jaimes Nájera, Dr. Máximo López López, Dr. Sergio Tomás Velázquez, Dra. Sara Cruz y Cruz, Dr. Oscar Rosas Ortiz, por disponer de su tiempo y conocimiento para corregir y evaluar mi trabajo.

Por otro lado, agradezco el gran apoyo brindado por mi hermano Carlos Romero Osnaya y por mis padres Berta Osnaya Ortega y Carlos Alejandro Romero Vargas. Por último expreso un especial agradecimiento a mi novia Mariana Zamora Mejía, por ser piedra angular en mi desarrollo personal en esta étapa de mi vida.

A mis abuelos, Enrique y Raimundo.

Resumen

Considerando materiales dieléctricos no homogéneos, bajo la aproximación de guiado débil, establecemos una analogía entre el estudio de guías de onda y el de potenciales exactamente solubles en mecánica cuántica.

En concreto, partiendo de las ecuaciones de Maxwell mostramos que el campo eléctrico en una guía de ondas obedece una ecuación diferencial de segundo orden que está en correspondencia con la ecuación de Schrödinger para un pozo de potencial.

Con el propósito de explorar el alcance de dicha analogía, presentamos el estudio detallado de un oscilador truncado y su correspondiente guía de ondas.

Además, en el contexto de la mecánica cuántica supersimétrica, usamos la analogía para diseñar guías de onda cuyo índice de refracción es exactamente soluble, con lo que se obtienen constantes de propagación hechas a la medida.

Abstract

For non-homogeneous dielectric materials and electromagnetic waves propagating in such media under the weakly guided condition, we study the properties of electromagnetic waveguides in connection with the exact solutions of some potential-wells in quantum mechanics.

To be concrete, departing from the Maxwell equations we arrive at the differential equation that is satisfied by the electric fields in the waveguide, and show that such equation is associated with the eigenvalue problem of a properly defined potential-well in quantum mechanics.

As an immediate example of the applicability of the model, we discuss in detail the connection between the guided modes of a waveguide characterized by a parabolic refractive index and the solutions of the eigenvalue problem of a truncated oscillator.

We take full advantage of such analogy by applying the supersymmetric formulation of quantum mechanics to design waveguides that admit exactly solvable guided modes, the propagation constants of which are defined under prescription.

Contents

Introduction

The study of light and its propagation through different media has been in the mind of physicists for as long as the study of nature goes. Even before Newton's and Huygen's debate about the nature of light, phenomena like reflection and refraction have captivated scholars and amateurs. Light have always presented subtleties to the human eye; illusions of finding a body of water in the middle of desert or misjudging the position of a fish swimming close to the surface of a tank are two examples of that. As an intangible entity, light is difficult to experiment with. Our knowledge of its behavior, both macroscopic and microscopic, is therefore a success by itself. However, more than a curiosity, light represents a very useful tool in our modern way of life. Its role in communications makes light essential for our society so that refining our knowledge of its nature and behavior opens the possibility to find new practical applications.

Light has different physical properties like amplitude, frequency, phase shifts and polarization. These properties encode information, the simplest example is a light bulb with configurations on/off that represent active or passive states of a given device. On the other hand, the properties of light may be conserved along its journey through a waveguide; the more clear the information is transmitted the better is the code received by the interpreter. Sending information from one end to another of the waveguide with minimum losses we speak of light in a guided mode. Such modes are characterized by a propagation constant, which measures the slope of the light ray with respect to the axis of the waveguide.

The study of waveguides and their modes is the subject of a big number of research papers, sientific monographs and academic books in optics. The novelty of the present work is the method employed to investigate the propagation of light since we implement approaches from quantum mechanics to the design of optical waveguides. Indeed, we study refractive indices of non-homogenous media through the analogy that can be established between waveguides and quantum wells.

The work addresses two types of problem, direct and inverse: 1) the direct problem consists of finding the propagation constants of guided modes provided a refractive index. 2) the inverse problem determines the refractive index admitting a set of propagation constants that are provided under prescription.

For the direct problem we will study an optical waveguide with parabolic dependence $n(r) = r^2$, where r is the distance from the axis of the waveguide to any point. Using the Maxwell equations we establish an analogy with a two-dimensional short-range oscillator-like system. The adjective "short-range" stands for a phenomenon that takes place only in a certain region of space. Consider for example a dielectric charged cylinder. Suppose non-uniform charge density and therefore a potential $V(\vec{r})$ that depends of the position vector $\vec{r}$. Outside the cylindrical body of radius a there is a cover of uncharged homogenous material with constant potential $V(r) = const.$ We have two distinguishable regions. Region I defines the domain where $V(r)$ varies continually and region II the domain where $V(r)$ is constant. We say that the potential is of short-range because the region where it varies is bounded. The point $r = a$ is called cutoff and determines the position at which the potential changes abruptly its behavior.

For the inverse problem we departure from a constant refractive index, defined over the whole real axis. An example would be provided by a system as large as it can be considered unbounded. Although the constant refractive index has analytic solution, we instead solve the analogous problem of a quantum free particle and then come back with solutions to the original problem. The free particle does not admit bounded modes. Using Darboux transformations, within the frame of quantum supersymmetry, we take the solutions of the quantum free particle potential to generate new refractive indices with as many propagation constants as we desire.

The work is organized as follows: In Chapter 1 we address a one-dimensional short-range oscillator. We study this system in depth. Following exact methods (solving the differential equation analytically) and the WKB approximation we find the bound states. Besides, with the exact solutions at hand we explore as well the scattering and resonant states of the system, making special emphasis on the role played by the wave number and the transmission coefficient. In Chapter 2 we study the two-dimensional version of the system of Chapter 1. We solve the bound states problem, and use the exact solutions to analyze scattering and resonant states. We analyze as well the probability density current which, contrary to the one-dimensional case, changes its flow in magnitude and direction. In Chapter we 3 use the Maxwell equations for an inhomogeneous non-magnetic dielectric medium to obtain the electric field satisfying the vectorial Helmholtz equation. We identify the transition from such equation onto a scalar Helmholtz equation for each scalar component of the field. Finally, the paraxial approximation gives place to a Schrödinger-like equation for the components of the field known as the paraxial Helmholtz equation. By comparison with the Schrödinger equation of the two-dimensional harmonic oscillator, we establish a quantum-classical analogy between an optical waveguide and a quantum well, which leads immediately to the propagation constants and guided modes. We also explore the problem of finding the propagation constants through an approximate method called the "quasi-plane approach". This method turns out to be similar to the

WKB approximation. Finally, in Chapter 4 we present a summary of the process of producing Hermitian and non-Hermitian potentials with real spectra, given that we know the solutions of a previous one. Although this technique was developed within the context of quantum mechanics, the analogy established in section 3 permits the application of the Darboux-transformations to generate propagation constants on demand.

We conclude the manuscript with a series of conclusions and perspectives in chapter 5. A very short appendix includes technical details about Laplacian operators.

Chapter 1

One dimensional case

Before solving the two dimensional short range potential we are interested in, it is appropriate to study first a one dimensional case. The insight gained by doing this will be useful in the next chapters, both as a guide of the challenges to be faced and as a reference for future comparison. We proceed by characterizing a piecewise potential over three different regions of the real line with a cutoff, and solving the corresponding Schrödinger equation. Continuity conditions are imposed to obtain a set of equations that determine the eigenstates, depending on the "kinetic" parameter k. As we shall see, k encodes information about the energy with respect to the height of the potential at the cutoff. This determines whether the particles may or may not be "trapped" by the potential under study.

1.1 Generalities

The potential of the one-dimensional oscillator is $V(x) = x^2$, with $x \in (-\infty, \infty)$. The general solution reads

$$\psi(x) = e^{-\frac{x^2}{2}} \left[A\ M\left(\frac{1-2E}{4}, \frac{1}{2}; x^2\right) + B\ xM\left(\frac{1-2E}{4} + \frac{1}{2}, \frac{3}{2}; x^2\right) \right], \tag{1.1}$$

where

$$M(\alpha, \beta; z) \equiv \sum_{n=0}^{\infty} \frac{(\alpha)_n}{(\beta)_n} \frac{z^n}{z!} \tag{1.2}$$

is the confluent hypergeometric (Kummer) function, also denoted as ${}_1F_1(a, b; z)$ [1].

We know that $M(\alpha, \beta, z)$ reduces to a polynomial if $\alpha = -n$, with n a positive integer (provided that β is not a negative integer). The degree of this polynomial is precisely n.

If $\alpha \neq -n$ then $M(\alpha, \beta, z)$ is a convergent series for all x. If $\alpha \neq -n$ the series $M(\alpha, \beta, z)$ has the asymptotic behavior

$$\lim_{|z|\to\infty} M(\alpha, \beta, z) = e^z z^{(\alpha-\beta)}. \tag{1.3}$$

Therefore, if $\alpha_1 \equiv \frac{1-2E}{4}$ and $\alpha_2 \equiv \frac{1-2E}{4} + \frac{1}{2}$ are not negative integers, the function (1.1) has the asymptotic behavior

$$\begin{aligned} \lim_{x\to\infty} \psi(x) &= \lim_{x\to\infty} e^{-\frac{x^2}{2}} \left[A\ x^{\frac{1}{2}-E} e^{x^2} + B\ x(x^{-\frac{3}{2}-E} e^{x^2}) \right] \\ &= (\text{some polynomial}) e^{\frac{x^2}{2}}. \end{aligned} \tag{1.4}$$

If $\alpha_1 = -n$, we have

$$\psi(x) = A\ e^{-\frac{x^2}{2}}\ M\left(-n, \frac{1}{2}; x^2\right) = A\ e^{-\frac{x^2}{2}}\ (-1)^n \frac{n!}{(2n)!} H_{2n}(x) \tag{1.5}$$

and

$$E = (2n) + \frac{1}{2}. \tag{1.6}$$

Hereafter $H_j(x)$ stands for the Hermite polynomials [2]. In this case the solution is proportional to $e^{-\frac{x^2}{2}} H_{2n}(x)$, which is an even function.

If $\alpha_2 = -n$, then

$$\psi(x) = e^{-\frac{x^2}{2}} B\, x M\left(\frac{1-2E}{4} + \frac{1}{2}, \frac{3}{2}; x^2\right) = B e^{-\frac{x^2}{2}}\ (-1)^n \frac{n!}{(2n+1)!2} H_{2n+1}(x), \tag{1.7}$$

and

$$E = (2n+1) + \frac{1}{2}. \tag{1.8}$$

In this case the solution is proportional to $e^{-\frac{x^2}{2}} H_{2n+1}(x)$, which is an odd function. Notice that $\alpha_1 = -n$ corresponds to even solutions while $\alpha_2 = -n$ refers to odd solutions. Condensing these expressions for the energy of even and odd functions in one single expression we get:

$$E = n + \frac{1}{2}; \quad n = 0, 1, 2, ... \tag{1.9}$$

Another consequence of the quantization is the rising of a set of functions that form an orthogonal basis. Any continuous or piece-wise continuous function defined in $(-\infty, \infty)$ may be expanded in terms of such basis [2]. This set of functions can be equipped with the inner product

$$(\phi_1, \phi_2) \equiv \int_{-\infty}^{\infty} \phi_1^*(x) \phi_2(x) e^{-x^2} dx. \tag{1.10}$$

In consequence a notion of orthogonality [2] can be associated to the Hermite polynomials:

$$(H_j(x), H_i(x)) \equiv \int_{-\infty}^{\infty} H_j^*(x) H_i(x) e^{-x^2} dx = 2^j \pi^{\frac{1}{2}} j! \delta_{ji}, \tag{1.11}$$

as well as a norm

$$|H_j(x)| = \sqrt{(H_j(x), H_j(x))}. \tag{1.12}$$

For a discussion of orthogonality of solutions related to a Sturm-Liouville problem see [2], and [3] for a more detailed discussion of orthogonality and completeness.

1.2 Solution to the piecewise Schrödinger equation

The solutions of the Schrödinger equation are, in principle, all we need to represent the quantum states of a system, the dynamics of which is ruled by a given Hamiltonian. In the case of short-range one-dimensional potentials the analytical solutions provide the information we need to make predictions. However, solving the same problem via approximate methods gives additional information about either the limiting form of solutions or the stability of eigenvalues. In the following we present the exact solution to the problem, from which we analyze bound, scattering and resonant states. Moving forward, next we apply the Wentzel-Kramers-Brillouin (WKB) method to address the search of bound states.

1.2.1 Analytical solution

The time dependent Schrödinger equation for a one-dimensional system reads

$$-\frac{\hbar^2}{2m}\frac{d^2}{dq^2}\Psi(q,t) + \widetilde{V}(q)\Psi(q,t) = i\hbar\frac{\partial}{\partial t}\Psi(q,t), \tag{1.13}$$

where q stands for position, t for time and $\widetilde{V}(q)$ for the potential of the system (the reason for the tilde notation will be cleared shortly). Assuming a harmonic dependence of time we write

$$\Psi(q,t) \equiv \psi(q) e^{-i\frac{E}{\hbar}t}, \tag{1.14}$$

where E is a constant to be determined. Substituting in (1.13) we get the stationary Schrödinger equation

$$-\frac{\hbar^2}{2m}\frac{d^2}{dq^2}\psi + \widetilde{V}(q)\psi = \mathcal{E}\psi, \tag{1.15}$$

where

$$\widetilde{V}(q) = \left\{ \begin{array}{l} \frac{1}{2}m\omega^2 q^2, \quad |q| \leqslant \widetilde{a} \\ \frac{1}{2}m\omega^2 \widetilde{a}^2, \quad |q| > \widetilde{a} \end{array} \right\}. \tag{1.16}$$

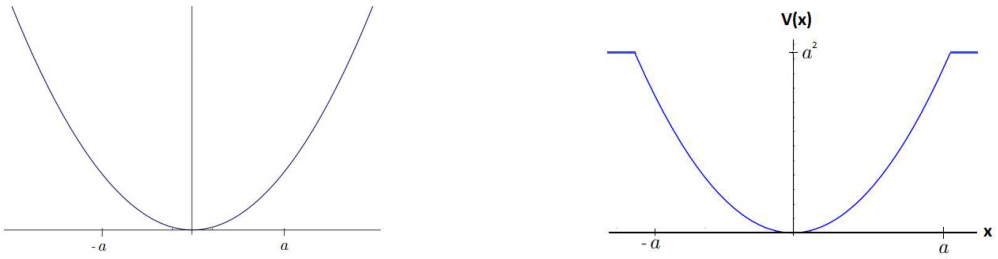

(a) (b)

Figure 1.1: (a) Potential of a harmonic oscillator. (b) Potential of the Short-range oscillator, see eq. (1.18).

Here $\hbar$ is the reduced Planck constant, q is the spatial coordinate, $\widetilde{a}$ is the specific value of q where the potential becomes constant, m is the mass of a particle interacting with the potential, ω is the natural frequency of the quantum harmonic oscillator and $\mathcal{E}$ its energy. Let $x = \sqrt{\frac{m\omega}{\hbar}}q$, $a = \sqrt{\frac{m\omega}{\hbar}}\widetilde{a}$ and $E = \frac{\mathcal{E}}{\hbar\omega}$, then (1.15) turns into

$$-\frac{1}{2}\frac{d^2}{dx^2}\psi + \frac{1}{2}V(x)\psi = E\psi. \tag{1.17}$$

where

$$V(x) = \begin{cases} x^2, & |x| \leqslant a \\ a^2, & |x| > a \end{cases}, \tag{1.18}$$

Eq. (1.17) is referred to as dimensionless Schrödinger equation. Potential (1.18) consists of three regions, see figure 1.1. In regions I ($-\infty < x < -a$) and III ($a < x < \infty$) the potential is constant. These regions represent a physical situation where the interaction no longer influences the dynamics of the system. Region II ($-a < x < a$) is called the interaction zone, and represents the domain where the influence of the potential is significant. This redefinition of physical quantities is helpful when performing large amounts of calculations, so we will not drag constants in the sequel. It is also helpful to plot our results using scaled quantities since, otherwise, we would deal with magnitudes as small as the scale of $\hbar$ ($=1.05\ 10^{-34} Js$) squared, which can be very cumbersome when operating

and plotting. One possible downside to such redefinitions could be that unit analysis of physical quantities is not immediate, but it suffices to change them back through their definitions for such analysis to be available again.

- **Region** I**:** $x < -a$

In this region $V(x) = a^2$. Therefore (1.17) reads

$$-\frac{1}{2}\frac{d^2}{dx^2}\psi(x) + \frac{1}{2}a^2\psi(x) = E\psi(x). \tag{1.19}$$

The solution of this equation follows immediatly:

$$\psi(x) = A_1 e^{ikx} + B_1 e^{-ikx}; \quad k \equiv \sqrt{2E - a^2}. \tag{1.20}$$

Notice that, whether $2E$ is shorter or larger than a^2, it will determine if $\psi(x)$ is a real exponential function or a complex one.

- **Region** II**:** $-a < x < a$

In this region $V(x) = x^2$. Equation (1.17) then reads

$$-\frac{1}{2}\frac{d^2}{dx^2}\psi + \frac{1}{2}x^2\psi = E\psi. \tag{1.21}$$

The appropriate change of dependent and independent variables reduces this equation to a confluent hypergeometric one. Let the solution be of the form $\psi(x) = u(x)e^{-\frac{x^2}{2}}$. Substituting it into (1.21) we arrive at

$$\frac{d^2}{dx^2}u(x) - 2x\frac{d}{dx}u(x) + (2E - 1)u(x) = 0. \tag{1.22}$$

Now let $\xi \equiv x^2$, then one gets

$$\xi\frac{d^2}{d\xi^2}u(\xi) + \left(\frac{1}{2} - \xi\right)\frac{d}{d\xi}u(\xi) + \left(\frac{2E-1}{4}\right)u(\xi) = 0 \tag{1.23}$$

which is the confluent hypergeometric equation, the general solution of which is well known [4]:

$$u(\xi) = A\ M\left(\frac{1-2E}{4}, \frac{1}{2}; \xi\right) + B\ \xi^{\frac{1}{2}} M\left(\frac{1-2E}{4} + \frac{1}{2}, \frac{3}{2}; \xi\right), \tag{1.24}$$

where A and B are arbitrary constants. Therefore, the complete solution for equation (1.21) in terms of x is:

$$\psi(x) = e^{-\frac{x^2}{2}} \left[A\ M\left(\frac{1-2E}{4}, \frac{1}{2}; x^2\right) + B\ xM\left(\frac{1-2E}{4} + \frac{1}{2}, \frac{3}{2}; x^2\right)\right]. \tag{1.25}$$

• **Region** $III : x > a$

In this case we also have

$$\psi = A_3 e^{ikx} + B_3 e^{-ikx}; \quad k = \sqrt{2E - a^2}. \tag{1.26}$$

We have found the solutions to the Schrödinger equations along the whole space, now we proceed to find the unknown coefficients through the continuity conditions that both, ψ and $\frac{d\psi}{dx}$ must fulfill.

1.3 Continuity conditions for the 1-D short range oscillator

The conditions that any solution of the Schrödinger equation must satisfy are as follows:

- Continuity at all points.
- Continuity of their derivatives at all points.

Let ψ_j and ϕ_j be two independent solutions for region j, and A_j,B_j be the corresponding arbitrary coefficients. We can summarize the continuity conditions as follows:

◦ Continuity at $x = -a$:

$$\begin{array}{rcl} A_1\psi_1(-a) + B_1\phi_1(-a) & = & A_2\psi_2(-a) + B_2\phi_2(-a) \\ A_1\psi_1'(-a) + B_1\phi_1'(-a) & = & A_2\psi_2'(-a) + B_2\phi_2'(-a) \end{array} \tag{1.27}$$

◦ Continuity at $x = a$:

$$\begin{array}{rcl} A_2\psi_2(a) + B_2\phi_2(a) & = & A_3\psi_3(a) + B_3\phi_3(a) \\ A_2\psi_2'(a) + B_2\phi_2'(a) & = & A_3\psi_3'(a) + B_3\phi_3'(a) \end{array} \tag{1.28}$$

where $(')$ stands for derivative with respect to x. We can write these sets equations as the matrix equations:

$$\begin{pmatrix} \psi_1 & \phi_1 \\ \psi_1' & \phi_1' \end{pmatrix}\Bigg|_{x=-a} \begin{pmatrix} A_1 \\ B_1 \end{pmatrix} = \begin{pmatrix} \psi_2 & \phi_2 \\ \psi_2' & \phi_2' \end{pmatrix}\Bigg|_{x=-a} \begin{pmatrix} A_2 \\ B_2 \end{pmatrix} \tag{1.29}$$

and

$$\begin{pmatrix} \psi_2 & \phi_2 \\ \psi_2' & \phi_2' \end{pmatrix}\Bigg|_{x=a} \begin{pmatrix} A_2 \\ B_2 \end{pmatrix} = \begin{pmatrix} \psi_3 & \phi_3 \\ \psi_3' & \phi_3' \end{pmatrix}\Bigg|_{x=a} \begin{pmatrix} A_3 \\ B_3 \end{pmatrix}. \tag{1.30}$$

We can simplify further if we rename the matrices acting on the coefficient vectors as M_1, M_2, N_1, N_2 respectively:

$$M_1 \begin{pmatrix} A_1 \\ B_1 \end{pmatrix} = M_2 \begin{pmatrix} A_2 \\ B_2 \end{pmatrix}, \qquad N_1 \begin{pmatrix} A_2 \\ B_2 \end{pmatrix} = N_2 \begin{pmatrix} A_3 \\ B_3 \end{pmatrix}. \tag{1.31}$$

It is simple to express the region 3 coefficients in terms of those of region 1:

$$\begin{pmatrix} A_3 \\ B_3 \end{pmatrix} = N_2^{-1} N_1 \begin{pmatrix} A_2 \\ B_2 \end{pmatrix} = N_2^{-1} N_1 M_2^{-1} M_1 \begin{pmatrix} A_1 \\ B_1 \end{pmatrix}. \tag{1.32}$$

Then

$$\begin{pmatrix} A_3 \\ B_3 \end{pmatrix} = M \begin{pmatrix} A_1 \\ B_1 \end{pmatrix}; \qquad M \equiv N_2^{-1} N_1 M_2^{-1} M_1. \tag{1.33}$$

In other words

$$A_3 = m_{1,1}\, A_1 + m_{1,2}\, B_1\ ; \qquad B_3 = m_{2,1}\, A_1 + m_{2,2}\, B_1, \tag{1.34}$$

where $m_{ij} \equiv$ the ij-th element of M. As we shall see in detail in the sequel, it is justified to set $B_3 = 0$. Then, equation (1.34) reads

$$A_3 = m_{1,1}\, A_1 + m_{1,2}\, B_1, \qquad 0 = m_{2,1}\, A_1 + m_{2,2}\, B_1. \tag{1.35}$$

It may be shown that the matrix M is of determinant equal to 1, and therefore unitary (see complement N III of [5]). Using this fact, (1.35) yields

$$m_{2,2}\, A_3 = A_1. \tag{1.36}$$

The latter result is useful to construct the transmission coefficient T. Indeed, the flux density of particles per time unit [6]

$$\widetilde{j}_\psi(q) \equiv \frac{\hbar}{2mi}\left(\psi^*(q)\frac{d}{dx}\psi(q) - \psi(q)\frac{d}{dx}\psi^*(q)\right). \tag{1.37}$$

Expressing $q$in terms of x we define a dimensionless current density

$$j_\psi(x) \equiv -\frac{i}{2}\left(\psi^*(x)\frac{d}{dx}\psi - \psi\frac{d}{dx}\psi^*(x)\right). \tag{1.38}$$

The transmission coefficient T is defined as follows

$$T \equiv \left|\frac{j_{\psi_3}}{j_{\psi_1}}\right| = \left|\frac{A_3}{A_1}\right|^2 = \left|\frac{1}{m_{2,2}}\right|^2. \tag{1.39}$$

As we shall see (1.39) contains the information needed to fully describe the system. Analyzing the character of k we shall see that bound, scattering, and resonant states flow naturally out of T.Let us go back to Equation (1.19) and rewrite it as

$$-\frac{d^2}{dx^2}\psi = k^2\psi. \tag{1.40}$$

From a mathematical point of view, this is an eigenvalue equation with no constraints on k. The possibilities for k are three:

- k is pure imaginary (bound states).
- k is pure real number (scattering states).
- k is complex (resonant states).

1.3.1 Bound states

Let k be pure imaginary $k = i\kappa$. Then

$$\sqrt{2E - a^2} = i\kappa \quad \Longrightarrow \quad 2E < a^2 \text{ and } \kappa = \sqrt{|2E - a^2|}. \tag{1.41}$$

This inequality defines an upper bound for the energy values which is half the height of the potential well. Substituting $k = i\kappa$ in the solutions for region I (equation 1.20) and region III (equation 1.26) we get

$$\psi = A_1 e^{-\kappa x} + B_1 e^{\kappa x};\ x < a, \tag{1.42}$$

and

$$\psi = A_3 e^{-\kappa x} + B_3 e^{\kappa x};\ x > a. \tag{1.43}$$

In order for ψ to be physically admissible, we impose the boundary condition $\lim_{x\to\pm\infty}\psi = 0$; which in turn fixes the values of A_1 and B_3 equal to zero. Going back to (1.39) we observe that $A_1 = 0$ implies a pole of T, and so, $m_{2,2}$ has a zero. Let us take the height of the well as $a^2 = 20$. Numerical solutions to the equation

$$m_{2,2}(E) = 0 \tag{1.44}$$

Energy values	
$E_0 = 0.5$	$E_5 = 5.499870551$
$E_1 = 1.499999994$	$E_6 = 6.49921014$
$E_2 = 2.499999873$	$E_7 = 7.495971211$
$E_3 = 3.499998269$	$E_8 = 8.482032284$
$E_4 = 4.499982932$	$E_9 = 9.423779007$

Table 1.1: Numerical solutions for equation (1.44) with $a = \sqrt{20}$

are shown in Table 1.1. The set of solutions is discrete as expected. All energy values are less than $10(= \frac{a^2}{2})$ as they should. It is also of interest that the numerical values of E are almost identical to those found for the harmonic oscillator $V(x) = x^2$, see equation(see equation (1.9)). In Figure 1.2 we show a comparison between some of the solutions for the short-range oscillator against the solutions for the harmonic oscillator. The plots are superimposed due to them being practically identical. This fact is in agreement with the values of the energy being practically the same.

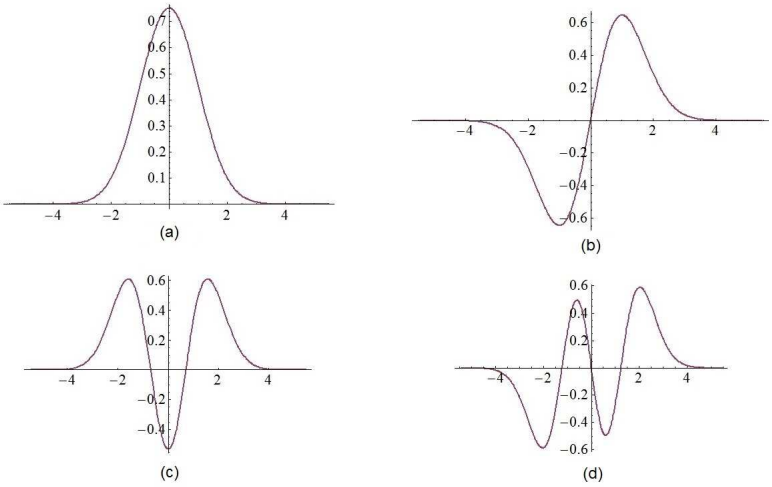

Figure 1.2: Comparison of the first four normalized bound states for a short-range well of height $a^2 = 20$ vs those of a conventional well, for energies (a) $E = 0.5$, (b) $E = 1.5$, (c) $E = 2.5$, (d) $E = 3.5$. The two plots appear superimposed on each other due to them being almost identical.

1.3.2 Scattering states

Now, let k be a real number. Then $k^2 \in \mathbb{R}^+$. In consequence

$$2E - a^2 > 0. \tag{1.45}$$

In this case, the energy is unbounded from above. Now, k is a real number. Therefore, the solutions corresponding to region I and region III are a linear combination of complex exponential functions. Taking into account that these functions represent ingoing (e^{-ikx}) and outgoing waves (e^{ikx}) we make the assumption that our system consists only of scattering of particles incident from the left of the well (i.e. no particles are incident from the right). Therefore, $B_3 = 0$ in equation (1.26), which leads us again to (1.35) and (1.39). This time there is no special conditions over $m_{2,2}$, the transmission coefficient is therefore a function of the continuous variable $E \in (\frac{a^2}{2}, +\infty)$. For $a^2 = 20$, the behavior of the transmission coefficient plot is shown in figure (1.3).

The plot of T reveals there some values of E such that $T(E) = 1$. Since T measures how many particles come out compared to how many go in, when a stream of particles with any of these energies hits the well from the left, it is guaranteed that the totality of them will come out heading right, no particle will be reflected and the transmission will be total.These energies are known as transparencies. Table 1.2 refers to transparencies present between energies $E = 10$ and $E = 20$.

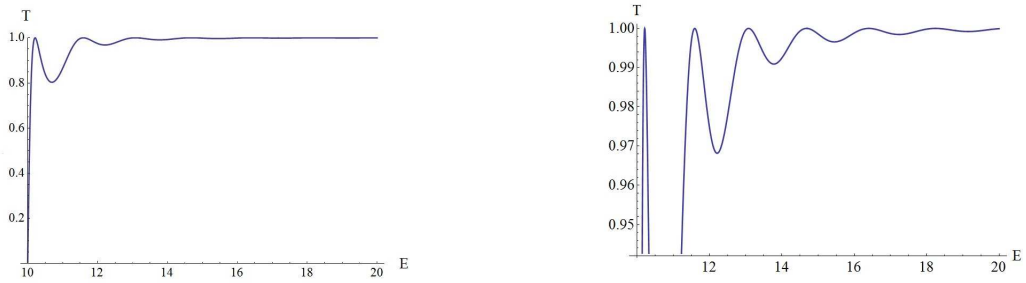

(a) (b)

Figure 1.3: (a) Transmission coefficient for the cutoff value $a = \sqrt{20}$. (b) Zoom in of the plot presented in (a)

1.3.3 Resonances and changes in the continuity equation

Let $k = k_r + i\,k_i$ be a non-trivial complex number (i.e. k_i is not zero). We will pay attention to how this changes the behavior of the probability density $\rho = |\Psi(x,t)|^2$. The

Transparencies	
$E_1 = 10.21$	$E_5 = 16.40$
$E_2 = 11.59$	$E_6 = 18.24$
$E_3 = 13.08$	$E_7 = 20.21$
$E_4 = 14.68$	

Table 1.2: Numerical values of the energy between $E = 10$ and $E = 20$ that result in transparencies for a well of height $a = \sqrt{20}$

time dependence of ρ is determined by the evolution operator $\hat{U}$,

$$\hat{U}\Psi(x,t) \equiv e^{-i\hat{H}t}\Psi(x,0), \tag{1.46}$$

where $\Psi(x,0) = \psi(x)$. For an eigenfunction $\psi(x)$ of $\hat{H}$ with eigenvalue E, the action of $\hat{U}$ reduces to

$$\hat{U}\Psi(x,t) = e^{-i\hat{H}t}\psi(x) = e^{-iEt}\psi(x). \tag{1.47}$$

Therefore, if E isa real then the probability density reads

$$\rho = |e^{-iEt}\psi(x)|^2 = |\psi(x)|^2. \tag{1.48}$$

However, for $k = k_r + i\,k_i$, we have $(k_r + i\,k_i)^2 = 2(E_r + i\,E_i) - a^2$, so that

$$k_r^2 - k_i^2 = 2E_r - a^2 \quad \text{and} \quad k_r k_i = E_i. \tag{1.49}$$

In this case, E is also a non-trivial complex number and (1.48) reads instead

$$\rho(x,t) = |e^{-iEt}\psi(x)|^2 = |e^{-i(E_r + i\,E_i)t}\psi(x)|^2 = |e^{-i\,E_r t}\psi(x)|^2 e^{2\,E_i t} = |\psi(x)|^2 e^{2\,E_i t}. \tag{1.50}$$

From (1.49) we notice that for bound states ($k_i = 0$) and for scattering states ($k_r = 0$) the imaginary part of the energy $E_i = 0$. In those cases equation (1.50) loses its time dependence and the stationary case is recovered. However, for non-trivial complex energies, we have found that ρ is no longer stationary. The probability density increases or decreases exponentially. If E_i is positive, at the limit $t \to \infty$ the probability density should diverge at any position. This makes no physical sense. Therefore, if we are to give any meaning to complex energies, E_i must be negative, which produces the probability density to decrease as time goes by (see figure 1.4). In turn, in light of (1.49), the sign of k_r is the opposite of that of k_i.

We notice as well the change that takes place in the solutions (1.20) and (1.26). The solution in region 1 now reads

$$\psi_1 = A_1 e^{i(k_r + ik_i)x} + B_1 e^{-i(k_r + ik_i)x} = A_1 e^{-k_i x} e^{ik_r x} + B_1 e^{k_i x} e^{-ik_r x}, \tag{1.51}$$

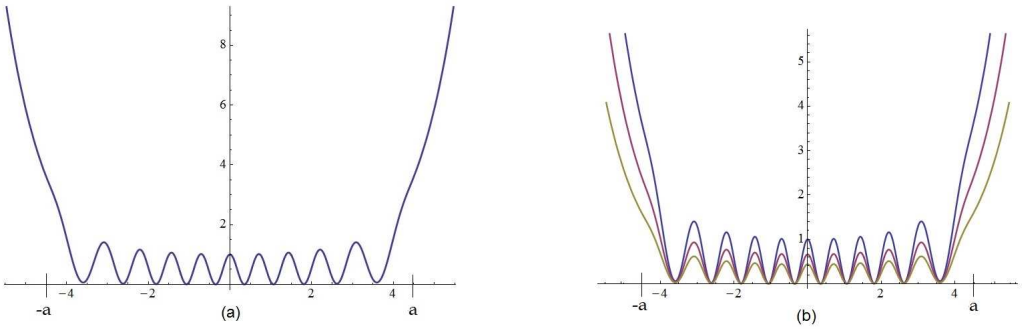

Figure 1.4: (a) Probability density distribution ρ along space of a resonant state with $k = 0.422 - 0.486$. (b) Time evolution of the state shown in (a) for $t = 0, 1, 2$ (from top to bottom); ρ decreases over time everywhere in space.

while for region 3 one has

$$\psi_3 = A_3 e^{i(k_r + ik_i)x} + B_3 e^{-i(k_r + ik_i)x} = A_3 e^{-k_i x} e^{ik_r x} + B_3 e^{k_i x} e^{-ik_r x}. \tag{1.52}$$

To find further information about k we shall assume now that there are no incoming waves, neither from the left nor from the right. Therefore we set $A_1 = 0$ and $B_3 = 0$:

$$\psi_1 = B_1 e^{k_i x} e^{-ik_r x}, \qquad \psi_3 = A_3 e^{-k_i x} e^{ik_r x}. \tag{1.53}$$

With these expressions in mind we use (1.38) to find the probability density current for regions 1 and 3,

$$j_1 = |B_1|^2 e^{2k_i x}(-k_r), \qquad j_3 = |A_3|^2 e^{-2k_i x}(k_r). \tag{1.54}$$

In order to make sense with our assumption of purely outgoing waves, j_1 be negative while j_3 should be positive. This means that $k_r > 0$. Since the real part of k is positive, from the discussion following (1.48) it follows that the imaginary part of k is negative, i.e. $k_i < 0$. Notice that the setting of $A_1 = 0$ in (1.53) leads again to condition (1.44). In conclusion, the values of $k \in \mathbb{C}$ located in the $4th$ quadrant of the complex plane such that satisfy being poles of T lead to the physical phenomena of purely outgoing waves. Therefore, for these energies the potential is working as a source of particles moving away from its core. This is essentially the resonance phenomena, which is a well fit model for decaying systems like radioactive atoms, or the modeling of scattering off a potential which absorbed some of the incident particles, kept them inside for a period of time, and then released them after the original source had been turned off. Table (1.3) presents the resonant energies of a short-range oscillator potential with height $a^2 = 20$.

The values of $k = k_r + ik_i$ that satisfy (1.44) in the fourth quadrant correspond to the purely outgoing wave solution (1.53). This set is discrete and that there seems to be an infinite amount of them. We present in Table 1.3 the first ten values of k (and their corresponding energies).

	$k_r + i\,k_i$	$E_r + i\,E_i$
k_1	$0.42219 - i\,0.48681$	$9.97063 - i\,0.20553$
k_2	$1.70080 - i\,0.51925$	$11.31155 - i\,0.88314$
k_3	$2.41611 - i\,0.54743$	$12.76895 - i\,1.32266$
k_4	$3.00351 - i\,0.57212$	$14.34687 - i\,1.71836$
k_5	$3.52816 - i\,0.59411$	$16.04747 - i\,2.09611$
k_6	$4.01505 - i\,0.61401$	$17.87180 - i\,2.46528$
k_7	$4.47668 - i\,0.63230$	$19.82043 - i\,2.83060$
k_8	$4.92023 - i\,0.64929$	$21.89354 - i\,3.19465$
k_9	$5.35023 - i\,0.66524$	$24.09120 - i\,3.55918$
k_{10}	$5.76972 - i\,0.68030$	$26.41343 - i\,3.92514$

Table 1.3: k and E values corresponding to purely outgoing waves solutions for $a^2 = 20$.

We point out that the last 7 energies presented in Table 1.3 barely display a pattern in their real part. This pattern goes as $E_r^n \approx E_r^{n-1} + 2$. An analogous pattern on the real part of k can barely be noticed too. This other pattern would behave $k_r^n \approx k_r^{n-1} + 0.5$. The search for a prediction of such an approximate behavior seems interesting and might be the subject of following studies in a near future.

1.4 Approximate method

Let us study our system through an approximate method now. We will use the WKB approach to quantum potentials. This method, born in the first era of quantum mechanics is most useful in the search of eigenvalues for bound states of the system rather than on the search of the exact form of the solution.

1.4.1 WKB solution for bound states

The stationary Schrödinger equation reads

$$-\frac{\hbar^2}{2m}\nabla^2\psi + V\psi = E\psi. \tag{1.55}$$

The WKB method proposes ψ to be of the form

$$\psi(r,\theta) = e^{\frac{i}{\hbar}S}, \tag{1.56}$$

where S is a function of the position $S(r,\theta)$ to be determined. Substituting in (1.55) and rearranging we get

$$\frac{(\nabla S)^2}{2m} - \frac{i\hbar}{2m}\nabla^2 S + V = E. \tag{1.57}$$

We shall assume that the system is in such a state that the following is true:

$$\left|\frac{(\nabla S)^2}{2m}\right| \gg \left|\frac{i\hbar}{2m}\nabla^2 S\right|. \tag{1.58}$$

With this in mind, we may dismiss the second term in (1.57), giving

$$\frac{\nabla S \cdot \nabla S}{2m} + V \approx E. \tag{1.59}$$

We can recognize that if we set $\nabla S(x) = p(x) \equiv \sqrt{2m(E - V(x))}$ =, the momentum of the particle, then (1.59) gets fulfilled since it would be exactly the expression of the total mechanical energy of a classical particle. From this observation a semi-classical approximation is born, in which quantum problems can be solved by introducing quantum corrections to the classic result. This corrected result would be used to compute the wave function along with its eigenvalues.

To explore the physical meaning of the condition (1.58). To be more clear we'll write it for a one dimensional system:

$$\left|\frac{\left(\frac{dS}{dx}\right)^2}{2m}\right| \gg \left|\frac{i\hbar}{2m}\frac{d^2S}{dx^2}\right|. \tag{1.60}$$

As we stated above, under this condition

$$\frac{dS}{dx} \approx p(x). \tag{1.61}$$

Substituting (1.61) in (1.60) we get

$$\begin{aligned} \left|\frac{p^2(x)}{2m}\right| &\gg \left|\frac{i\hbar}{2m}\frac{dp(x)}{dx}\right| = \left|\frac{i\hbar}{2m}\left(-\sqrt{\frac{m}{2(E-V(x))}}\frac{dV(x)}{dx}\right)\right| \\ &= \left|\frac{i\hbar}{2m}\frac{mF}{p(x)}\right| \end{aligned} \tag{1.62}$$

where we have used a relation from Newtonian mechanics, associating a force F with the potential $V(x)$ through $F = -\frac{dV(x)}{dx}$. This expression makes it clear that the semi-classical approximation is valid in those regions where, either the force acting over the particle is weak, *i.e.* $V(x)$ varies slowly or the classical momentum is large. Notice that this last condition makes the WKB approximation not valid near the classical turning points where $E \approx V(x) \leftrightarrow p(x) \approx 0$.

Let S be expanded in a power series of $i\hbar$

$$S = S_0 + i\hbar S_1 + (i\hbar)^2 S_2 + \cdots \tag{1.63}$$

By expanding S as a series of powers of $\hbar$ we make it evident that we will get quantum corrections with each successive power of $\hbar$ considered. Introducing this series in (1.57) we get a corresponding set of equations. As long as (1.58) is fulfilled these set of equations will determine the wave function. In most cases it is sufficient to work only with the zeroth and first order approximations. As a first approach we will only work with these two (order 0 and order 1). The set of differential equations obtained is

$$\frac{|\nabla S_0|^2}{2m} + V = E, \qquad \nabla S_0 \cdot \nabla S_1 - \frac{1}{2}\nabla^2 S_0 = 0. \tag{1.64}$$

Our focus is on the 1-dimensional short range oscillator. Being that the case we will solve the one-dimensional version of (1.64). That is,

$$\frac{1}{2m}\left|\frac{dS_0}{dx}\right|^2 + V = E, \qquad \frac{dS_0}{dx}\frac{dS_1}{dx} - \frac{1}{2}\frac{d^2 S_0}{dx^2} = 0. \tag{1.65}$$

These equations can be easily integrated and we obtain

$$S_0 = \pm \int^r p(x)\ dx + C, \qquad S_1 = -\ln\left(\frac{1}{\sqrt{p(x)}}\right), \tag{1.66}$$

where C is an arbitrary constant that comes with the indefinite integral of $p(x)$.

The solution for ψ is then

$$\begin{aligned} \psi &= \exp\left[(\tfrac{i}{\hbar})(S_0 + i\hbar S_1)\right] = \exp\left[\pm(\tfrac{i}{\hbar})\textstyle\int p(x)\,dx + C + ln\left(\frac{1}{\sqrt{p(x)}}\right)\right] \\ &= \frac{1}{\sqrt{p(x)}}\ \exp\left[\pm\frac{i}{\hbar}\left(\int p(x)\ dx + C\right)\right]. \end{aligned} \tag{1.67}$$

For a given bounded energy, any one-dimensional potential well is divided in three regions. Let $x_{1,2}$ be turning points, that is they are such that $p(x) = 0$. The values of $p(x)$ satisfy

$$p(x) = \begin{cases} i\tilde{p}(x) \equiv i\sqrt{2m(V(x) - E)} & , \quad x < x_1 \\ \sqrt{2m(E - V(x))} & , \quad x_1 < x < x_2 \\ i\tilde{p}(x) \equiv i\sqrt{2m(V(x) - E)} & , \quad x > x_2 \end{cases} \tag{1.68}$$

Notice that, in their respective domains, $p(x) > 0$ and $\tilde{p}(x) > 0$. Then, according to (1.67), the general solution for each region reads

$$\psi(x) = \begin{cases} A_1 \dfrac{1}{\sqrt{\tilde{p}(x)}} \exp\left[\dfrac{1}{\hbar}\left(\displaystyle\int_x^{x_1} \tilde{p}(x)\ dx\right)\right] + A_2 \dfrac{1}{\sqrt{\tilde{p}(x)}} \exp\left[-\dfrac{1}{\hbar}\left(\displaystyle\int_x^{x_1} \tilde{p}(x)\ dx\right)\right], & x < x_1 \\ N \cos\left(\displaystyle\int p(x)dx + \alpha\right), \qquad x_1 < x < x_2 \\ B_1 \dfrac{1}{\sqrt{\tilde{p}(x)}} \exp\left[\dfrac{1}{\hbar}\left(\displaystyle\int_{x_2}^{x} \tilde{p}(x)\ dx\right)\right] + B_2 \dfrac{1}{\sqrt{\tilde{p}(x)}} \exp\left[-\dfrac{1}{\hbar}\left(\displaystyle\int_{x_2}^{x} \tilde{p}(x)\ dx\right)\right], & x > x_2 \end{cases} \tag{1.69}$$

where A_i, B_i, N and α are constants to be determined through boundary conditions. Since we are focused on bound states, we need to make sure the wave function is an acceptable physical state. Therefore, $A_1 = 0, B_1 = 0$. The function $\psi(x)$ now reads

$$\psi(x) = \begin{cases} A_2 \dfrac{1}{\sqrt{\tilde{p}(x)}} \exp\left[-\dfrac{1}{\hbar}\left(\displaystyle\int_x^{x_1} \tilde{p}(x)\ dx\right)\right] & , \quad x < x_1 \\ N \cos\left(\displaystyle\int p(x)dx + \alpha\right) & , \quad x_1 < x < x_2 \\ B_2 \dfrac{1}{\sqrt{\tilde{p}(x)}} \exp\left[-\dfrac{1}{\hbar}\left(\displaystyle\int_{x_2}^{x} \tilde{p}(x)\ dx\right)\right] & , \quad x > x_2 \end{cases} \tag{1.70}$$

Since the WKB approximation is not valid close to the turning points we cannot use this formulas to sew the solution across the turning points by using continuity conditions. However, a set of connection formulas exist that allow us to link the outside of the well with the inside. The connection formulas establish that, assuming we know for sure the asymptotic behavior of the wave function on one side of the turning point, then we

can be sure that the wave function has a matching behavior on the other side. This correspondences work only in the direction specified. To know more in more detail about the connection formulas and its derivation we refer the reader to [7].

The following two sets of equations are read as follows: What is on the left of the arrow is the expression of ψ far away to the left of the turning point. What is on the right of the arrow is the expression of ψ far away to the right of the turning point. The direction of the arrow states which asymptotic expression of the wave function determines with certainty its asymptotic form on the other side of the turning point. For the turning point $x = x_1$ we have

$$\begin{aligned}
\psi(x) = \tfrac{A}{\sqrt{\tilde{p}(x)}} \exp\left[-\tfrac{1}{\hbar}\int_x^{x_1} \tilde{p}(x)\, dx\right] \quad &\Longrightarrow \quad \psi(x) = \tfrac{2A}{\sqrt{p(x)}} \cos\left(\tfrac{1}{\hbar}\int_{x_1}^{x} p(x)\, dx - \frac{\pi}{4}\right); \\
\psi(x) = \tfrac{A\sin\eta}{\sqrt{\tilde{p}(x)}} \exp\left[\tfrac{1}{\hbar}\int_x^{x_1} \tilde{p}(x)\, dx\right] \quad &\Longleftarrow \quad \psi(x) = \tfrac{A}{\sqrt{p(x)}} \cos\left(\tfrac{1}{\hbar}\int_{x_1}^{x} p(x)\, dx - \frac{\pi}{4} + \eta\right),
\end{aligned} \tag{1.71}$$

while for the turning point $x = x_2$ it results

$$\begin{aligned}
\psi(x) = \tfrac{2A}{\sqrt{p(x)}} \cos\left(\tfrac{1}{\hbar}\int_x^{x_2} p(x)\, dx - \frac{\pi}{4}\right) \quad &\Longleftarrow \quad \tfrac{A}{\sqrt{\tilde{p}(x)}} \exp\left[-\tfrac{1}{\hbar}\int_{x_2}^{x} \tilde{p}(x)\, dx\right]; \\
\psi(x) = \tfrac{A}{\sqrt{p(x)}} \cos\left(\tfrac{1}{\hbar}\int_x^{x_2} p(x)\, dx - \frac{\pi}{4} + \eta\right) \quad &\Longrightarrow \quad \tfrac{A\sin\eta}{\sqrt{\tilde{p}(x)}} \exp\left[\tfrac{1}{\hbar}\int_{x_2}^{x} \tilde{p}(x)\, dx\right].
\end{aligned} \tag{1.72}$$

According to the connection formulas (1.71) and (1.72), the first line of (1.70) implies that in the region $(x_1 < x < x_2)$ ψ has the form

$$\psi = A\cos\left(\int_{x_1}^{x} p(x)dx - \frac{\pi}{4}\right), \quad x_1 < x < x_2. \tag{1.73}$$

On the other hand, through the connection formulas again, the third line of (1.70) forces ψ in the same region $(x_1 < x < x_2)$ to be of the form

$$\psi = B\cos\left(\int_{x}^{x_2} p(x)dx - \frac{\pi}{4}\right), \quad x_1 < x < x_2. \tag{1.74}$$

Let us focus on (1.74) and look for the conditions in which it matches equation (1.73).

By adding a zero inside the argument of the cosine we get

$$\begin{aligned}
\psi &= B\cos\left(\int_x^{x_2} p(x)dx + \left(\int_{x_1}^{x} p(x)dx - \int_{x_1}^{x} p(x)dx\right) - \frac{\pi}{4}\right) \\
&= B\cos\left(\int_{x_1}^{x_2} p(x)dx - \int_{x_1}^{x} p(x)dx - \frac{\pi}{4}\right) \\
&= B\cos\left(\int_{x_1}^{x_2} p(x)dx - \int_{x_1}^{x} p(x)dx - \frac{\pi}{2} + \frac{\pi}{4}\right) \\
&= B\cos\left(\int_{x_1}^{x_2} p(x)dx - \frac{\pi}{2} - \int_{x_1}^{x} p(x)dx + \frac{\pi}{4}\right) \\
&= B\cos\left(\int_{x_1}^{x_2} p(x)dx - \frac{\pi}{2}\right)\cos\left(-\int_{x_1}^{x} p(x)dx + \frac{\pi}{4}\right) \\
&\quad -B\sin\left(-\int_{x_1}^{x} p(x)dx + \frac{\pi}{4}\right)\sin\left(\int_{x_1}^{x_2} p(x)dx - \frac{\pi}{2}\right), \quad x_1 < x < x_2
\end{aligned} \tag{1.75}$$

For this to have the form of (1.73) it should be true that

$$\int_{x_1}^{x_2} p(x)\ dx = \left(n + \frac{1}{2}\right)\pi, \qquad n = 0, 1, 2, ... \tag{1.76}$$

With this in mind we go back to (1.75) and find

$$\psi = B\cos(n\pi)\cos\left(\int_{x_1}^{x} p(x)\ dx - \frac{\pi}{4}\right) = (-1)^n B\cos\left(\int_{x_1}^{x} p(x)\ dx - \frac{\pi}{4}\right). \tag{1.77}$$

Comparing (1.77) with (1.73) we conclude that the connection formulas are in agreement as long as

$$\int_{x_1}^{x_2} p(x)dx = \left(n + \frac{1}{2}\right)\pi, \qquad A = (-1)^n B \tag{1.78}$$

This equation is the quantization condition for the WKB method. We would like to point out that this condition was derived from the connection formulas under the assumption that the WKB applicability condition (1.58) holds. We will show with an example how effective it can be to find the eigenvalues of the harmonic oscillator short range potential.

1.5 WKB quantization of the 1-dimensional short range oscillator

In this section we are going to apply the WKB quantization formula (1.78) to a specific potential. This formula reads

$$\int_{x_1}^{x_2} p\, dx = \pi\hbar\left(n + \frac{1}{2}\right). \tag{1.79}$$

The one-dimensional short range quantum harmonic oscillator potential $V(x)$ reads

$$V(x) = \begin{cases} \frac{1}{2}m\omega^2 x^2, & |x| < a \\ \frac{1}{2}m\omega^2 a^2, & |x| \geqslant a \end{cases} \tag{1.80}$$

Therefore the momentum inside the well is

$$p(x) = \sqrt{2m(E - V(x))} = \sqrt{2mE - m^2\omega^2 x^2}. \tag{1.81}$$

In turn, the left side of (1.79) reads

$$\begin{aligned} \int_{x_1}^{x_2} p(x')\, dx' &= \int_{x_1}^{x_2} \sqrt{2mE - m^2\omega^2 x'^2}\, dx' = \int_{x_1}^{x_2} \sqrt{a + cx'^2}\, dx' \\ &= \frac{2cx\sqrt{a + cx'^2}}{4c}\Big|_{x=x_1}^{x=x_2} + \frac{4a}{8}\int_{x_1}^{x_2} \frac{dx'}{\sqrt{a + cx'^2}} dx' \\ &= \tfrac{1}{2}x\sqrt{a + cx'^2}\Big|_{x=x_1}^{x=x_2} + \tfrac{1}{2}a\left(\frac{-1}{\sqrt{-c}} arcsin\left(\frac{2cx'}{\sqrt{-4ac}}\right)\right)\Big|_{x=x_1}^{x=x_2}, \end{aligned} \tag{1.82}$$

where $a \equiv 2mE$, $c \equiv -m^2\omega^2$. In the last two lines we used results from [8] (pgs. 94, 95). By substituting the definitions of a and c we have

$$\begin{aligned} \int_{x_1}^{x_2} p(x')\, dx' &= \tfrac{1}{2}x\sqrt{2mE - m^2\omega^2 x^2}\Big|_{x=x_1}^{x=x_2} \\ &\quad + \tfrac{1}{2}(2mE)\left(\frac{-1}{\sqrt{m^2\omega^2}} \arcsin\left(\frac{2(-m^2\omega^2)}{\sqrt{-4(2mE)(-m^2\omega^2)}}x\right)\right)\Big|_{x=x_1}^{x=x_2} \\ &= \tfrac{1}{2}x\sqrt{2mE - m^2\omega^2 x^2}\Big|_{x=x_1}^{x=x_2} + \left(\frac{-E}{\omega}\right)\arcsin\left(\sqrt{\frac{m\omega^2}{2E}}x\right)\Big|_{x=x_1}^{x=x_2}. \end{aligned} \tag{1.83}$$

Now, x_1 and x_2 are turning points i.e. points where $p^2 = 2mE - m^2\omega^2 = 0$. Therefore,

$$\sqrt{2mE - m^2\omega^2 x^2}\Big|_{x=x_1,x_2} = 0, \qquad x_{1,2} \equiv \pm\sqrt{\frac{2E}{m\omega^2}}. \tag{1.84}$$

With this in mind, (1.83) results in

$$\begin{aligned}\int_{x_1}^{x_2} p(x')\,dx' &= \left(\tfrac{-E}{\omega}\right)\arcsin\left(\sqrt{\tfrac{m\omega^2}{2E}}\sqrt{\tfrac{2E}{m\omega^2}}\right) - \arcsin\left(\sqrt{\tfrac{m\omega^2}{2E}}\left(-\sqrt{\tfrac{2E}{m\omega^2}}\right)\right) \\ &= \left(\tfrac{-E}{\omega}\right)(\arcsin(1) - \arcsin(-1)) = \left(\tfrac{-E}{\omega}\right)\left(\tfrac{\pi}{2} - \tfrac{3\pi}{2}\right) = \left(\tfrac{E\pi}{\omega}\right)\end{aligned} \tag{1.85}$$

Combining (1.85) with (1.79) we finally get

$$E = \left(n + \frac{1}{2}\right)\hbar\omega \tag{1.86}$$

As we can see, the WKB quantization formula yielded exactly the quantization of the energy corresponding to a conventional oscillator, *i.e* an oscillator whose potential dependence goes as $\frac{1}{2}m\omega^2x^2$ all along the real line.

Up to this moment we have found the bound states energy values for a short range one-dimensional oscillator through two different methods. On one hand we solved the Schrödinger equation for the three regions arising due to the potential joints. On the first and third regions the potential is constant and we have as solutions Bessel equations. Inside the well the solution to the squared dependence of the potential is a product of two functions: a Gaussian dependence and a linear combination of Hypergeometric Functions. The matching of these conditions gives place to a transcendental equation which we solved numerically.

On the other hand we have the WKB method just presented This method is designed to be applied to potentials which divide the domain in three regions, which is our case. Although the method clearly shows that the solution in the classical forbidden regions is asymptotically evanescent, the WKB quantization condition matches exactly the quantization of the conventional harmonic oscillator which is a potential that does not acknowledge the short range action of the potential. This leads us to infer that the conventional oscillator is good enough to predict the energies of the more realistic, short range potential; at least as good as the WKB method. However, the exact solution for the three regions found by us and the actual matching of them, result in numerical values that differ with the other methods' values in a degree of 10^{-2}. Although a difference so small might be not relevant for most applications, a more subtle phenomena would benefit greatly of more precise results to compare with finer experimental measurements.

Chapter 2

Solving the 2-D short-range oscillator potential

For the solving of the two-dimensional version of the system addressed in Chapter 1 we shall follow a similar path to that already used. However, a second dimension adds complexity to the mathematical structure so that some caution is necessary. From now on, any symbol that may have appeared in the previous chapter holds its own meaning. Let the potential $V(r')$ be defined as

$$V(r') = \begin{cases} \frac{1}{2}m\omega^2 r'^2; & r' \leqslant a' \\ a'^2; & r' > a' \end{cases} \tag{2.1}$$

where r' is the polar radial coordinate, m is the mass of the incident particle and ω is the harmonic oscillator natural frequency. See Figure 2.1 for a three-dimensional representation of this potential.

In polar coordinates, the Laplacian operator reads

$$\nabla'^2\psi = \frac{\partial^2\psi}{\partial r'^2} + \frac{1}{r'}\frac{\partial\psi}{\partial r'} + \frac{1}{r'^2}\frac{\partial^2\psi}{\partial\theta^2}, \tag{2.2}$$

where θ is the polar coordinate. The stationary Schrödinger equation for the 2-dimensional harmonic oscillator reads

$$-\frac{\hbar^2}{2m}\left(\frac{\partial^2\psi}{\partial r'^2} + \frac{1}{r'}\frac{\partial\psi}{\partial r'} + \frac{1}{r'^2}\frac{\partial^2\psi}{\partial\theta^2}\right) + \frac{1}{2}m\omega^2 r'^2\psi = E'\psi, \tag{2.3}$$

where E' is the energy. We define dimensionless variables just as in the one-dimensional system. Using

$$r \equiv \sqrt{\frac{m\omega}{\hbar}}r'; \quad E \equiv \frac{E'}{\hbar\omega}, \tag{2.4}$$

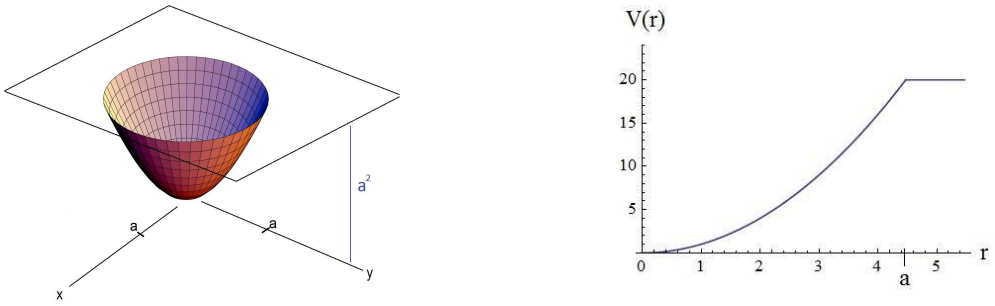

(a) (b)

Figure 2.1: (a) Three dimensional representation of a short-range 2-dimensional harmonic potential. (b) Plot of the short-range square dependence of $V(r)$with respect to $r \in (0, \infty)$.

the dimensionless Schrödinger equation reads $\nabla^2\psi + (2E - V(r))\,\psi = 0$, explicitly

$$-\frac{1}{2}\left(\frac{\partial^2\psi}{\partial r^2} + \frac{1}{r}\frac{\partial\psi}{\partial r} + \frac{1}{r^2}\frac{\partial^2\psi}{\partial\theta^2}\right) + \frac{1}{2}V(r)\psi = E\psi. \tag{2.5}$$

where the dimensionless potential $V(r)$ is defined as

$$V(r) = \begin{cases} r^2; & r \leqslant a \\ a^2; & r > a \end{cases} \tag{2.6}$$

A differential equation defined over a given set of variables admits separable solutions whenever [9]:

- The factors comprising the solution lead to ordinary differential equations (ODE), each on its own independent variable.
- At least one of such ODE is linked with a Sturm-Liouville problem.
- At least one of the independent variables is constained in a finite interval.

The differential equation (2.5)-(2.6) satisfies teh above criteria, so we propose the solution:

$$\psi(r, \theta) = R(r)\Theta(\theta). \tag{2.7}$$

Substituting (2.7) into (2.5), and dividing the result by ψ, we arrive at the relationship

$$\left(\frac{1}{R}\frac{d^2R}{dr^2} + \frac{1}{R}\frac{1}{r}\frac{dR}{dr} - V(r) + 2E\right)r^2 = -\frac{1}{\Theta}\frac{d^2\Theta}{d\theta^2}. \tag{2.8}$$

Notice that the left- and the right-hand side of (2.8) depend on independent variables. Therefore, they must be equal to a constant l^2. Thus, we write

$$-\frac{1}{\Theta}\frac{d^2\Theta}{d\theta^2} = l^2, \tag{2.9}$$

and

$$\left(\frac{1}{R}\frac{d^2R}{dr^2} + \frac{1}{R}\frac{1}{r}\frac{dR}{dr} - V(r) + 2E\right) r^2 = l^2. \tag{2.10}$$

The solution to the former equation is easily found to be

$$\Theta(\theta) = B_1 e^{il\theta} + B_2 e^{-il\theta}, \tag{2.11}$$

where B_1 and B_2 are constants to be determined.

Before solving the radial equation (2.10) we will show that the continuity conditions of this two dimensional system reduce to continuity conditions for the one dimensional case, the radial coordinate.

2.1 Continuity conditions in polar coordinates

The continuity conditions required by the solution of the Schrödinger equation are

$$\psi_<(r,\theta)|_{r=a} = \psi_>(r,\theta)|_{r=a}, \qquad \nabla\psi_<(r,\theta)|_{r=a} = \nabla\psi_>(r,\theta)|_{r=a}. \tag{2.12}$$

The subscript $<$ stands for the function within the well ($r < a$) while $>$ refers to the function outside the well ($r > a$). Writing explicitly the gradient in polar coordinates, $\nabla\psi \equiv \frac{\partial\psi}{\partial r}\hat{r} + \frac{1}{r}\frac{\partial\psi}{\partial\theta}$, we find

$$\Theta(\theta)R_<(r)\Big|_{r=a} = \Theta(\theta)R_>(r)\Big|_{r=a}, \tag{2.13}$$

$$\Theta(\theta)\frac{dR_<(r)}{dr}\Big|_{r=a} = \Theta(\theta)\frac{dR_>(r)}{dr}\Big|_{r=a}, \qquad \frac{R_<}{a}\frac{d\Theta}{d\theta}\Big|_{r=a} = \frac{R_>}{a}\frac{d\Theta}{d\theta}\Big|_{r=a}. \tag{2.14}$$

As the continuity conditions do not depend on θ we cancel the factors $\Theta(\theta)$ and $\frac{d\Theta}{d\theta}$ from both sides of these equations. Therefore, the continuity conditions (2.12) can be stated in terms of the radial function as follows.

$$R_<(r)|_{r=a} = R_>(r)|_{r=a}, \qquad \frac{dR_<(r)}{dr}(r)\Big|_{r=a} = \frac{dR_>(r)}{dr}\Big|_{r=a}. \tag{2.15}$$

Once the Schrödinger equation is solved within and without the well, equations (2.15) will adjust the corresponding coefficients so the solution"gets glued" in such a way that

both, it and its derivative are continuous. The reducing of continuity conditions for $\psi(r,\theta)$ to the continuity of $R(r)$ allows to continue the analysis of the stationary system taking into account the behavior of $R(r)$ only. This is possible due to the symmetry of the potential, which essentially allows the separability of variables.

2.2 Solution to the piece-wise radial equation

As stated in chapter 1, solving a problem by approximate methods (even if we are able to solve it in closed form) can be a nurturing exercise. In the following we will solve the two-dimensional harmonic oscillator in closed form. The analytic expressions will naturally give bound, scattering and resonant states. Afterwards, we will revisit the case of bound states applying the WKB method.

2.2.1 Analytical solution

• **Within the well** $(r < a)$

The potential is given as a piece-wise function of r. Therefore, $R(r)$ will be also a piece-wise function. In the domain $0 < r < a$, $V(r) = r^2$. Therefore the equation to be solved is

$$r^2R'' + rR' - (r^4 - 2Er^2 + l^2)R = 0, \tag{2.16}$$

where the prime ($'$) stands for derivative with respect to r. Dividing by r^2 we get

$$R'' + \frac{1}{r}R' + (-r^2 + 2E - \frac{l^2}{r^2})R = 0. \tag{2.17}$$

As in the one-dimensional case, we first define a new variable ξ as follows

$$\xi \equiv r^2. \tag{2.18}$$

In terms of ξ, our differential equation reads

$$\xi\frac{d^2R}{d\xi^2}(\xi) + \frac{dR}{d\xi}(\xi) - \frac{l^2}{4\xi}R(\xi) + \frac{2E-\xi}{4}R(\xi) = 0. \tag{2.19}$$

Now we propose $R(\xi)$ to have the form

$$R(\xi) = e^{-p\xi}\ \xi^q\ u(\xi), \tag{2.20}$$

where p and q are constants such that $u(r)$ satisfies a confluent hypergeometric equation. Taking the first and second derivative of (2.20), and substituting them into equation (2.19), we get

$$\xi\frac{d^2u}{d\xi^2}+(2q+1-2p\xi)\frac{du}{d\xi}+\left[\xi^{-1}(-\frac{l^2}{4}+q^2)+\left(\frac{2E}{4}-p(2q+1)\right)+\xi(p^2-\frac{1}{4})\right]u=0. \quad (2.21)$$

Making

$$p=\frac{1}{2}\ ;\ q=\frac{l}{2}, \quad (2.22)$$

eq. (2.21) takes the form

$$\xi\frac{d^2u}{d\xi^2}+(\gamma-\xi)\frac{du}{d\xi}-\alpha u=0, \quad (2.23)$$

where $\gamma\equiv l+1$ and $-\alpha\equiv\frac{E}{2}-\frac{l}{2}-\frac{1}{2}$.

On the other hand, in order to get single-valued (2.11), the parameter l must take integer values. The latter implies that $\gamma(=l+1)$ takes integer values as well, denoting again the Kummer function as $M(\alpha,\gamma;\xi)$. Unlike the one-dimensional version of the problem, the pair of solutions

$$M(\alpha,\gamma;\xi),\qquad \xi^{1-\gamma}M(1+\alpha-\gamma,2-\gamma;\xi), \quad (2.24)$$

is not enough since one of them is not well defined for γ an integer number [4]. From the theory of hypergeometric equations we know that the appropiate pair of solutions depends on whether γ is shorter, equal or larger than 1. Therefore, the solution of (2.23) will depend on the profile of l.

◦ **Case** $l>0$

In this case $\gamma>1$. Thus, the general solution of equation (2.23) reads

$$u(\xi)=A\,M(\alpha,\gamma;\xi)+B\,U(\alpha,\gamma;\xi), \quad (2.25)$$

where A and B are arbitrary constants, and $U(\alpha,\gamma;\xi)$ is the Tricomi function (also called Hypergeometric Function of the second kind).

Taking into account that $\xi=r^2$, the solution for the radial function is

$$\begin{aligned} R(r) &= e^{-\frac{r^2}{2}}r^l u(r) \\ &= A\,e^{-\frac{r^2}{2}}r^l M(\tfrac{1}{2}(1+l-E),1+l;r^2)+B\,e^{-\frac{r^2}{2}}r^l U(\tfrac{1}{2}(1+l-E),1+l;r^2). \end{aligned} \quad (2.26)$$

Before going further we need to make sure $R(r)$ does not diverge at $r = 0$. Recall that for positive integer values of $\gamma > 1$ the behavior of $M(\alpha, \gamma; \xi)$ and $U(\alpha, \gamma; \xi)$ close to $r = 0$ are, respectively [10]

$$\lim_{\xi \to 0} M(\alpha, \gamma; \xi) = 1 \ , \qquad \lim_{\xi \to 0} U(\alpha, \gamma; \xi) \sim \xi^{1-\gamma}. \tag{2.27}$$

As $\xi = r^2$ and $l > 0$, then the behavior of the first and second solutions near $r = 0$ turns out to be

$$\begin{array}{rcl} \lim_{r\to 0} e^{-\frac{r^2}{2}} r^l M(\frac{1}{2}(1+l-E), 1+l; r^2) & = & r^l, \\ \lim_{r\to 0} e^{-\frac{r^2}{2}} r^l U(\frac{1}{2}(1+l-E), 1+l; r^2) & = & (r^l)(r^2)^{1-(l+1)} = r^{-l}. \end{array} \tag{2.28}$$

Therefore, the only physically admissible solution in this case is

$$R(r) = R_l(r) = e^{-\frac{r^2}{2}} r^l M\left(\frac{1}{2}\left(1 + l - E\right), 1 + l; r^2\right). \tag{2.29}$$

◦ **Case** $l = 0$

If $l = 0$ then $\gamma = 1$. The two independent solutions for equation (2.23) are again $M(\alpha, \gamma, \xi)$ and $U(\alpha, \gamma, \xi)$. In this case, close to $r = 0$ [10]

$$\lim_{r \to 0} M(\alpha, \gamma; \xi) = 1 \ ; \quad \lim_{r \to 0} U(\alpha, \gamma; \xi) \sim -\frac{1}{\Gamma(\alpha)} \ln(\xi) \tag{2.30}$$

To analyze the behavior of the complete solution $R(r)$ remember that $\xi = r^2$ and $l = 0$. Then the behavior of the first and second solutions near $r = 0$ is

$$\begin{array}{rcl} \lim_{r\to 0} e^{-\frac{r^2}{2}} (r^0) M(\frac{1}{2}(1-E), 1; r^2) & = & (1)(1)(1) = 1, \\ \lim_{r\to 0} e^{-\frac{r^2}{2}} (r^0) U(\frac{1}{2}(1-E), 1; r^2) & = & -\frac{1}{\Gamma(\frac{1}{2}(1-E))} \ln(r^2). \end{array} \tag{2.31}$$

In this case, the second solution is not admissible. Then

$$R_0 = e^{-\frac{r^2}{2}} M\left(\frac{1}{2}(1-E), 1; r^2\right). \tag{2.32}$$

◦ **Case** $l < 0$

$l < 0 \Rightarrow \gamma < 1$. In this case the function $M(\alpha, \gamma; \xi)$ is not well defined, but $\xi^{1-\gamma} M(1 + \alpha - \gamma, 2 - \gamma; \xi)$ is well defined instead. $U(\alpha, \gamma; \xi)$ still works as a second independent solution, therefore, for $l < 0$ we have

$$\xi^{1-\gamma} M(1 + \alpha - \gamma, 2 - \gamma; \xi) \ , \qquad U(\alpha, \gamma; \xi). \tag{2.33}$$

The behavior of these solutions near $\xi = 0$ is as follows

$$\lim_{\xi\to 0} \xi^{1-\gamma} M(1+\alpha-\gamma, 2-\gamma; \xi) = \xi^{1-\gamma}(1) \ , \qquad \lim_{\xi\to 0} U(\alpha,\gamma;\xi) \sim \frac{\Gamma(1-\gamma)}{\Gamma(1+\alpha-\gamma)}. \quad (2.34)$$

Considering $\xi = r^2$, one has

$$\begin{aligned} \lim_{r\to 0} e^{-\frac{r^2}{2}} r^{-l} M(\tfrac{1}{2}(1-l-E), -l+1; r^2) &= r^{-l} = r^{|l|} \to 0, \\ \lim_{r\to 0} e^{-\frac{r^2}{2}} r^{l} U(\tfrac{1}{2}(1-l-E), 1-l; r^2) &= r^{l}(\text{constant}) \to r^{-|l|}. \end{aligned} \quad (2.35)$$

Then, the physically acceptable function is

$$R_l(r) = e^{-\frac{r^2}{2}} r^{-l} M\left(\frac{1}{2}(1-l-E), -l+1; r^2\right) = e^{-\frac{r^2}{2}} r^{|l|} M\left(\frac{1}{2}(1+|l|-E), |l|+1; r^2\right). \quad (2.36)$$

Notice how we wrote in the last equation $-l$ as $|l|$. We did this on purpose to show the "symmetry" of the solution $R(r)$ for $l < 0$ compared with the case $l > 0$ (equation (2.29)).

This symmetry under change of sign of l is a consequence of l appearing as l^2 in the radial equation (2.17). It becomes clear that whether l is shorter, equal or larger than 0, for all integer values of l the only acceptable solution for $R(r)$ is that given by the Kummer function $M(\alpha, \beta; z)$. We conclude that for every l the solution within the well is given by

$$R_l(r) = e^{-\frac{r^2}{2}} r^{|l|} M\left(\frac{1}{2}(1+|l|-E), 1+|l|; r^2\right). \quad (2.37)$$

By writing $|l|$, both cases, positive and negative values of l are covered by the same expression.

2.2.2 The two dimensional harmonics oscillator

As pointed out earlier in the reminder of the one-dimensional harmonic oscillator, the Kummer function is either a polynomial or a convergent series. If $\alpha \equiv \frac{1}{2}(1+|l|-E)$ is not a negative integer, the Kummer function is a series that behaves asymptotically as

$$\begin{aligned} \lim_{z\to\infty} M(\alpha,\beta,z) &= e^z z^{(\alpha-\beta)}, \\ \lim_{r\to\infty} M(\tfrac{1}{2}(1+|l|-E), 1+|l|, r^2) &= e^{r^2} r^{-(1+|l|+E)}, \\ \lim_{r\to\infty} R(r) = e^{-\frac{r^2}{2}} r^{|l|} \left(e^{r^2} r^{-(1+|l|+E)}\right) &= \left(r^{-(1+E)}\right) e^{\frac{r^2}{2}} \to \infty, \end{aligned} \quad (2.38)$$

which is not a suitable behavior for a physical state. Therefore α must be a negative integer $\alpha = -n$. In this case the Kummer function is a polynomial and the asymptotic behavior of $R(r)$ results in

$$\lim_{r\to\infty} R(r) = (\text{some polynomial})\, e^{-\frac{r^2}{2}}. \tag{2.39}$$

Now the solution has an appropriate behavior to be a physical state. As a consequence,

$$-n = \tfrac{1}{2}(1 + |l| - E) \quad \Rightarrow \quad E = 2n + |l| + 1. \tag{2.40}$$

Substituting $\alpha = -n$ in the confluent hypergeometric equation (2.23) we get the associated Laguerre equation, the solutions of which are the associated Laguerre polynomials

$$M(-n, 1 + |l|; r^2) = \frac{|l|!n!}{(|l| + n)!} L_n^{|l|}(r^2); \quad |l| \leqslant n, \tag{2.41}$$

with

$$E = 2n + |l| + 1 = m + 1; \qquad m \equiv 2n + |l|. \tag{2.42}$$

As indicated above, the set of solutions can be equipped with the inner product

$$(\phi_1(\xi), \phi_2(\xi)) \equiv \int_0^\infty \phi_1^*(\xi)\phi_2(\xi)e^{-\xi}\xi^{|l|}d\xi. \tag{2.43}$$

As consequence, the notion of orthogonality for the associated Laguerre polynomials is introduced as follows

$$(L_j^{|l|}(\xi), L_i^{|l|}(\xi)) \equiv \int_{-\infty}^\infty L_j^{|l|}(\xi)L_i^{|l|}(\xi)e^{-\xi}\xi^{|l|}d\xi = \frac{(j + |l|)!}{j!}\delta_{ji}. \tag{2.44}$$

Consistently, for the norm we write

$$|L_j^{|l|}| = \sqrt{\left(L_j^{|l|}, L_j^{|l|}\right)}. \tag{2.45}$$

As we can see, the energy E is defined by two parameters (n, l) that take different integer values to sum m. Since these parameters determine also the state ψ, then two or more states may have the same energy. The amount of different states belonging to the same energy is better calculated by solving the problem in cartesian coordinates.

Proposing the solution in the form $R(x, y) = X(x)Y(y)$, and $V(x, y) = x^2 + y^2$, together with the Laplacian in Cartesian coordinates, the two dimensional Schrödinger equation can be separated into two Schrödinger equations, each associated with a one-dimensional harmonic oscillator depending on only of the variables. Thus, the complete solution

$$\psi(x, y) = A\ e^{-x^2} H_{n_x(x)} H_{n_y(y)}, \tag{2.46}$$

and

$$E = E_x + E_y = (n_x + \frac{1}{2}) + (n_y + \frac{1}{2}) = n_x + n_y + 1 \equiv m + 1. \tag{2.47}$$

Given a fixed m there are $m + 1$ pairs (n_x, n_y) that satisfy (2.47), see Table 2.1. Since a change of coordinates does not affect the dynamical behavior of a physical system, the degeneration of the two dimensional harmonic oscillator is $deg(E_m) = m + 1$.

n_x	0	1	2	...	m
n_y	m	$m-1$	$m-2$	...	1

Table 2.1: Pairs of (n_x, n_y) that added equal m.

Once again we refer the reader to [2] for a discussion of orthogonality of solutions related to a Sturm-Liouville problem and to [3] for a more detailed discussion of orthogonality and completeness.

2.2.3 Solution outside the well $r > a$

Outside the well, the potential has the form $V(r) = a^2$. Therefore equation (2.10) reads

$$\left(\frac{1}{R}\frac{d^2R}{dr^2} + \frac{1}{R}\frac{1}{r}\frac{dR}{dr} + k^2\right) r^2 = l^2, \tag{2.48}$$

where $k^2 = 2E - a^2$. Let $y = kr$. By expressing (2.49) in terms of y we get the Bessel equation:

$$\frac{d^2R}{dy^2} + \frac{1}{y}\frac{dR}{dy} + \left(1 - \frac{l^2}{y^2}\right) R(y) = 0. \tag{2.49}$$

The solutions corresponding to this equation depend on k. As indicated above, there are three possibilities:

- k is pure imaginary
- k is real
- k is complex

2.2.3.1 Bound states

If $k = i\kappa$ with $\kappa \in \mathbb{R}$, we get

$$-\kappa^2 = k^2 = 2E - a^2 < 0 \quad \Rightarrow \quad E < a^2. \tag{2.50}$$

The values of the energy are bounded by half the height of the potential well. Substituting $k = i\kappa$ in (2.49), and making $x = \kappa r$, we have a differential equation for R in terms of x:

$$\frac{d^2R}{dx^2} + \frac{1}{x}\frac{dR}{dx} - \left(1 + \frac{l^2}{x^2}\right) R(x) = 0, \tag{2.51}$$

the solutions of which are the modified Bessel functions $I(\kappa r)$ and $K(\kappa r)$. Therefore,

$$R_>(r) = CI_l(\kappa r) + DK_l(\kappa r), \tag{2.52}$$

where C and D are arbitrary constants. Bound states correspond to solutions that vanish asymptotically. Thus, we need to pay attention to the behavior of the solutions at $r \to \infty$ [11]

$$\lim_{r\to\infty} I_l(\kappa r) = \frac{e^{\kappa r}}{\sqrt{r}}, \qquad \lim_{r\to\infty} K_l(\kappa r) = \frac{e^{-\kappa r}}{\sqrt{r}}. \tag{2.53}$$

Note that $I_l(\kappa r)$ diverges while $K_l(\kappa r)$ goes to zero. Therefore, we discard $I_l(\kappa r)$, so the solution outside the interaction region is

$$R_>(r) = CK_l(\kappa r), \tag{2.54}$$

where C is a normalization constant. This leads to the following continuity conditions:

$$AR_l(a) = CK_l(\kappa a), \qquad AR_l'(a) = CK_l'(\kappa a), \tag{2.55}$$

where (') stands for derivative with respect to r and A is a normalization constant. These equations can be written as a matrix equation:

$$\begin{pmatrix} R_l(r) & -K_l(\kappa a) \\ R_l'(r) & -K_l'(\kappa a) \end{pmatrix} \begin{pmatrix} A \\ C \end{pmatrix} = \begin{pmatrix} 0 \\ 0 \end{pmatrix}. \tag{2.56}$$

As $A \neq 0$ and $C \neq 0$, the matrix on the left-hand side must be non-singular, which means

$$\det \begin{pmatrix} R_l(a) & -K_l(\kappa a) \\ R_l'(a) & -K_l'(\kappa a) \end{pmatrix} = 0. \tag{2.57}$$

For a and l fixed, this equation defines a discrete set of energies, each of them associated to a physical state of a particle captured by the potential well. In Table (2.2) we present

numerical solutions to (2.57) for $a^2 = 20$. We notice that odd and even values of the energy appear with even or odd values of $|l|$. Besides, just as in the one-dimensional case, the energy values are almost dentical to those of the two-dimensional oscillator ($V(r) = r^2$ for $0 < r < \infty$). Recall that the latter is

$$\psi_{conv}(r) = (R_{conv})\left(e^{i|l|\theta}\right) = \left(\sqrt{\frac{n!}{\pi(n+|l|)!}}\right) r^{|l|}e^{-\frac{r^2}{2}}L_n^{|l|}(r^2)e^{il\theta}. \tag{2.58}$$

It would not be a surprise if the radial profile of the solutions coincide in both cases. As examples, we present in Figure 2.2 the profile of $R(r)$ compared with the solution of the two-dimensional oscillator for $l = 0, 1, 2, 3$, and quantum number $n = 1 \leftrightarrow E = 4$. As expected, the plots of both functions appear superimposed one over the other, differing only at scales of 10^{-10} around the cutoff $r = a$.

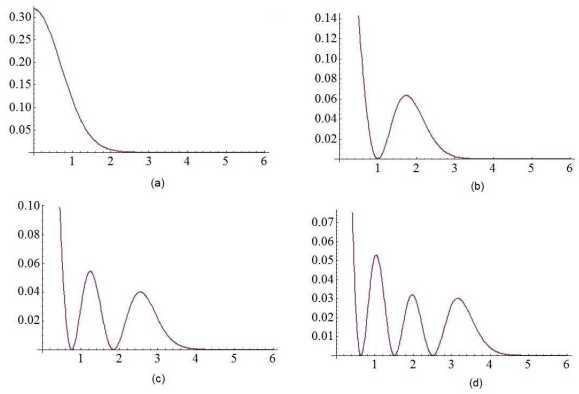

Figure 2.2: Profile comparison between bound states solutions of the two-dimensional short range oscillator vs those of the conventional oscillator potential, for values $l = 0, 1, 3, n = 1 \leftrightarrow E = 4$. The plots of both systems are so similar to each other that their plots appear superimposed.

8.96279		8.96752		8.97883		8.99051		8.99773
	7.99163		7.99390		7.99700		7.99999	
6.99816		6.99848		6.99999		6.99999		
	5.99968		5.9999		5.99999			
4.99995		4.99999		4.99999				
	3.99999		3.99999					
2.99999		2.99999						
	1.99999							
0.99999								
$\|l\|$=0	$\|l\|$=1	$\|l\|$=2	$\|l\|$=3	$\|l\|$=4	$\|l\|$=5	$\|l\|$=6	$\|l\|$=7	$\|l\|$=8

Table 2.2: Numerical solutions for energy values corresponding to admitted values of l.

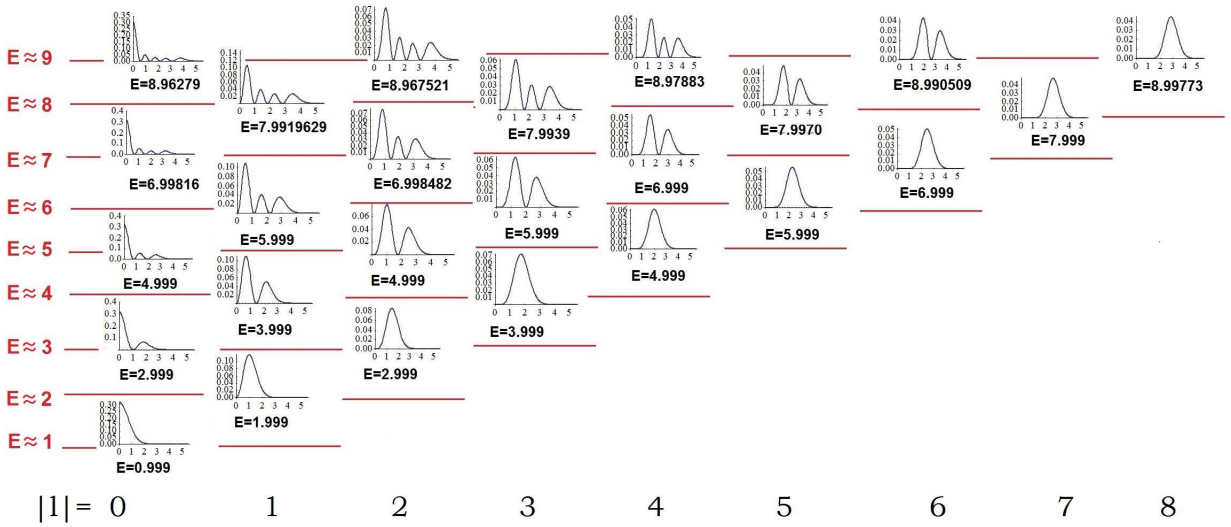

Figure 2.3: Normalized radial distribution of probability corresponding to the values shown in Table 2.2.

2.2.3.2 Time evolution of a superposition of bound states

The time evolution of a quantum state is given by the evolution operator U defined as [5]

$$\psi(\vec{r},t) = \hat{U}\psi(\vec{r}) \equiv e^{-\frac{i}{\hbar}\hat{H}t}\psi(\vec{r}) \tag{2.59}$$

It is well known [5] that for the eigenfunctions $\psi(\vec{r})$ of the Hamiltonian $\hat{H}$ with eigenenergy E, the action of U reduces to

$$\hat{U}\psi(\vec{r}) = e^{-\frac{i}{\hbar}Et}\psi(\vec{r}). \tag{2.60}$$

For the probability density we find

$$|\psi(\vec{r},t)|^2 = |e^{-\frac{i}{\hbar}Et}\psi(\vec{r})|^2 = |\psi(\vec{r})|^2. \tag{2.61}$$

The probability density of one eigen-state does not change with time and it only depends on r. However, we can get a dynamic behavior of the probability density by considering $\psi(\vec{r})$ as a superposition of two eigenfunctions. Let

$$\psi_s(\vec{r}) = A_1\psi_1(\vec{r}) + A_2\psi_2(\vec{r}), \tag{2.62}$$

where $\psi_1(\vec{r})$ and $\psi_2(\vec{r})$ are eigenfunctions with eigenvalues E_1 and E_2, respectively. Then,

$$\Psi_s(\vec{r},t) = \hat{U}\psi(\vec{r}) = e^{-\frac{i}{\hbar}E_1t}A_1\psi_1(\vec{r}) + e^{-\frac{i}{\hbar}E_2t}A_2\psi_2(\vec{r}), \tag{2.63}$$

which leads to the probability density

$$\rho_s(r,t) = |A_1\psi_1(\vec{r})|^2 + |A_2\psi_2(\vec{r})|^2 + 2\,Re\left[A_1\psi_1(\vec{r})\,A_2\psi_2^*(\vec{r})\,e^{i(E_2-E_1)t}\right] \tag{2.64}$$

In order to have a graphical representation of how this superposition evolves over the time we fix $\theta = 0$. That is, $\psi_j(\vec{r}) = \psi_j(r)e^{i(\theta=0)} = \psi_j(r)$. Thus, we are focusing on the radial profile of the probability density since $\psi_j \in \mathbb{R}$. Then

$$\rho_s(r,t) = |A_1\psi_1(r)|^2 + |A_2\psi_2(r)|^2 + 2\,A_1\,\psi_1(r)\,A_2\,\psi_2(r)\,\cos\left[(E_2-E_1)t\right]. \tag{2.65}$$

In this case the probability density depends on t (as long as $E_1 \neq E_2$). The coefficients A_1 and A_2 weight the contribution of the states in the superposition. We choose them such that ψ_s is a balanced superposition $A_1 = A_2 = \frac{1}{\sqrt{2}}$. In Figure 2.4a we show the probability density at $t = 0$ for a balanced superposition $A_1 = A_2 = \sqrt{\frac{1}{2}}$, while Figure 2.4b presents the time evolution of $\rho(t)$ for $t = 0, \frac{\pi}{4}, \frac{\pi}{2}, \frac{3\pi}{4}, \pi$. In Figure 2.5a and 2.5b we present the time evolution of a superposition of ψ_1 and ψ_2 for two cases of unbalanced weights.

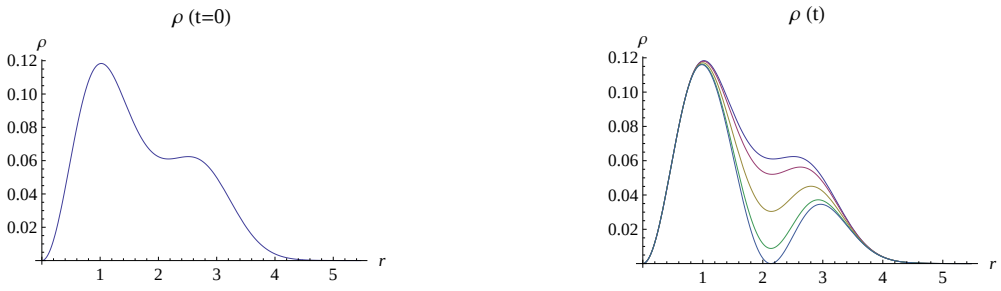

(a) (b)

Figure 2.4: (a) Radial profile of the probability density $\rho_s(r, t = 0)$ of a balanced superposition ψ_s with $A_1 = A_2 = \sqrt{\frac{1}{2}}$, and (b) its subsequent time evolution for $t = 0, \frac{\pi}{4}, \frac{\pi}{2}, \frac{3\pi}{4}, \pi$.

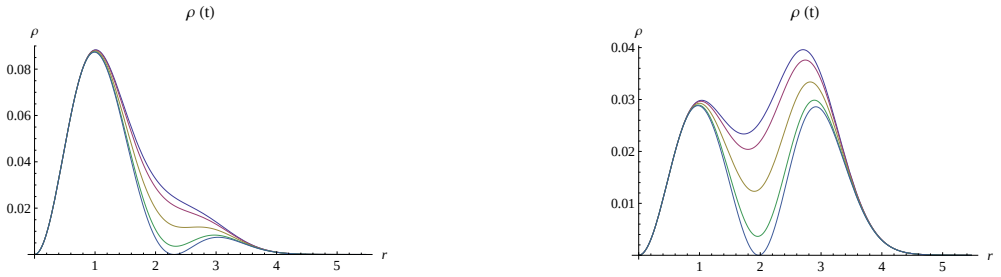

(a) (b)

Figure 2.5: Time evolution of the radial profile of the probability density ρ_s of two unbalanced superpositions ψ_s with weights (a) $A_1 = \sqrt{\frac{3}{4}}$, $A_2 = \sqrt{\frac{1}{4}}$, and (b) $A_1 = \sqrt{\frac{1}{4}}$, $A_2 = \sqrt{\frac{3}{4}}$ respectively; for $t = 0, \frac{\pi}{4}, \frac{\pi}{2}, \frac{3\pi}{4}, \pi$.

2.2.3.3 Scattering states

We now consider the case of k real.

$$0 < k^2 = 2E - a^2 \Rightarrow E > \frac{a^2}{2}. \tag{2.66}$$

E is clearly positive, unbounded, and greater than $\frac{a^2}{2}$, which is the least upper bound for bound states. Therefore $k =$ leads to scattering states. Using $x \equiv kr$, the radial equation

(2.49) for region II ($r > a$) reads

$$\frac{d^2R}{dx^2} + \frac{1}{x}\frac{dR}{dx} + \left(1 - \frac{l^2}{x^2}\right) R(x) = 0. \tag{2.67}$$

The solutions to this equation are the Bessel functions of first and second kind, $J_l(kr), N_l(kr)$.[1] Therefore, the general solution to the radial equation in this region is

$$R_>(r) = C_1 J_l(kr) + C_2 N_l(kr). \tag{2.68}$$

2.2.3.4 Boundary condition for scattering states

In every scattering system there is a chance that the particle might not get scattered by the potential in the interaction region but goes into the interaction region. On the other hand, the scattered particles come out in a superposition of $J_l(kr)$ and $N_l(kr)$. However, it can be shown that, due to the radial symmetry of the system, at long distances the scattered waves behave like $\frac{e^{ikr}}{\sqrt{r}}$. Let

$$z(r) \equiv r^{\frac{1}{2}} R(r) \rightarrow R(r) = r^{-\frac{1}{2}} z(r) \tag{2.69}$$

By substitution in the radial equation (2.10) we get a differential equation for $z(r)$:

$$z^{''}(r) + \left(2E - V(r) - \frac{l^2 - \frac{1}{4}}{r^2}\right) z(r) = 0 \tag{2.70}$$

At the asymptotic limit $r \rightarrow \infty$, we have $1/r^2 \rightarrow 0$ and $V(r) = a^2$. Then,

$$z_\infty^{''}(r) + \left(2E - a^2\right) z_\infty(r) = 0. \tag{2.71}$$

Therefore

$$z_\infty(r) = f e^{ikr} + D e^{-ikr}, \qquad R_\infty(r) = f\frac{e^{ikr}}{\sqrt{r}} + D\frac{e^{-ikr}}{\sqrt{r}}, \tag{2.72}$$

with f and D arbitrary coefficients. As we assumed no incoming waves, we set $D = 0$. The asymptotic form of the wave function is

$$\lim_{r\rightarrow\infty} \psi_\infty(r, \theta) \rightarrow f(\theta)\frac{e^{ikr}}{\sqrt{r}}. \tag{2.73}$$

where $f(\theta)$ is called the scattering amplitude. Therefore, outside the interaction region, the wave function has the asymptotic boundary form

$$\lim_{r\rightarrow\infty} \psi_\infty(r, \theta) \rightarrow e^{ikr\cos\theta} + f(\theta)\frac{e^{ikr}}{\sqrt{r}}. \tag{2.74}$$

[1] $N_l(x)$ is also called the Newmann function.

The first term accounts for the unscattered particles while the second term stands for the scattered ones.

Expanding the incident wave in terms of Bessel functions [4] we get

$$\lim_{r\to\infty}\psi(r,\theta)\to\sum_n i^n J_n(kr)e^{in\theta}+f(\theta)\frac{e^{ikr}}{\sqrt{r}}. \tag{2.75}$$

Taking into account the asymptotic behavior of the Bessel function $J_l(kr)$ [11], we write

$$\lim_{r\to\infty}\psi(r,\theta)\longrightarrow\sum_n i^n\sqrt{\frac{2}{\pi kr}}\cos\Big(kr-\frac{n\pi}{2}-\frac{\pi}{4}\Big)e^{in\theta}+f(\theta)\frac{e^{ikr}}{\sqrt{r}}, \tag{2.76}$$

and expanding further the cosine as a sum of exponentials we arrive at

$$\lim_{r\to\infty}\psi(r,\theta)\;\to\;\sum_n i^n\sqrt{\frac{2}{\pi kr}}\left(\frac{1}{2}\right)\left(e^{i(kr-\frac{n\pi}{2}-\frac{\pi}{4})}+e^{-i(kr-\frac{n\pi}{2}-\frac{\pi}{4})}\right)e^{in\theta}+f(\theta)\frac{e^{ikr}}{\sqrt{r}}.$$

So that

$$\begin{aligned}\lim_{r\to\infty}\psi(r,\theta)\;\to\;&\frac{e^{-ikr}}{\sqrt{r}}\left(\sum_n i^n\sqrt{\frac{1}{2\pi k}}e^{-i(-\frac{n\pi}{2}-\frac{\pi}{4})}e^{in\theta}\right)\\&+\frac{e^{ikr}}{\sqrt{r}}\left(\sum_n i^n\sqrt{\frac{1}{2\pi k}}e^{i(-\frac{n\pi}{2}-\frac{\pi}{4})}e^{in\theta}+f(\theta)\right).\end{aligned} \tag{2.77}$$

On the other side, taking into account the assymptotic behavior of $J_l(kr)$ and $N_l(kr)$, the exact solution

$$\psi(r,\theta)=\sum_n\left(C_1J_n(kr)+C_2N_n(kr)\right)e^{in\theta} \tag{2.78}$$

behaves as

$$\psi(r,\theta)=\sum_n C_1\sqrt{\frac{2}{\pi kr}}\cos\Big(kr-\frac{n\pi}{2}-\frac{\pi}{4}\Big)+C_2\sqrt{\frac{2}{\pi kr}}\sin\Big(kr-\frac{n\pi}{2}-\frac{\pi}{4}\Big)e^{in\theta}. \tag{2.79}$$

Now, expanding the cosine and sine functions in terms of exponential functions and associating factors of $e^{\pm ikr}$ we find

$$\begin{aligned}\psi(r,\theta)\;=\;&\frac{e^{-ikr}}{\sqrt{r}}\left(\sum_n\sqrt{\frac{1}{2\pi k}}e^{-i(-\frac{n\pi}{2}-\frac{\pi}{4})}(C_1-\tfrac{1}{i}C_2)e^{in\theta}\right)\\&+\frac{e^{ikr}}{\sqrt{r}}\left(\sum_n\sqrt{\frac{1}{2\pi k}}e^{i(-\frac{n\pi}{2}-\frac{\pi}{4})}(C_1+\tfrac{1}{i}C_2)e^{in\theta}\right).\end{aligned} \tag{2.80}$$

Comparing this asymptotic behavior with the asymptotic boundary condition (2.77) we find

$$C_1 = i^n - iC_2, \qquad f(\theta) = \sum_n \sqrt{\frac{1}{2\pi k}} e^{-i(\frac{n\pi}{2}+\frac{\pi}{4})} e^{in\theta}(C_1 - iC_2 - i^n). \tag{2.81}$$

Substituting the former in the latter, f can be written in terms of C_2 as

$$f(\theta) = \sqrt{\frac{2}{\pi k}} e^{-\frac{\pi}{4}} \sum_n i^{-(n+1)} C_2 e^{in\theta}. \tag{2.82}$$

Now, denoting the derivative with respect to r with a prime ($'$), the continuity conditions (2.15) demand

$$AR_l(kr) = C_1 J_l(kr) + C_2 N_l(kr), \qquad AR_l'(kr) = C_1 J_l'(kr) + C_2 N_l'(kr), \tag{2.83}$$

with A an arbitrary coefficient that can be eliminated to give

$$C_1 = C_2 \frac{W(N_l(ka), R_l(a))}{W(R_l(a), J_l(ka))}. \tag{2.84}$$

Combining this expression with the first one in (2.81) we find

$$C_2 = i^n \left(\frac{W(N_l(ka), R_l(a))}{W(R_l(a), J_l(a))} + i \right)^{-1}. \tag{2.85}$$

Therefore, (2.82) reads

$$\begin{aligned} f(\theta) &= \sqrt{\tfrac{2}{\pi k}} e^{-i\frac{\pi}{4}} \sum_n \left(i \frac{W(N_l(ka), R_l(a))}{W(R_l(a), J_l(ka)} - 1 \right)^{-1} e^{in\theta} \\ &= \sqrt{\tfrac{2}{\pi k}} e^{-i\frac{\pi}{4}} \sum_n \frac{W(R_l(a), J_l(ka))}{W(H_l^{(1)}(ka), R_l(a))} e^{in\theta} \end{aligned} \tag{2.86}$$

Here $H_l^{(1)}(x)$ is the Hankel function of first kind $H_l^{(1)}(x) \equiv J_l(x) + iN_l(x)$. The steps to go from the former to the latter involve the use of properties of determinants.

In practice, the physical quantity that is actually measured is the differential scattering cross section $\frac{d\sigma(\theta)}{d\theta}$, defined as

$$\frac{d\sigma(\theta)}{d\theta} \equiv |f(\theta)|^2. \tag{2.87}$$

The nature of this definition will be explored below. In Figure 2.6 we present the behavior of (2.87) for $-\frac{\pi}{2} < \theta < \frac{\pi}{2}$, and corresponding to the height $a^2 = 20$, for the scattering energy: $E = 11$. This plots reveals the scattering is locally maximized with global maximum at $\theta = 0$, which corresponds to the straightforward direction.

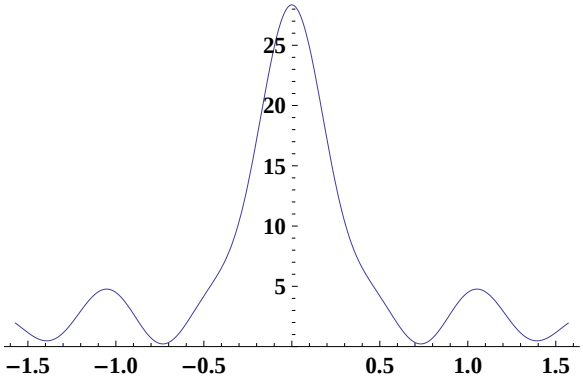

Figure 2.6: Differential scattering cross section $\frac{d\sigma}{d\theta}(\theta)$ for fixed energy $E = 11$ and height $a^2 = 20; \theta \in (-\frac{Pi}{2}, \frac{Pi}{2})$

2.2.3.5 Relation between $f(\theta)$ and the differential scattering cross-section

In this section clarify the physical meaning of the differential scattering cross section $\frac{d\sigma}{d\theta}$. First, consider the spatial description illustrated in Figure 2.7. At the top left we

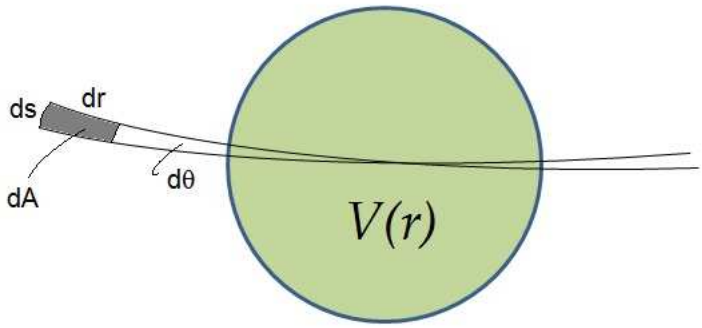

Figure 2.7: Spatial scattering of two adjacent particles due to a potential $V(r)$.

have pictured a physical detector, located at a large distance as an infinitesimal arc $ds^{'}$ covering the angle $d\theta$. In a time interval $dt^{'}$, the number of particles that will go through the detector are those situated at a distance no further than $dr = v\,dt$, where v is the mean speed of the particle flux.

Defining ψ_{sc} as the scattered wave function and considering $\rho = |\psi_{sc}|^2$, the number of

particles scattered into the area dA is

$$dn = \rho\, dA = |\psi_{sc}|^2 dr^{'} ds^{'} \tag{2.88}$$

where $dr^{'}$ and $ds^{'}$ are the differential distances that limit the differential area dA. We now write

$$dr = \sqrt{\frac{m\omega}{\hbar}} dr^{'}, \quad dt = \omega dt^{'} ds^{'} \equiv r^{'} d\theta = \sqrt{\frac{\hbar}{m\omega}} r d\theta \tag{2.89}$$

so that

$$v^{'} = \frac{dr^{'}}{dt^{'}} = \sqrt{\frac{\hbar\omega}{m}} \frac{dr}{dt} = \sqrt{\frac{\hbar\omega}{m}} v, ds^{'} \equiv r^{'} d\theta = \sqrt{\frac{\hbar}{m\omega}} r d\theta \tag{2.90}$$

and

$$ds^{'} \equiv r^{'} d\theta = \sqrt{\frac{\hbar}{m\omega}} r d\theta, \tag{2.91}$$

where $v \equiv \frac{dr}{dt}$ is the dimensionless speed. Furthermore, the De-Broigle length λ and wave number k can be expressed free of units

$$\lambda \equiv \sqrt{\frac{m\omega}{\hbar}} \lambda^{'} \quad ; k \equiv \sqrt{\frac{\hbar}{m\omega}} k^{'} \tag{2.92}$$

so that

$$p^{'} = \hbar k^{'}; \qquad m v^{'} = \hbar k^{'}. \tag{2.93}$$

Then

$$m\sqrt{\frac{\hbar\omega}{m}} v = \hbar \sqrt{\frac{m\omega}{\hbar}}\, k; \qquad v = k. \tag{2.94}$$

Having (2.91) in mind we can write (2.88) in terms of the dimensionless variables $\{r, s, v\}$ to find

$$dn = |\psi_{sc}|^2 \left(v^{'} dt^{'}\right) \left(r^{'} d\theta\right) = |\psi_{sc}|^2 \left(\sqrt{\frac{\hbar\omega}{m}} v dt^{'}\right) \left(\sqrt{\frac{\hbar}{m\omega}} r d\theta\right). \tag{2.95}$$

Thus

$$\frac{dn}{dt^{'}} = |\psi_{sc}|^2 \sqrt{\frac{\hbar\omega}{m}} \sqrt{\frac{\hbar}{m\omega}}\, v r\, d\theta. \tag{2.96}$$

We have obtained an expression for the number of particles per time interval. Now, we want to compute how is this rate compared with the incident flux of particles $|\overrightarrow{j^{'}_{inc}}|$. Again, using definitions (2.4) it is straightforward to show

$$|\overrightarrow{j^{'}}| = \sqrt{\frac{\hbar\omega}{m}}\, |\overrightarrow{j}|, \qquad \overrightarrow{j} \equiv -\tfrac{i}{2}(\psi^* \nabla\psi - \psi \nabla\psi^*). \tag{2.97}$$

where ψ^* denotes the complex conjugate of ψ and $\overrightarrow{j_{inc}}$ is the dimensionless probability density current. Then, the differential cross-section is defined as

$$d\sigma^{'} \equiv \frac{dn/dt^{'}}{|\overrightarrow{j_{inc}^{'}}|} = \frac{|\psi_{sc}|^2\sqrt{\frac{\hbar\omega}{m}}\sqrt{\frac{\hbar}{m\omega}}\,vr\,d\theta}{\sqrt{\frac{\hbar\omega}{m}}\,|\overrightarrow{j_{inc}}|} = \frac{|\psi_{sc}|^2\sqrt{\frac{\hbar}{m\omega}}\,vr\,d\theta}{|\overrightarrow{j_{inc}}|}. \tag{2.98}$$

Given the incident wave function $\psi_{inc} = e^{ikr\cos(\theta)}$, we have

$$|\overrightarrow{j_{inc}}| = k. \tag{2.99}$$

In turn, the differential cross-section reads

$$d\sigma^{'} = \frac{|\psi_{sc}|^2\sqrt{\frac{\hbar}{m\omega}}\,vr\,d\theta}{k} = |\psi_{sc}|^2\sqrt{\frac{\hbar}{m\omega}}\,r\,d\theta. \tag{2.100}$$

where we used equation (2.94) to cancel k with v. At this point, we define the dimensionless differential *scattering* cross-section by

$$d\sigma \equiv \sqrt{\frac{m\omega}{\hbar}}d\sigma^{'} = \frac{|\psi_{sc}|^2\,vr\,d\theta}{k} = |\psi_{sc}|^2\,r\,d\theta \tag{2.101}$$

Given that

$$|\psi_{sc}|^2 = \left|\frac{f(\theta)}{\sqrt{r}}e^{ikr}\right|^2 = \frac{|f(\theta)|^2}{r} \tag{2.102}$$

then it follows from (2.101),

$$\frac{d\sigma}{d\theta} = |f(\theta)|^2 \tag{2.103}$$

which is the relation between the differential scattering cross-section and the scattering amplitude $f(\theta)$ presented in equation (2.87). In Figure 2.8 we present the scattering pattern of a plane wave of energy $E = 80$ tnat is scattered by the potential $V(r) = r^2$.

Figure 2.6 shows that global maximum of the scattering amplitude is reached at the straightforward direction ($\theta = 0$). Fig. 2.8 shows the probability density of the complete function, which involves scattered and unscattered particles. Notice that, at some angles the probability density has local maxima. Besides, the straightforward direction $\theta = 0$ presents a deep minimum.

2.2.3.6 Phase shift of a scattered state and optical theorem

We now revisit the concept of phase shift. In the scattering processes, the particle is either scattered or it goes right through the scatterer without being deflected. In both

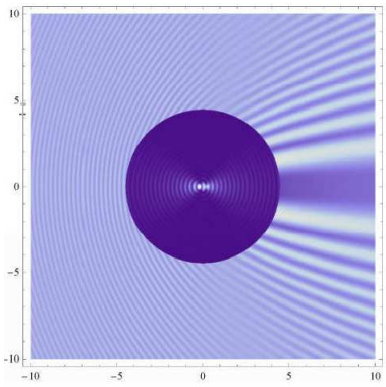

Figure 2.8: Probability density of a plane wave carrying an energy $E = 80$ being scattered by a potential $V(r) = r^2$. Bright areas represent larger values.

cases a phase shift takes place. To see this we write the solution to the radial equation outside the well (2.49) as $R_l = C_1 J_l(kr) + C_2 N_l(kr)$. Then

$$\lim_{r\to\infty} R_l = C_1\sqrt{\frac{2}{\pi kr}}\cos\left(kr - l\tfrac{\pi}{2} - \tfrac{\pi}{4}\right) + C_2\sqrt{\frac{2}{\pi kr}}\sin\left(kr - l\tfrac{\pi}{2} - \tfrac{\pi}{4}\right). \tag{2.104}$$

Defining $C_1 \equiv C\cos(\delta_l)$, $C_2 \equiv -C\sin(\delta_l)$, $\frac{C_2}{C_1} = -\tan(\delta_l)$; (2.104) becomes

$$\lim_{r\to\infty} R_l = C_1\sqrt{\frac{2}{\pi kr}}\left[\cos\left(kr - l\frac{\pi}{2} - \frac{\pi}{4}\right) - \tan(\delta_l)\sin\left(kr - l\frac{\pi}{2} - \frac{\pi}{4}\right)\right], \tag{2.105}$$

or equivalently

$$\lim_{r\to\infty} R_l = C\sqrt{\frac{2}{\pi kr}}\cos\left(kr - l\frac{\pi}{2} - \frac{\pi}{4} + \delta_l\right). \tag{2.106}$$

In absence of scatterer, the solution for all r would be

$$R_l = C_1 J_l(kr) + C_2 N_l(kr). \tag{2.107}$$

Then

$$\lim_{r\to\infty} R_l = C_1\frac{kr}{2}^{l} + C_2\frac{kr}{2}^{-l}, \tag{2.108}$$

and the boundary condition at origin must be $R_l(0) = 0$, which would imply $C_2 = 0$. Then $\tan(\delta_l) = 0 \leftrightarrow \delta_l = 0$. In other words, the presence of a scatterer leads to phase shifts $\delta_l \neq 0$. The complete wave function outside the well is

$$\psi_{II}(r,\theta) = e^{ikr\cos\theta} + R_>(r) = \sum_l i^l J_l(kr)e^{il\theta} + f(\theta)\frac{e^{ikr}}{\sqrt{r}}. \tag{2.109}$$

More precisely, the asymptotic behavior is

$$\begin{aligned}\lim_{r\to\infty}\psi_{II}(r,\theta) &= \sum_l i^l\sqrt{\frac{2}{\pi kr}}\left(\cos(kr-l\tfrac{\pi}{2}-\tfrac{\pi}{4})\right)e^{il\theta}+f(\theta)\frac{e^{ikr}}{\sqrt{r}}\\ &= \sum_l i^l\sqrt{\frac{2}{\pi kr}}\left(\frac{e^{i(kr-l\frac{\pi}{2}-\frac{\pi}{4})}+ie^{i(kr-l\frac{\pi}{2}-\frac{\pi}{4})}}{2}\right)e^{il\theta}+f(\theta)\frac{e^{ikr}}{\sqrt{r}}.\end{aligned} \tag{2.110}$$

On the other hand,one gets (2.106) holds for $r\to\infty$. Using it to write the full wave function $\psi_{II}(r,\theta)$ one gets

$$\begin{aligned}\lim_{r\to\infty}\psi_{II}(r,\theta) &= \sum_l C_l\sqrt{\frac{2}{\pi kr}}\cos\left(kr-l\tfrac{\pi}{2}-\tfrac{\pi}{4}+\delta_l\right)e^{il\theta}\\ &= \sum_l C_l\sqrt{\frac{2}{\pi kr}}e^{il\theta}\left(\frac{e^{i(kr-l\frac{\pi}{2}-\frac{\pi}{4}+\delta_l)}+e^{i(kr-l\frac{\pi}{2}-\frac{\pi}{4}+\delta_l)}}{2}\right).\end{aligned} \tag{2.111}$$

Equating (2.110) with (2.111), and factorizing $e^{\pm ikr}$, we find

$$C_l=i^le^{i\delta_l},\qquad f(\theta)=\sqrt{\frac{1}{2\pi k}}e^{-i\frac{\pi}{4}}\sum_l\left(e^{2i\delta_l}-1\right)e^{il\theta}, \tag{2.112}$$

which can be rewritten as follows

$$f(\theta)=\sqrt{\frac{1}{2\pi k}}e^{-i\frac{\pi}{4}}\sum_l\left(2i\sin(\delta_l)\right)e^{i\delta_l}e^{il\theta}. \tag{2.113}$$

Then the *total* scattering cross-section σ is given by

$$\begin{aligned}\sigma_{total} &\equiv \int_0^{2\pi}\sigma(\theta)d\theta=\int_0^{2\pi}|f|^2d\theta=\frac{4}{2\pi k}\sum_n\sum_l\left(i\sin\delta_ne^{i\delta_n}\right)\left(-i\sin\delta_le^{-i\delta_l}\right)\underbrace{\int_0^{2\pi}e^{i(n-l)\theta}d\theta}_{2\pi\,\delta_{nl}}\\ &= \tfrac{4}{k}\textstyle\sum_l\sin^2(\delta_l);\qquad \delta_{nl}\equiv\text{Kronecker delta}\end{aligned} \tag{2.114}$$

Equation (2.114) is known as the optical theorem, this shows that for $\delta=n\frac{\pi}{2}$; with n integer, the total scattering is maximized.

2.2.3.7 Total scattering maximization

In search of an expression determining the energies that maximize σ_{total} we proceed to write the continuity conditions for ψ in terms of its phase shift

$$AR_l(a)=C_l\left(J_l(ka)-\tan(\delta_l)N_l(ka)\right),\qquad AR_l'(a)=C_l\left(J_l'(ka)-\tan(\delta_l)N_l'(ka)\right). \tag{2.115}$$

These lead to

$$\tan(\delta_l) = -\frac{J_l(ka)R_l'(a) - R_l J_l'(ka)}{R_l N_l'(ka) - N_l(ka)R_l'(a)}. \tag{2.116}$$

Considering:

$$\delta_l = n\tfrac{\pi}{2} \Longleftrightarrow \tan(\delta_l) \to \infty, \quad \text{and} \quad N_l(ka)R_l'(a) - R_l N_l'(ka) = 0, \tag{2.117}$$

or, in terms of a Wronskian:

$$W\left(N_l(ka), R_l(a)\right) = 0, \tag{2.118}$$

the solutions define a discreet set of energies. These are the energy values that maximize σ_{total}. In Figure 2.12 we present both $\tan(\delta_l)$ and σ_{total} for $a^2 = 20$ and $l = 1$. We would like to point out that σ_{total} is maximized at the energies for which $\tan(\delta_1) \to \infty \Leftrightarrow \delta_1 = \frac{n\pi}{2}$; with n an integer. We also present a table with the energy values where the divergence of $\tan(\delta_1)$ takes place.

Divergences of $tan(\delta_l)$
10.1022
10.8366
13.8175
26.1781*
186.138*

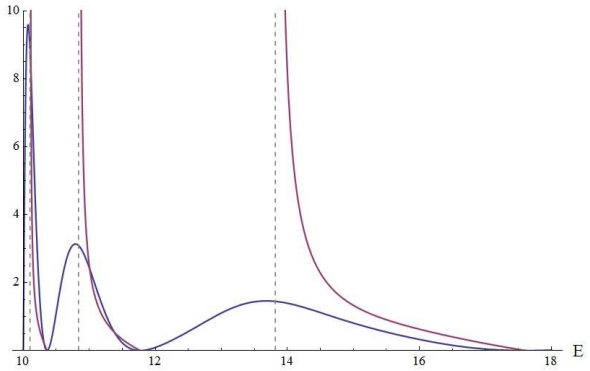

Figure 2.9: $\tan(\delta_1)$ (blue) and σ_{total} (purple) as a function of the energy E. The table shows the first energy values for which $\tan(\delta_1)$ diverges. These values are also those which maximize σ_{total} (*Not shown in figure for visual clarity).

2.3 Resonances

We have already seen the consequences of k being a pure imaginary number or k being a pure real number. To exhaust the possibilities of k we allow now k to have non-trivial real and imaginary parts $k = k_r + ik_i$. Let us gauge what physical implications does this value of k carry.

2.3.1 Time dependence of probability and current density for a 2-dimensional short range potential

Recall that $\Psi(r,t)$ is determined by the evolution operator as

$$\Psi(r,t) = \hat{U}\Psi(r,0) = e^{-i\frac{\hat{H}t}{\hbar}}\Psi(r,0), \tag{2.119}$$

where $\Psi(r,0) \equiv \psi(r)$. When $\psi(r)$ is an eigenfunction of $V(r)$ with eigenvalue E the action of $\hat{U}$ reduces to

$$\Psi(r,t) = e^{-i\frac{Et}{\hbar}}\psi(r). \tag{2.120}$$

When k is a non-trivial complex number there is a non-trivial $E = E_r + iE_i$ related to it.

$$(k_r + ik_i)^2 = 2(E_r + iE_i) - a^2, \tag{2.121}$$

then $k_r^2 - k_i^2 = 2E_r - a^2$ and $k_r k_i = E_i$. Let $\hat{H}$ be such that $E = E_r + iE_i$ is an eigenvalue, the probability density reads

$$\rho \equiv |\Psi(r,t)|^2 = |e^{-i\frac{Et}{\hbar}}\Psi(r,0)|^2 = e^{-i\frac{(E_r+iE_i)t}{\hbar}}|\Psi(r,0)|^2 = e^{\frac{2E_i t}{\hbar}}|\Psi(r,0)|^2. \tag{2.122}$$

From the last equation we can see that complex energies give rise to ρ not being stationary anymore, but a function of time. Observe as well that E_i cannot be positive, since in that case, the probability density would increase over time over the whole space. Therefore, E_i must be negative. In consequence, the last of equations (2.121) implies that k_r and k_i are of opposite sign.

2.3.1.1 Probability density current for radially symmetrical 2-D short range potentials

Recall the general definition of the probability density current

$$\vec{j}_\psi \equiv \frac{\hbar}{2mi}(\psi(x')^*\nabla\psi(x') - \psi(x')\nabla\psi(x')^*). \tag{2.123}$$

Contrary to the use of adimensional variables used previously, in this subsection we shall keep the physical constants explicitly. Previously we could define appropiate adimensional variables due to knowing the explicit form of the potential ($V(r) = \frac{1}{2}m\omega^2 r^2$). In the present calculations we want to keep the potential $V(r)$ as general as possible. Defining the probability density velocity as

$$\vec{v}_\psi \equiv \frac{\vec{j}}{\rho} = \frac{\vec{j}}{\psi\psi^*} = \frac{\hbar}{2mi}\left(\frac{\nabla\psi}{\psi} - \frac{\nabla\psi^*}{\psi^*}\right), \tag{2.124}$$

we notice that it would be useful to know the form of $\frac{\nabla\psi}{\psi}$. We recall that, due to the radial symmetry of the potential, $\psi(r,\theta)$ reads

$$\psi(r,\theta) = R(r)\, e^{il\theta}. \tag{2.125}$$

We recall too the nabla operator in polar coordinates

$$\nabla \equiv \frac{\partial}{\partial r}\hat{r} + \frac{1}{r}\frac{\partial}{\partial\theta}\hat{\theta}. \tag{2.126}$$

With these in mind we find

$$\frac{\nabla\psi}{\psi} = \frac{R'}{R}\hat{r} + il\frac{1}{r}\hat{\theta} = \frac{R'^*}{R^*}\hat{r} - il\frac{1}{r}\hat{\theta}. \tag{2.127}$$

where R' stands for the derivative of R with respect to r. Susbtituting (2.127) in (2.124) we get

$$\vec{v} = \frac{\hbar}{m}\left(Im\left(\frac{R'}{R}\right)\hat{r} + \frac{l}{r}\hat{\theta}\right). \tag{2.128}$$

Notice that for bound states and scattering states $R(r)$ is real. Therefore the radial component of $\vec{j}_\psi$ is zero, and $\vec{j}_\psi$ only spins around with a speed proportional to $\frac{l}{r}$. Let us pay attention to the region outside the well. We express the solution for $r > a$ in terms of the Hankel functions as

$$R(r) = C_1 J_l(kr) + C_2 N_l(kr) = \frac{1}{2}\left((C_1 - iC_2)H_l^{(1)}(kr) + (C_1 + iC_2)H_l^{(2)}(kr)\right) \tag{2.129}$$

For a moment, let us assume there are only outgoing waves, that is

$$C_1 + iC_2 = 0. \tag{2.130}$$

Then

$$\frac{R'}{R} = \frac{k\frac{d}{dr}H_l^{(1)}(r)}{H_l^{(1)}(r)} = k\frac{d}{dr}ln\left(H_l^{(1)}(r)\right). \tag{2.131}$$

At the assymptotic regime

$$\begin{aligned}\lim_{r\to\infty}\frac{R'}{R} &= k\frac{d}{dr}ln\left(\sqrt{\frac{2}{\pi r}}e^{i(r-l\frac{\pi}{2}-\frac{\pi}{4})}\right) = k\frac{d}{dr}\left(i(r-l\tfrac{\pi}{2}-\tfrac{\pi}{4}) - \tfrac{1}{2}ln(x) + \tfrac{1}{2}ln(\tfrac{2}{\pi})\right)\\ &= (k_r + ik_i)i - \tfrac{1}{2r},\end{aligned} \tag{2.132}$$

this reveals that

$$\lim_{r\to\infty} Im\left(\frac{R'}{R}\right) = k_r. \tag{2.133}$$

With this in mind, we take the limit of equation (2.128) and find

$$\lim_{r\to\infty} \vec{v} = \frac{\hbar}{m}\lim_{r\to\infty}\left(Im\left(\frac{R'}{R}\right)\hat{r} + \frac{l}{r}\hat{\theta}\right) = \frac{\hbar}{m}k_r\,\hat{r}. \tag{2.134}$$

Since this expression was obtained bu assuming only outgoing waves, k_r has to be of a positive nature in order to have $\vec{v}$ pointing outwards. Since we already found that k_r and k_i are of opposite signs, it is certain that k_i is negative. We can conclude then, that non-trivial values of k laying in the $4\,th$ quadrant of the Complex plane correspond naturally to a physical situation where only outgoing waves are present. This situation can represent for example, a potential well that had been bombarded with incoming particles, trapped them for a period of time, and then expelled them long after the bombarding source had been turned off. This kind of phenomena where only outgoing waves are present are called resonances. We make special emphasis that result (2.134) is valid for any scatterer as long as it is short-range (constant after some cutoff value $r = a$) and radially symmetric.

Since $R(r) \in \mathbb{R}$ for bound states and scattering states, then the radial component of $\vec{j}$ is zero and $\vec{j}$ flows parallel to $\hat{\theta}$. E doesn't figure at all and the behavior of $\vec{j}$ is determined only by l. Figure (2.10a) represents the vector field $\vec{j}$ for any of these state with angular number $l = 1$. Figure (2.10b) shows the analogue case for $l = -1$. Notice how the arrows indicate that for $l = -1$, $\vec{j}$ flows in the opposite direction, a fact expected from (2.128). The background intensity stands for the magnitude of $\vec{j}$. Notice too the rapid decay of $|\vec{j}| \propto \frac{1}{r}$. These plots for $\vec{j}$ show that, although equation (2.51) depends on l only as its square l^2, the actual states corresponding to l and $-l$ are different by nature. Therefore, despite having the same energy, these states are totally different. This is basically the notion of degeneration discussed in the reminder of the two dimensional oscillator.

Figure (2.11a) shows the behavior of $\vec{j}$ for the resonant state $k = 2.07807 - i\,0.53121$ with $l = 1$. Notice that unlike bound states and resonant states, the behavior of $\vec{j}$ isn't purely angular. Notice too that the magnitude of $\vec{j}$ has a constant asymptotic behavior, a fact know from equation (2.133). This is reflects the fact that the probability density at any point decreases over time. We notice as well there's an interesting interference pattern within the well, one that hadn't been apparent from the analytical expression. The presence of this pattern for $\vec{j}$ supports the interpretation of resonant states consisting of trapped particles which are "bouncing" back and forth inside the well for a period of time that might be long after the source of particles has been turned off.

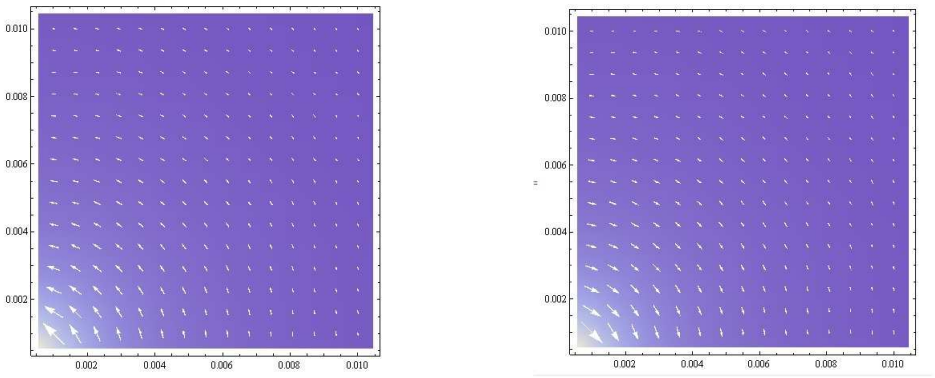

(a) (b)

Figure 2.10: The probability density current of stationary states for a well with cutoff $a = \sqrt{20}$ and angular parameters (a) $l = 1$ and (b) $l = -1$. Notice that for positive values of l the flow of $\vec{j}$ is counter-clockwise while for negative values it is clock-wise. (Bright areas correspond to higher values)

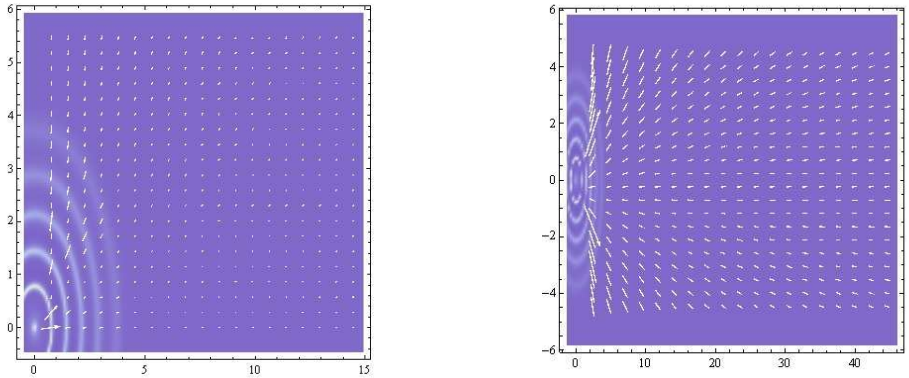

(a) (b)

Figure 2.11: (a) Probability density current corresponding to a resonant state for $l = 1$, $a = \sqrt{20}$ and $k = 2.07807 - i\,0.53121$. (b) Zoom out of (a): The probability density current is clearly non-circular and of constant magnitude far away from the well, in agreement with equation (2.134). (Bright areas correspond to higher values)

2.3.1.2 Purely-outgoing waves condition implications

We saw in the previous subsection that the purely outgoing waves condition requires coefficients C_1 and C_2 to satisfy

$$0 = C_1 + iC_2, \qquad \frac{C_1}{C_2} = -i. \tag{2.135}$$

From equation (2.129) $R(r)$ reads

$$R(r) = \frac{1}{2}(C_1 - iC_2)\, H_l^{(1)}(kr). \tag{2.136}$$

If we combine (2.135) with (2.84) we find that the purely outgoing waves condition leads to

$$\frac{W(N_l(ka), R_l(a))}{W(R_l(a), J_l(ka))} = -i. \tag{2.137}$$

The values of k that satisfy this equation correspond to the purely outgoing wave solution (2.135). The set of k values that satisfy this condition is discrete and that there seems to be an infinite amount of them. We present in figure (2.12) the first three values of k (and their corresponding energies) that satisfy (2.137) for $l = 1$, $a = \sqrt{20}$. We also present the probability density plot corresponding to k_1; bright areas correspond to higher values. We observe that we have some stationary waves of finite height inside the well. However, as we go beyond $r = a$ the probability density spikes up evidenced by the brightest areas barely beyond the well boundary $r = a$. The spike up is due to the probability density leaking out from the interaction region as time goes on.

	$k_r + i\,k_i$	$E_r + i\,E_i$
k_1	$2.07807 - i\,0.53121$	$12.0181 - i\,0.551944$
k_2	$3.26843 - i\,0.58238$	$15.1717 - i\,0.951735$
k_3	$4.24562 - i\,0.622788$	$18.8187 - i\,1.32206$

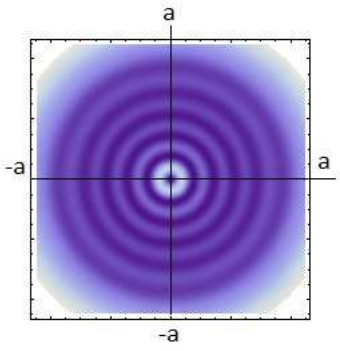

Figure 2.12: The table shows k and E values corresponding to purely outgoing waves solutions for $l = 1$ and $a^2 = 20$. Probability density corresponding to the first resonant state for $l = 1$, $a = \sqrt{20}$: $E = 12.0181 - i\,0.551944$.

2.4 Energy quantization for a two dimensional radial potential using the WKB method

In this section we will use an approximate method to compute the solution of the stationary Schrödinger equation. There is literature dealing with a generalized WKB method for approximating the solutions of quantum wells in two or three dimensions, *e.g.* (Van Horn and Salpeter(2010) and Shirnov and Nurlygayanov (1975). However, we will sort our way to use the one dimensional WKB approximation theory explained above to solve our two dimensional system. The stationary Schrödinger equation in polar coordinates reads

$$-\frac{\hbar^2}{2m}\nabla^2\psi(r,\theta)+V\psi=E\psi. \tag{2.138}$$

After separating variables through the ansatz $\psi=R(r)e^{il\theta}$, we get

$$R''(r)+\frac{1}{r}R'(r)-\frac{l^2}{r^2}R(r)+\left(\frac{2m}{\hbar^2}\right)(E-V(r))\,R(r)=0, \tag{2.139}$$

where (') denotes derivative with respect to r.

Let $R(r)=r^{-\frac{1}{2}}u(r)$, equation (2.139) turns into

$$u''+\left(\left(\frac{2m}{\hbar^2}\right)(E-V(r))-\left(\frac{l^2-\frac{1}{4}}{r^2}\right)\right)u=0 \tag{2.140}$$

Here it is where we introduce our WKB hypothesis. Let $u\equiv e^{i\frac{S}{\hbar}}$. Upon substitution in (2.140) we find

$$\frac{i}{\hbar}S''-\frac{1}{\hbar^2}S'^{\,2}+\frac{2mE}{\hbar^2}-\left(\frac{2m}{\hbar^2}\right)\underbrace{\left(V(r)+\left(\frac{\hbar^2}{2m}\right)\left(\frac{l^2-\frac{1}{4}}{r^2}\right)\right)}_{V_{ef}}=0. \tag{2.141}$$

Multiplying by $(-\frac{\hbar^2}{2m})$,

$$\frac{1}{2m}S'^2-\frac{i\hbar}{2m}S''+V_{ef}=E. \tag{2.142}$$

We have defined an effective potential V_{ef}. This equation has exactly the same form as equation (1.57) with V_{ef} playing the role of V. Therefore, (it seems at first) there is no problem in following the theory of the 1-D WKB approximation presented before, with $u(r)$ in the place of $\psi(x)$, $V_{ef}(r)$ instead of $V(x)$ and $r\in(0,\infty)$ in the place of $x\in(-\infty,\infty)$.

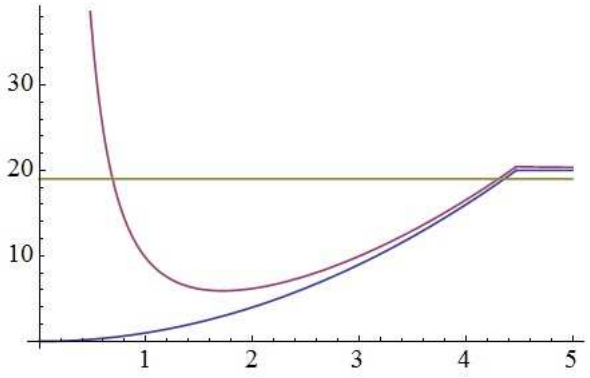

Figure 2.13: Potentials $V(r)$(blue), $V_{ef}(r)$ (purple), and a bound energy (golden) that defines two classical turning points ($l \neq 0$).

We focus our attention on bound states of the effective potential

$$V_{ef}(r) = \begin{cases} V(r) + \left(\frac{\hbar^2}{2m}\right)\left(\frac{l^2 - \frac{1}{4}}{r^2}\right), & 0 < r < a \\ V(a) + \left(\frac{\hbar^2}{2m}\right)\left(\frac{l^2 - \frac{1}{4}}{a^2}\right), & r \geqslant a. \end{cases} \tag{2.143}$$

where

$$V(r) = \begin{cases} \frac{1}{2}m\omega^2 r^2, & 0 < r < a \\ \frac{1}{2}m\omega^2 a^2, & r \geqslant a \end{cases} \tag{2.144}$$

The energy of a bound state is that which does not exceed $V_{ef}(r \to \infty)$. That is

$$\begin{array}{rcl} E & < & V_{ef}(r \to \infty) \\ E & < & V(r \to \infty) + 0 \\ E & < & V(a) \\ E & < & \frac{1}{2}m\omega^2 a^2 \end{array} \tag{2.145}$$

For $l \neq 0$ there are two points $r = r_{1,2}$ such that $V(r_{1,2}) = E$. These are the turning points for the effective potential. The case $l = 0$ presents a different situation, which has only one classical turning point. From (2.143) we can see that in the case $l = 0$ the

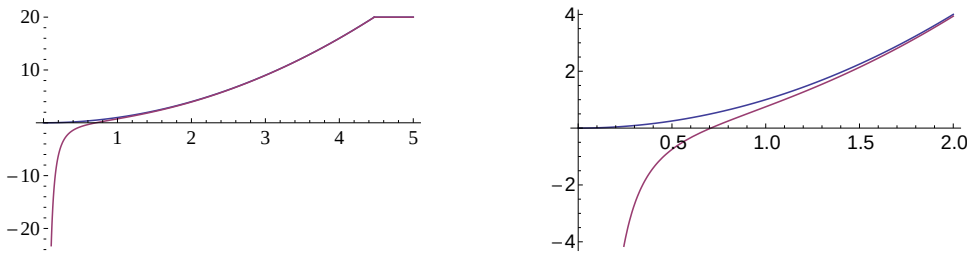

(a) (b)

Figure 2.14: (a) Potentials $V(r)$ (top) V_{ef} and for $l = 0$ (bottom). (b) Zoom in of (a). Notice that the case $l = 0$ has no returning point close to the origin.

potential decreases infinitely as $r \to 0$ with no turning point (See figure 2.14). Therefore, the formulas obtained by the 1-dimensional WKB method above does not apply. From now on, we'll work with the assumption $l \neq 0$.

Let

$$p_{ef}(x) \equiv \begin{cases} i\tilde{p_{ef}}(x) \equiv i\sqrt{2m(V_{ef}(x) - E)} & , \quad r < r_1 \\ \sqrt{2m(E - V_{ef}(x))} & , \quad r_1 < r < r_2 \\ i\tilde{p_{ef}}(x) \equiv i\sqrt{2m(V_{ef}(x) - E)} & , \quad r > r_2 \end{cases} \tag{2.146}$$

the domain of this effective potential gets subdivided in three regions $0 < r \leqslant r_1$, $r_1 < r < r_2$ and $r_2 \leqslant r$. Analogous to the 1-dimensional case, for the solution to be physically acceptable, $u(r)$ for the regions inside and outside the potential well reads

$$u(x) = \begin{cases} A_2 \dfrac{1}{\sqrt{\tilde{p_{ef}}(r)}} \exp\left[-\dfrac{1}{\hbar}\left(\displaystyle\int_r^{r_1} \tilde{p_{ef}}(r)\ dr\right)\right] & , \quad r < r_1 \\ N \cos\left(\displaystyle\int p_{ef}\ dr + \alpha\right) & , \quad r_1 < r < r_2 \\ B_2 \dfrac{1}{\sqrt{\tilde{p_{ef}}(r)}} \exp\left[-\dfrac{1}{\hbar}\left(\displaystyle\int_{r_2}^{r} \tilde{p_{ef}}(r)\ dr\right)\right] & , \quad r > r_2 \end{cases} \tag{2.147}$$

Appealing to the connection formulas (1.71) and (1.72) again, and proceeding as showed in the 1-dimensional derivation, the quantization condition for $V_{ef}(r)$ reads

$$\frac{1}{\hbar}\int_{r_1}^{r_2} p_{ef}(r)\ dr + \frac{\pi}{2} \quad = \quad \pi(n+1). \tag{2.148}$$

Therefore

$$\begin{aligned}\pi(n+\tfrac{1}{2}) &= \frac{1}{\hbar}\int_{r_1}^{r_2} p_{ef} = \int_{r_1}^{r_2} dr\sqrt{\frac{2mE}{\hbar^2} - \frac{m^2\omega^2 r^2}{\hbar^2} - \frac{l^2}{r^2} + \frac{\frac{1}{4}}{r^2}} \\ &= \int_{y_1}^{y_2} \frac{dy}{2y}\sqrt{Ay^2+By+C},\end{aligned} \tag{2.149}$$

where $A \equiv -\frac{m^2\omega^2}{\hbar^2}$, $\quad B \equiv \frac{2mE}{\hbar^2}$, $\quad C \equiv -l^2 + \frac{1}{4}$.

From the tables presented in [8] (pgs. $94-97$) we get to a simple expression:

$$\pi\left(n+\frac{1}{2}\right) = \frac{B\sqrt{-C}+2C\sqrt{-A}}{2\sqrt{AC}}. \tag{2.150}$$

Having in mind the definitions

$$A \equiv -\tfrac{m^2\omega^2}{\hbar^2}, \qquad B \equiv \tfrac{2mE}{\hbar^2}, \qquad C \equiv -l^2+\tfrac{1}{4}, \tag{2.151}$$

eq. (2.150) can be simplified to get a discretization equation for E

$$\pi n = \pi\left(\frac{\left(\frac{2mE}{\hbar^2}\right)\sqrt{l^2-\frac{1}{4}} + 2(-l^2+\frac{1}{4})\sqrt{\frac{m^2\omega^2}{\hbar^2}}}{4\sqrt{(-\frac{m^2\omega^2}{\hbar^2})(-l^2+\frac{1}{4})}}\right). \tag{2.152}$$

Then

$$\frac{E}{\hbar\omega} = 2n+1+\sqrt{l^2-\frac{1}{4}}. \tag{2.153}$$

Note that this quantization result has the same functional form for the energies as the one found when we solved the problem by finding the exact solutions. However, there is a substantial difference. In (2.153) a term $(+\frac{1}{4})$ adding to l^2 is present. Perhaps for $l \gg 1$ this term can be ignored but not for lower values of l. This "failure" has been noted before by many authors. The first one was Langer (1937) when he studied the connection formulas for a three dimensional radial problem. The three dimensional radial problem poses the same issue of a wrong eigenvalue prediction, arising also from the centrifugal term of the effective potential. Until then, the solution to finding the correct value for E was to make an unfounded substitution by hand. To be more clear, the 2-dimensional equivalent (which is our case) of what they did was to replace $(l^2-\frac{1}{4})$ for l^2, and it worked.

In his paper Langer noticed that the source of the issue was that the effective potential grows out of proportion as the turning point nearest to the origin is close enough. In that case, the WKB approximation requisite (1.58) no longer gets fulfilled, therefore giving

inaccurate results. The way he solved the problem was to make a change of variables $r = e^x$, $u = e^{\frac{x}{2}} v$. This shows that the point $r = 0$ is now mapped unto the point $x \to -\infty$. In this manner the issue is avoided and previously unfounded substitution is found.

In the book Semiclassical Physics (1997) pgs. 76, 78, M. Brack and R. K. Bhaduri talk about the Langer corrections in two and three dimensions. In particular they mention that Langer's correction works for $l = 0$ in the 3-dimensional case but not in the 2-dimensional one. They mention that other authors made further mappings along the Langer mapping in other to demonstrate that even for $l = 0$ the substitution $l^2 - \frac{1}{4} \to l^2$ is valid and that the correct energy values are

$$E = (2n + 1 + l)\,\hbar\omega. \tag{2.154}$$

Chapter 3

Electromagnetic waveguides

In order to establish a connection between quantum states and optical waves we shall study a system whose description resembles that of a short range potential well. In the following pages we will study the propagation of waves within a cylindrical dielectric fiber (waveguide, for short) under certain conditions, those which will take us from the Maxwell equations onto a Schrödinger-like equation. An optical waveguide consists of a large slim dielectrical material called "the core", through which a wave will propagate due to total internal refraction. This material is surrounded by a covering with a lower refractive index than the core. This covering is called "the clad". A waveguide's length is too large compared to its width, so much that they can be modelled as infinitely large. They can have an arbitrary shape cross-section, but the most common type is a circular cross-section, see figure (3.1).

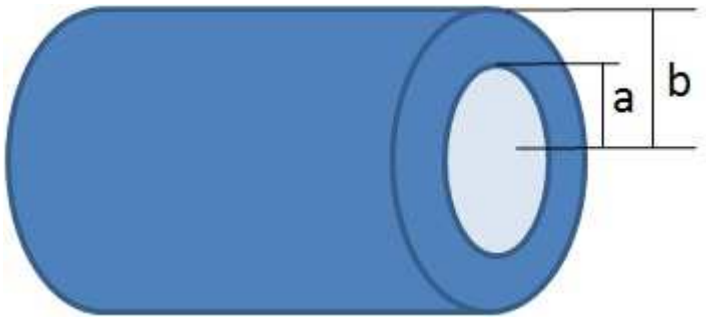

Figure 3.1: Cylindrical waveguide corresponding to a circular cross-section. The core (inner) radius is of length= a, while the clad (outer) radius is of length = b.

3.1 The Helmholtz equation for optical fibers

The Maxwell equations for a inhomogeneous dielectric media read

$$\begin{array}{rclcrcl} \nabla \cdot \vec{D}(\vec{r},t) & = & 0, & & \frac{\partial}{\partial t}\vec{D}(\vec{r},t) & = & \nabla \times \vec{H}(\vec{r},t), \\ \nabla \cdot \vec{B}(\vec{r},t) & = & 0, & & -\frac{\partial}{\partial t}\vec{B}(\vec{r},t) & = & \nabla \times \vec{E}(\vec{r},t), \end{array} \tag{3.1}$$

with constitutive relations

$$\vec{D}(\vec{r},t) = \epsilon_0 \epsilon(\vec{r}) \vec{E}(\vec{r},t), \qquad \vec{B}(\vec{r},t) = \mu_0 \vec{H}(\vec{r},t). \tag{3.2}$$

Let $\vec{E}(\vec{r},t) = \vec{E}(\vec{r})e^{-i\omega t}$, with the aid of

$$\nabla \times \left(\nabla \times \vec{E}(\vec{r}) \right) = \nabla \left(\nabla \cdot \vec{E}(\vec{r}) \right) - \nabla^2 \vec{E}(\vec{r}), \tag{3.3}$$

the Maxwell equations can be worked out to find

$$\nabla^2 \vec{E}(\vec{r}) + \underbrace{\epsilon(\vec{r})}_{n^2(\vec{r})} k_0^2 \vec{E}(\vec{r}) + \nabla \left(\frac{1}{\epsilon(\vec{r})} \nabla \epsilon(\vec{r}) \cdot \vec{E}(\vec{r}) \right) = 0, \tag{3.4}$$

where it has been pointed out the well-known relation between the dielectric permittivity and the refractive index $\epsilon(\vec{r}) = n^2(\vec{r})$. k_0 stands for the wave number in the clad where the refractive index is n_0.

We restrict our analysis to fibers such that ϵ varies slowly enough to allow the third term of (3.4) to be dismissed. In that case,

$$\nabla^2 \vec{E}(\vec{r}) + k_0^2 n(r)^2 \vec{E}(\vec{r}) = 0. \tag{3.5}$$

This equation is known as the (vectorial) Helmholtz equation. It is our starting point for what is going to be a useful way to study quantum potentials with classical experiments. In quantum mechanics the information of the system is encoded in the wave function, which is a scalar quantity. If we are looking for an analogy with optic fibers it is only natural that we search for a scalar function to compare with. The form of equation (3.5) makes us wonder if the operator ∇^2 could somehow act on each scalar component of $\vec{E}$, therefore inheriting its current form. In appendix A we present an observation on Laplacians and under what conditions is it possible to manipulate them in this way.

As pointed out, if we expand $\vec{E}$ in Cartesian components, equation (3.6) implies that each component obeys

$$\nabla^2 U(\vec{r}) + k_0^2 n(r)^2 U(\vec{r}) = 0; \quad \vec{r} = (r, \phi, z). \tag{3.6}$$

3.2 The paraxial approximation

Since we are interested in waves whose amplitude depends weakly on z, we assume that, within a distance of $\Delta z = \lambda$,

$$\begin{aligned} |\Delta U| &\ll |U|, \\ |\left(\tfrac{\partial}{\partial z} U\right) \Delta z| &\ll |U|, \\ |\left(\tfrac{\partial}{\partial z} U\right) \lambda| &\ll |U|. \end{aligned} \tag{3.7}$$

$$\left|\left(\frac{\partial}{\partial z} U\right)\right| \ll \left|\frac{U}{\lambda}\right|, \quad \text{and} \quad \left|\left(\frac{\partial}{\partial z} U\right)\right| \ll \left|U \frac{k}{2\pi}\right|. \tag{3.8}$$

In a similar form,

$$\left|\left(\tfrac{\partial^2}{\partial z^2} U\right)\right| \ll \left|\tfrac{k}{2\pi} \tfrac{\partial}{\partial z} U\right|. \tag{3.9}$$

Let us assume a harmonic profile on z: $U = u(r, \phi, z) e^{ik_0 n_0 z}$, where $u(r, \phi, z)$ is a slow varying function of z. Substituting this in equation (3.6) we arrive to

$$\begin{gathered} \nabla_T^2 u(r, \phi, z) + \tfrac{\partial^2}{\partial z^2} u(r, \phi, z) + 2ik_0 n_0 \tfrac{\partial}{\partial z} u(r, \phi, z) + k_0^2 (n(r)^2 - n_0^2) u(r, \phi, z) = 0, \\ \nabla_T^2 \equiv \nabla^2 \psi = \tfrac{1}{r} \tfrac{\partial}{\partial r} \left(r \tfrac{\partial \psi}{\partial r}\right) + \tfrac{1}{r^2} \tfrac{\partial \psi}{\partial^2 \phi}, \end{gathered} \tag{3.10}$$

where ∇_T^2 is called the transverse Laplacian. Using (3.9) to dismiss the second term in equation (3.10), it reads

$$\nabla_T^2 u(r, \phi, z) + 2ik_0 n_0 \frac{\partial}{\partial z} u(r, \phi, z) + k_0^2 (n(r)^2 - n_0^2) u(r, \phi, z) = 0. \tag{3.11}$$

It is well known that the paraxial approximation (3.8) is valid in the weakly guiding regime, where the refractive index is nearly constant, i.e.

$$n^2(r) \equiv n_0^2 + \Delta n(r); \quad \Delta n(r) \ll 1. \tag{3.12}$$

Then, for a refractive index characterized by a parabolic profile given by

$$n^2(r) = n_0^2 (1 - \omega^2 r^2), \quad \omega^2 r^2 \ll 1, \tag{3.13}$$

we identify $\Delta n(r) \equiv -n_0^2 \omega^2 r^2$. Applying (3.13) in (3.11) we get

$$\frac{1}{2n_0 k_0^2} \nabla_T^2 u(r, \phi, z) - \frac{n_0^2 \omega^2 r^2}{2n_0} u(r, \phi, z) = -i \left(\frac{1}{k_0}\right) \frac{\partial u(r, \phi, z)}{\partial z}. \tag{3.14}$$

Pay close attention to the left and right sides of this equation. The Laplacian of a function is essentially a second derivative. therefore, on the left side we've got the Laplacian of a function being summed with a term involving the function weighted with a polynomial, while on the right side we've got a first derivative with respect to an independient variable z. This is essentially a Shcrödinger equation. At this stage, we propose u has the form $u = \psi(r)e^{-i\beta k_0 z}$. Substituting this expression in (3.14) along with (3.13) we find

$$\nabla_T^2\psi - k_0^2 n_0^2\omega^2 r^2\psi = -2\beta k_0^2 n_0\psi, \tag{3.15}$$

which can be rewritten as

$$-\frac{1}{2k_0^2 n_0}\nabla_T^2\psi + \frac{1}{2}n_0\omega^2 r^2\psi = \beta\psi. \tag{3.16}$$

3.3 Classical-Quantum analogy for a stratified fiber

Equation (3.16) leads us to think of stablishing an analogy between optical fibers with a parabolic refractive index and short range quantum wells. Consider the following solutions to the parabolic refractive index fiber and the quantum harmonic oscillator respectively:

$$\begin{aligned} \text{Electric}: &\quad -\tfrac{1}{2k_0^2 n_0}\nabla_r^2\psi(r) + \tfrac{1}{2}n_0\omega^2 r^2\psi(r) = \beta\psi(r); \\ \text{Quantum}: &\quad -\tfrac{\hbar^2}{2m}\nabla_r^2\psi(r) + \tfrac{1}{2}m\omega^2 r^2\psi(r) = E\psi(r). \end{aligned} \tag{3.17}$$

Comparing these expressions we notice that we have arrived at the exact same equation if we realize that electric quantities are playing the role of quantum ones. In particular β is playing the role of E. Therefore the solution ψ and β seeked for the waveguide is exactly that of the short-range oscillator, see eq. (2.3), with $\beta \leftrightarrow E$.

Furthermore ,we can follow the steps following eq. (2.3) and define an adimensional variable and a redefinition of the refractive index as it was done in (2.5) and (2.6). Being an optic fiber with a cilindrical cross section, the boundary is set at $r = a$ as in the short-range oscillator and the boundary analysis of (2.12) is valid here too. The requirements for physical admissibility presented in (2.28), (2.31), and (2.35) apply here as well.

This leads us to the Kummer function being the final expression for our solution as in (2.29) i.e.

3.3.1 Solution to the paraxial approximation

$$\psi(r) = e^{-\frac{r^2}{2}}r^{|l|}M\left(\frac{1}{2}(1+|l|-B), 1+|l|; r^2\right); \quad r = \sqrt{k_0 n_0\omega}r, \quad B = \frac{\beta k_0}{\omega}. \tag{3.18}$$

We would like to make a pause here to emphasize something. In chapter 2 we realized that the radial profile of the solutions of the short-range problem were not appreciably distinguishable. We noticed it too how similar the energy values are compared to those arising from the conventional potential. Analogous comparisons were made in chapter 1, where the short-range version of the problem had eigenfunctions and eigenvalues so similar to the conventional version of the problem that they are practically indistinguishable. Taking advantage of the classical-quantum analogy, this leads us to think that it is reasonable to adopt (3.20) as the solution of the waveguide, even though the functional form of solution (3.20) corresponds to an unbounded interaction region and not to a short-range interaction. Along the same lines, we proceed to quantize the propagation constant β as we did in chapter 2, by demanding the first argument of the Kummer function to be equal to a negative integer.

As seen in equation (2.40) in the reminder of the Quantum Harmonic Oscillator, we know that in order for ψ to be a physical state (guided inside the fiber) we should demand

$$-n = \frac{1}{2}(1 + |l| - B); \quad n = 0, 1, 2, ... \tag{3.19}$$

$$B = 2n + 1 + |l|, \qquad \text{and} \qquad \beta = (2n + 1 + |l|)\frac{\omega}{k_0}. \tag{3.20}$$

Therefore, for guided modes the complete solution $U(r, \phi, z)$ reads

$$U(r, \phi, z) = e^{ik_0(n_0-\beta)z}\psi(r)e^{il\phi} \tag{3.21}$$

3.4 The quasi-plane wave approach

In this section we'll follow an approximate method that seeks to approximate the problem to the much simpler one of a plane wave, but allowing its amplitude and phase to depend of r. The justification of this method rests in the assumption that the waves travel almost parallel to the axis of the guide, which leads to the assumption that the wave is locally plane. This method is pretty similar to the WKB approximations discussed in chapters 1 and 2. However, in those discussions, it was the method which provided us of the varying phase S, while in this method, S is proposed of a certain form and then developed further. For more details of this approach see [12].

As seen in the previous section of this work, the three Cartesian components of $\vec{E}$ satisfy equation (3.6) i.e.

$$\nabla^2 U(\vec{r}) + k_0^2 n(r)^2 U(\vec{r}) = 0; \quad \vec{r} = (r, \phi, z); \quad U \equiv E_j \;\; j = x, y, z\,. \tag{3.22}$$

Suppose U to be of the form

$$U(r,\phi,z) = \alpha(r,\phi,z)e^{-ik_0 S(r,\phi,z)}, \tag{3.23}$$

where $\alpha(r,\phi,z)$ and $S(r,\phi,z)$ are slowly varying real functions with respect to $\lambda_0 \equiv \frac{2\pi}{k_0}$. Under this hypothesis, $S(r,\phi,z)$ satisfies approximately the Eikonal equation from optic physics

$$|\nabla S|^2 \approx n^2, \tag{3.24}$$

as well as the fact that the light rays travel in the direction of ∇S. Let

$$k_0 S(r,\phi,z) \equiv k_0 s(r) + l\phi + \beta k_0 z. \tag{3.25}$$

Substituting this in (3.23) and in (3.24) we get respectively,

$$U(r,\phi,z) = \alpha(r,\phi,z)e^{-i(k_0 s(r)+l\phi+\beta k_0 z)}, \tag{3.26}$$

and

$$\left(k_0 \frac{d}{dr}s(r)\right)^2 + \left(\frac{l}{r}\right)^2 + (\beta k_0)^2 = n^2(r)k_0^2. \tag{3.27}$$

Then

$$(k_r)^2 + (k_\phi)^2 + (k_z)^2 = n^2(r)k_0^2, \tag{3.28}$$

where we have defined $k_r \equiv k_0 \frac{ds}{dr}$, $k_\phi \equiv \frac{l}{r}$, $k_z \equiv k_0\beta$. From this we get an expression for the unknown quantity $s(r)$

$$k_0 s(r) = \int k_r dr = \int \pm\sqrt{n^2(r)k_0^2 - \left(\frac{l}{r}\right)^2 - (\beta k_0)^2}dr. \tag{3.29}$$

Since k_r appears squared in (3.28) we can discard the minus sign of the square root without any loss of generality. From equation (3.13) we substitute the value of $n^2(r)$ in (3.29) to get

$$\begin{aligned} \int k_r dr &= \int \sqrt{(n_0^2 - n_0^2\omega^2 r^2)k_0^2 - \left(\frac{l}{r}\right)^2 - (\beta k_0)^2}dr \\ &= \int \frac{dr}{r}\sqrt{-n_0^2\omega^2 k_0^2 r^4 + \left(n_0^2 - \beta^2\right)k_0^2 r^2 - l^2}. \end{aligned} \tag{3.30}$$

In simplified form

$$\int k_r dr = \int \frac{dr}{r}\sqrt{Ar^4 + Br^2 + C}; \quad A \equiv -n_0^2\omega^2 k_0^2;\ B \equiv \left(n_0^2 - \beta^2\right)k_0^2;\ C \equiv -l^2. \tag{3.31}$$

Notice that $B > 0$ by necessity. Otherwise, the radicand would be negative for all values of β. We shall define another variable to carry out the integration more clearly. Let $y \equiv r^2$, then

$$\int k_r dr \;=\; \int \tfrac{dy}{2y}\sqrt{Ay^2+By+C};\quad y \equiv r^2\ ;\ \tfrac{dr}{r} = \tfrac{dy}{2y}. \tag{3.32}$$

The solution to this integral can be found in tables. Its expression depends on the character of the coefficients A, B, C. Since $A < 0, B > 0$ and $C < 0$, the corresponding expression in our case is

$$\begin{aligned}\int k_r(y)dy &= \tfrac{1}{2}\int \frac{dy}{y}\sqrt{Ay^2+By+C} \\ &= \tfrac{1}{2}\sqrt{Ay^2+By+C} + \tfrac{B}{4}\left(\tfrac{-1}{\sqrt{-A}}\right)\arcsin\left(\tfrac{2Ay+B}{\sqrt{B^2-4AC}}\right) \\ &\qquad + \tfrac{C}{2}\left(\tfrac{1}{\sqrt{-C}}\right)\arcsin\left(\tfrac{By+2C}{|y|\sqrt{B^2-4AC}}\right).\end{aligned} \tag{3.33}$$

with the conditions

$$\begin{array}{lrcl} 1. & A & < & 0 \\ 2. & C & < & 0 \\ 3. & B^2-4AC & > & 0 \\ 4. & \sqrt{B^2-4AC} & > & |2Ay+B| \end{array} \tag{3.34}$$

Conditions 1 and 2 are already satisfied. For the case $l = 0$ ($C = 0$) the result (3.33) changes in the factor following $\frac{1}{2}C$. However, the presence of precisely the factor $\frac{1}{2}C$ nullifies that change, making (3.33) still valid for $l = 0$.

Condition 4 can be explored in two ways. The first one is to develop the absolute value in its two possibilities ($|x| = \pm x$) and find that there exist two numbers y_1 and y_2 (roots of $Ay^2 + By + C = 0$) that bound the domain of $y : y_1 < y < y_2$. The second one is to take the square of it to find that $Ay^2 + By + C > 0$ is satisfied within those bounds.

Condition 3 guarantees that $B^2 - 4AC > 0$ *i.e.* there are always two points $y_{1,2} = \frac{1}{2A}(-B \pm \sqrt{B^2-4AC})$. On the other hand, by substituting the values of A,B and C we find a bound for β,

$$\beta^2 < n_0^2 - \frac{1}{k_0}2n_0\omega|l|. \tag{3.35}$$

Likewise, since the upper bound for β^2 must be non-negative, we get a bound for $|l|$ too.

$$0 < n_0^2 - \frac{1}{k_0}2n_0\omega|l|, \qquad |l| \leqslant \frac{k_0 n_0}{2\omega}. \tag{3.36}$$

The modes of the fiber are determined by imposing the self-consistency condition that the wave reproduces itself after one helical period of travel between r_1 and r_2 and back.

The azimuthal path length corresponding to an angle 2π must correspond to a multiple of 2π phase shift, *i.e.* $k_\phi 2\pi r = 2\pi l;\ l = 0, 1, 2, ...$ This condition is evidently satisfied since $k_\phi = \frac{l}{r}$. Furthermore, the radial round-trip path length must correspond to a phase shift equal to an integer multiple of 2π:

$$2\int_{r_1}^{r_2} k_r dr = 2\pi m; \quad m = 0, 1, 2, ... \tag{3.37}$$

The value $m = 0$ corresponds to the integral equaling zero, which can only happen in the case $y_1 = y_2$. For this to be true we would require that $\sqrt{B^2 - 4AC} = 0$, which would technically be a violation of condition 3. To sort this issue, remember that condition 3. ensures there are two values along the radial direction between which the quasi-plane bounces off. In the limit where this return points are very close to each other *i.e.* $y_1 \to y_2 \Rightarrow \sqrt{B^2 - 4AC} \to 0$. Then, we are in the presence of a quasi-plane wave with a wave vector $\vec{k} = (k_r, k_\phi, k_z)$ that has no radial component *i.e.* $k_r = 0$. This wave does not bounce along the radial direction, it rather exists confined to a fixed value $r_0 = \sqrt{y_1} = \sqrt{y_2}$. This self-consistency condition provides the characteristic equation from which the propagation constants β_{lm} of the modes are determined.From (3.32) and (3.33), we see that, in terms of y, (3.37) reads

$$\begin{aligned} \pi m &= \int_{r1}^{r2} k_r dr = \frac{1}{2}\int_{y1}^{y2} k_r(y) dy \\ &= \left(\frac{1}{2}\right)\left(\sqrt{Ay^2 + By + C} + \left(\frac{B}{2}\right)\int \frac{dy}{\sqrt{Ay^2 + By + C}} + C\int \frac{dy}{y\sqrt{Ay^2 + By + C}}\right)\Bigg|_{y_1}^{y_2}. \end{aligned} \tag{3.38}$$

Thus

$$\begin{aligned} \pi m &= \frac{1}{2}\sqrt{Ay^2 + By + C}\Big|_{y_1}^{y_2} \\ &\quad + \frac{B}{4}\left(\frac{-1}{\sqrt{-A}}\arcsin\left(\frac{2Ay+B}{\sqrt{B^2-4AC}}\right)\right)\Bigg|_{y_1}^{y_2} + \frac{C}{2}\left(\frac{1}{\sqrt{-C}}\arcsin\left(\frac{By+2C}{|y|\sqrt{B^2-4AC}}\right)\right)\Bigg|_{y_1}^{y_2}, \end{aligned} \tag{3.39}$$

where $y_{1,2} \equiv \frac{1}{2A}\left(-B \pm \sqrt{B^2 - 4AC}\right)$. Then

$$\pi m = \frac{B\sqrt{-C} + 2C\sqrt{-A}}{2\sqrt{AC}}, \tag{3.40}$$

where

$$A \equiv -n_0^2\omega^2 k_0^2, \qquad B \equiv \left(n_0^2 - \beta^2\right)k_0^2, \qquad C \equiv -l^2. \tag{3.41}$$

So that

$$\pi m = \pi \left(\frac{(n_0^2 - \beta^2)k_0^2|l| - 2l^2 n_0 \omega k_0}{4 n_0 \omega k_0 |l|} \right), \tag{3.42}$$

and

$$\beta = \pm n_0 \sqrt{1 - 2\frac{\omega}{k_0 n_0}(|l| + 2m)}. \tag{3.43}$$

In order for β to be real the radicand of the previous expression must be non-negative. This stablishes a bound for m:

$$0 \leqslant 1 - 2\frac{\omega}{k_0 n_0}(|l| + 2m), \qquad m \leqslant \frac{1}{2}\left(\frac{n_0 k_0}{2\omega} - |l| \right). \tag{3.44}$$

Given a fixed number l, equation (3.43) gives a finite discrete set of values for β. Let us explore a little further the expression for β. Let $x \equiv -2\frac{\omega}{k_0 n_0}(|l| + 2m)$. From (3.44) we've got

$$1 + x \geqslant 0 \quad \Rightarrow \quad 1 \geqslant |x|. \tag{3.45}$$

Therefore, we can make use of the Taylor series for $\sqrt{1+x}$

$$\sqrt{1+x} = 1 + \frac{1}{2}x - \frac{1}{8}x^2 + \frac{1}{16}x^3 - \cdots \tag{3.46}$$

Note that if the physical conditions were such as to let us dismiss the third term and beyond, then we could approximate β to a more insightful expression. That is, if $1 \gg |\frac{2\omega}{k_0 n_0}(|l| + 2m)|$, then

$$\beta \approx n_0 - \frac{\omega}{k_0}(|l| + 2m); \quad m = 0, 1, 2, ... \quad |l| = 0, 1, 2, ... \tag{3.47}$$

Up to this point we have found that the solution for the quasi-plane approximation is

$$U = \alpha e^{-ik_0 s(r)} e^{-il\phi} e^{-i\beta k_0 z}, \tag{3.48}$$

with β given by (3.47).

3.5 Comparison between the paraxial approximation against the quasi-plane picture

Let us compare the two solutions found for the optical fiber, in particular the propagation constant *i.e* the coefficient that comes with the z dependence.

- **Paraxial propagation constant**

By means of the paraxial approximation we found

$$U(r,\phi,z) = \psi(r)e^{ik_0(n_0-\beta)z}e^{il\phi}. \tag{3.49}$$

In this case the propagation constant is

$$\begin{aligned} &k_0(n_0-\beta) = k_0\left(n_0 - (2n+1+|l|)\tfrac{\omega}{k_0}\right) = k_0 n_0 - (2n+|l|+1)\omega; \\ &|l| = 0,1,2,..., \qquad n = 0,1,2,... \end{aligned} \tag{3.50}$$

- **Quasi-planar propagation constant**

On the other hand, the quasi-plane approach gave us

$$U = \alpha e^{-ik_0 s(r)}e^{-il\phi}e^{-i\beta k_0 z}, \tag{3.51}$$

with propagation constant

$$\begin{aligned} &k_0\beta = k_0(n_0 - \tfrac{\omega}{k_0}(|l|+2m)) = k_0 n_0 - (2m+|l|)\omega, \\ &|l| = 0,1,2,... \qquad m = 0,1,2,... \end{aligned} \tag{3.52}$$

At first glance the functional form of (3.50) and (3.52) are basically the same. However, there is a fundamental difference: All values of β from one approach can be matched with the other approach by an appropriate selection of l, n and m with *one exception*. For $l = 0$ and $n = 0$ in (3.50) the $(+1)$ gives as a result $k_0 n_0 - \omega$, while for $l = 0$ and $m = 0$ in (3.52) the propagation constant is equal to $k_0 n_0$. It appears that the paraxial approximation gives us an extra lower level that is not accessible through the quasi-plane approach. The non-agreement of the propagation constants obtained by different methods is no reason to worry. As stated before, solving the problem by an approximate method is an exercise to compare the results found through a simpler method against those found through the complexity of an analytical solution. If any conclusion can be made about this discrepancy is that, for the approximate result (3.52) to resemble the analytical result (3.50), a strong approximation had to be made (3.46)-(3.47), one that is not clear to hold for every value of l and m. Therefore, in the case of the two-dimensional short-range oscillator, the quasi-plane approximation proves insufficient where the exact method prevails.

Chapter 4

Balanced gain-and-loss waveguides

In this chapter we will study a one dimensional fiber assuming its refractive index $n(x)$ is a continuous and derivable function of the position x. We will take advantage of the analogy between optical wave guides and quantum systems described in chapter 2. A more general way to establish this analogy for an arbitrary potential $V(x)$ is obtained by comparing

$$\left[-\frac{1}{2k_0^2 n_*}\frac{d^2}{dx^2} - n(x) + n_*\right] E(x) = \varepsilon E(x); \qquad E(x) := E_y(x,z)|_{z=0} \tag{4.1}$$

with

$$\left[-\frac{\hbar^2}{2m}\frac{d^2}{dx^2} + V(x)\right]\psi(x) = \mathcal{E}\psi(x). \tag{4.2}$$

We get the identification [13]

$$k_0^2 \longleftrightarrow \frac{mw}{\hbar}, \quad [-n(x) + n_*]\, n_* \longleftrightarrow \frac{V(x)}{\hbar w}, \quad \varepsilon n_* \longleftrightarrow \frac{\mathcal{E}}{\hbar w}, \tag{4.3}$$

where ω is any reference value of frequency in terms of which the energy of the quantum system can be measured. Then, the $E_y(x,z) = E(x)\exp(ik_0\varepsilon n_* z)$ may be associated with the solutions $\psi(x,t) = \psi(x)\exp(i\mathcal{E}t/\hbar)$ of the related Schrödinger equation, where $z \leftrightarrow t\sqrt{\omega\hbar/m}$. The link between (4.1) and (4.2) is even more clear after introducing the changes $x \to \chi/\left(k_0\sqrt{2}\right)$ and $x \to \chi\sqrt{\hbar/(2m\omega)}$, which gives

$$\left[-\frac{d^2}{d\chi^2} + (-n(\chi) + n_*)\, n_*\right] E(\chi) = \varepsilon n_* E(\chi), \quad \left[-\frac{d^2}{d\chi^2} + \mathcal{V}(\chi)\right]\psi(\chi) = \widetilde{\mathcal{E}}\psi(\chi) \tag{4.4}$$

where $\hbar\omega\chi = V$ and $\hbar\omega\widetilde{\mathcal{E}} = \mathcal{E}$. In the following we will take full advantage of the above mathematical relationship, providing solutions to the paraxial Helmholtz equation

from the space of solutions of the quantum mechanical problem. The objective is to provide refractive indices on demand locating propagating constants inherited from the solutions to the quantum version of the problem while producing balanced wave-loss guides. Keeping this in mind we will apply teh Darboux method [14] as it has been developed in supersymmetric (Susy) quantum Mechanics [15] to deform the eigenfunctions of a given refractive index into the eigenfunctions of another one. The approach is useful to add a concrete number of eigenvalues to the propagation constants of $n(x)$, through a process of transforming $n(x)$ and $E(x)$ into new functions. The application of this method once adds a single value ϵ corresponding to the first order Susy (Darboux) transformation. Applied twice it will add a second eigenvalue. In such a case we would be working with a $2nd$ order Susy transformation. By performing this process $k-$times we will have k additional eigenvalues at the expense of transforming $n(x)$ $k-$ times. The Darboux method has been elegantly summarized in the finite-difference algorithm for higher order supersymmetry introduced in [16]. A concise summary is presented next.

4.1 Supersymmetric finite-difference algorithm

We briefly revisit the generalities of the finite-difference algorithm for higher order supersymmetry, the complete details of this rich procedure can be consulted in [16]. Let $f_k(x;\epsilon) := fk(x;\epsilon_1,\epsilon_2,,\epsilon_{k1},\epsilon)$, with $k \geqslant 1$, the Darboux transformation of an exactly solvable potential $V_{k1}(x;\epsilon_{k1})$ produces a new potential $V_k(x;\epsilon)$ in the form

$$V_k(x;\epsilon) = V_{k-1}\left(x;\epsilon_{k-1}\right) + 2\beta_k'(x;\epsilon), \quad k = 1,2,\ldots, \tag{4.5}$$

where $\beta_k(x;\epsilon)$, usually called the superpotential, is solution of the Riccati equation with the initial potential V_{k-1},

$$-\beta_k'(x;\epsilon) + \beta_k^2(x;\epsilon) = V_{k-1}\left(x;\epsilon_{k-1}\right) - \epsilon, \tag{4.6}$$

and ϵ is a constant to be determined.Let β be of the form

$$\beta_k(x;\epsilon) = -\frac{d}{dx}\ln u_{(k)}(x;\epsilon). \tag{4.7}$$

This transformation linearizes equation (4.6) by providing the eigenvalue problem

$$-u_{(k)}''(x;\epsilon) + V_{k-1}\left(x;\epsilon_{k-1}\right)u_{(k)}(x;\epsilon) = \epsilon u_{(k)}(x;\epsilon), \quad k = 1,2,\ldots, \tag{4.8}$$

where $f'(x) = \frac{df}{dx}$. Thus, the superpotential 4.7 may be constructed from the eigenfunctions $u_k(x;\epsilon)$ of $V_{k-1}(x;\epsilon_{k-1})$ that belong to the eigenvalue ϵ (usually called

factorization constant). The "transformation functions" u_k are not required to be square-integrable in $Dom(V_{k1})$, since they are just a mathematical tool to find β. The finite-difference algorithm [16] states that the solutions of (4.6) are the result of a finite-difference operation performed on β_{k1},

$$\beta_k(x;\epsilon) = -\beta_{k-1}(x;\epsilon_{k-1}) - \frac{\epsilon_{k-1}-\epsilon}{\beta_{k-1}(x,\epsilon_{k-1}) - \beta_{k-1}(x;\epsilon)}. \tag{4.9}$$

The superpotentials β_k built at each step are guaranteed to solve the Riccati equation (4.6) and are linked to the eigenvalue problem (4.8), which is defined by the potential of the previous step V_{k1} through the new factorization constant ϵ. In turn, the solutions $\psi_(k)(x;\epsilon)$ of the new eigenvalue equation

$$-\psi''_{(k)}(x;\epsilon) + V_k(x;\epsilon)\psi_{(k)}(x;\epsilon) = \mathcal{E}\psi_{(k)}(x;\epsilon), \quad k = 1,2,\ldots, \tag{4.10}$$

are obtained as the Darboux-deformation of the previous ones

$$\mathcal{N}^{-1}_{(k)}\psi_{(k)}(x;\epsilon) = \psi'_{(k-1)}(x;\epsilon_{k-1}) + \beta_k(x;\epsilon)\psi_{(k-1)}(x;\epsilon_{k-1}), \tag{4.11}$$

where N_k^{-1} stands for normalization. An intersting fact arising from the method is the recognition of an additional solution to equation (4.10), which is not included in the transformation (4.11), given by the expression

$$\psi^M_{(k)}(x;\epsilon) = \mathcal{N}^M_{(k)}u^{-1}_{(k)}(x;\epsilon) = \mathcal{N}^M_{(k)}\exp\left[\int \beta_k(x;\epsilon)dx\right]. \tag{4.12}$$

The above function was introduced by Mielnik [16], it is known as missing state and satisfies (4.10). Thus, if (4.12) is square-integrable in $Dom(V_k)$, then ϵ must be added to the set of eigenvalues of V_k.

4.2 Adding propagation constants under prescription

Our interest is in generating refractive indices $n(x)$ with exact solutions to the paraxial Helmholtz equation (4.1). The finite-difference algorithm for higher order supersymmetry described above provides an elegant way to achieve this goal. The key step is to have an already known exactly solvable refractive index $n_0(x)$, the point-spectrum of which is inherited to another refractive index $n_1(x;\epsilon)$, defined by the Darboux transformation

$$(-n_1(x;\epsilon) + n_{1,*})\frac{n_{1,*}}{n_{0,*}} = -n_0(x) + n_{0,*} + \frac{\sqrt{2}}{k_0 n_{0,*}}\beta'_1(x;\epsilon) \tag{4.13}$$

where the superpotential $\beta_1(x;\epsilon)$ is solution of the nonlinear Riccati equation

$$-\frac{\sqrt{2}}{k_0}\beta_1'(x;\epsilon)+\beta_1^2(x;\epsilon)=n_{0,*}\left[-n_0(x)+n_{0,*}-\epsilon\right]. \tag{4.14}$$

where ϵ is still yet to be determined. To simplify notation, without loss of generality, hereafter we make $n_{k,*}=n_{0,*}:=n_*$, with $k=1,2,...$ As pointed out in equation (4.8), the transformation $\beta_1\equiv-\frac{d}{dx}ln(u_1(x;\epsilon))$ leads to $u_1(x;\epsilon)$ satisfying an eigenvalue equation that determines both $u_1(x;\epsilon)$ and ϵ,

$$-u''(x;\epsilon)+V_0(x;\epsilon)u(x;\epsilon)=\epsilon u(x;\epsilon). \tag{4.15}$$

where $f'(x)\equiv\frac{df}{dx}$. We insist, that the function u need not be a physical solution, so the eigenvalue ϵ is not fixed in any sense. It is free for us to choose.

The new refractive index (4.13) defines its own paraxial Helmholtz equation

$$\left[-\frac{1}{2k_0^2n_*}\frac{d^2}{dx^2}-n_1(x;\epsilon)+n_*\right]E_{(1)}(x;\epsilon)=\varepsilon E_{(1)}(x;\epsilon). \tag{4.16}$$

Since $n_1(x;\epsilon)$ is a new refractive index, it defines its own guided modes. However, it is not necessary to solve the eigenvalue equation itself, since the solutions to $n_1(x)$ are related to those of $n_0(x)$ by the "deformation"

$$\mathcal{N}_{(1)}^{-1}E_{(1)}(x;\epsilon)=E_{(0)}'(x)+\beta_1(x,\epsilon)E_{(0)}(x). \tag{4.17}$$

where $f'(x)\equiv\frac{df}{dx}$ and N_1 stands for normalization. The set of eigenvalues of $n_1(x)$ are exactly those of $n_0(x)$, or it may also include the factorization constant ϵ. In such case, the corresponding eigenfunction is called a "*Missing state*" and is expressed as

$$E_{(1)}^M(x;\epsilon)=\mathcal{N}_{(1)}^M\exp\left[\int\beta_1(x;\epsilon)dx\right]. \tag{4.18}$$

So, if $n_0(x)$ had N guided modes, after the first Susy step we have a new potential $n_1(x;\epsilon)$ that has $N+1$ levels where the extra eigenvalue ϵ is free for us to choose as long as it is a solution of equation (4.15). This procedure can be repeated as many times as needed. Since each step can provide a single additional "energy", if we seek to have at hand k guided modes, we can repeat the process $k-$ times. It is conventional in this supersymmetric approach to include the new eigenvalue below the lowest eigenvalue of the previous point-spectrum. This obeys the fact that the oscillation theorem prevents the construction of regular superpotentials β_k if the factorization constant ϵ is above the

lowest propagation constant of n_{k-1}. indeed, the real and imaginary parts of (4.14) give place to the nonlinear differential equation

$$\left[-\frac{1}{2k_0^2 n_*}\frac{d^2}{dx^2} - n_0(x) + n_*\right]\alpha(x;\epsilon) = \epsilon\alpha(x;\epsilon) - \frac{1}{2k_0^2 n_*}\frac{\lambda^2}{\alpha^3(x;\epsilon)}, \quad \lambda \in \mathbb{R} \tag{4.19}$$

which we will deduce next.

4.2.1 Balanced gain and loss waveguides

In contraposition to the method exposed up to this point there is a Darboux-deformation method that produces complex valued refractive indices parting from real valued ones. This can be done by the method introduced in [17]. Equations (4.16)-(4.18) are still valid. The eigenvalues arising from it will be real and the additional value ϵ can be incorporated at any position of the point-spectrum [19]. Let $\beta \equiv \beta_{\mathrm{R}} + i\beta_{\mathrm{I}}$ with β_{R} and β_{I} real functions,

$$\begin{aligned} \beta_{\mathrm{R}}' + \beta_{\mathrm{R}}^2 - \beta_{\mathrm{I}}^2 + \epsilon - V &= 0, \\ -\beta_{\mathrm{I}}' + 2\beta_{\mathrm{I}}\beta_{\mathrm{R}} &= 0. \end{aligned} \tag{4.20}$$

From the second line we immediately get

$$\frac{d}{dx}\ln\beta_{\mathrm{I}} = 2\beta_{\mathrm{R}}. \tag{4.21}$$

This last equation suggest the ansatz

$$\beta_{\mathrm{R}}(x) \equiv -\frac{d}{dx}\ln\alpha(x), \tag{4.22}$$

with $\alpha(x)$ a function to be determined. In terms of $\alpha(x)$ the imaginary part of β reads

$$\beta_{\mathrm{I}}(x) = \frac{\lambda}{\alpha^2(x)}. \tag{4.23}$$

To get real functions β_{R} and β_{I} it will be enough to consider α and λ real. Substituting (4.22), and (4.23) in (4.14) yields the nonlinear differential equation

$$\left[-\frac{1}{2k_0^2 n_*}\frac{d^2}{dx^2} - n_0(x) + n_*\right]\alpha(x;\epsilon) = \epsilon\alpha(x;\epsilon) - \frac{1}{2k_0^2 n_*}\frac{\lambda^2}{\alpha^3(x;\epsilon)}, \quad \lambda \in \mathbb{R}, \tag{4.24}$$

which is named after Ermakov [20]. Note that (4.24) coincides with the paraxial Helmholtz equation (4.5) when $\lambda = 0$. The solutions to the Ermakov eqution is the nonlinear superposition

$$\alpha(x;\epsilon) = \left[a u_{(1);1}^2(x;\epsilon) + b u_{(1);1}(x;\epsilon) u_{(1);2}(x;\epsilon) + c u_{(1);2}^2(x;\epsilon)\right]^{\frac{1}{2}}, \tag{4.25}$$

where $u_{(1);1}$ and $u_{(1);2}$ are two-linearly independent solutions of (4.1) for with $\varepsilon = \epsilon$. The α-function is real-valued and free of zeros in Dom n_0 if the set $\{a, b, c\}$ is composited by positive numbers fulfilling

$$b^2 - 4ac = -4\frac{\lambda^2}{W_0^2}, \tag{4.26}$$

where $W_0 = W\left(u_{(1);1}, u_{(1);2}\right) = \text{const}$ is the Wronskian of $u_{(1);1}$ and $u_{(1);2}$. Using (4.25), the complex-valued superpotential acquires a simple form

$$\beta_1(x;\epsilon) = -\frac{1}{2}\frac{d}{dx}\ln v(x;\epsilon) + i\frac{\lambda}{v(x;\epsilon)} = -\left[\frac{v'(x;\epsilon) - i2\lambda}{2v(x;\epsilon)}\right], \tag{4.27}$$

where

$$v(x;\epsilon) = a u_{(1);1}^2(x;\epsilon) + b u_{(1);1}(x;\epsilon) u_{(1);2}(x;\epsilon) + c u_{(1);2}^2(x;\epsilon). \tag{4.28}$$

Then, the Darboux transformation gives the complex-valued refractive index

$$n_1(x;\epsilon) = n_0(x) + \frac{1}{k_0^2 n_*}\frac{d}{dx}\left[\frac{v'(x;\epsilon) - i2\lambda}{2v(x;\epsilon)}\right]. \tag{4.29}$$

On the other hand, it may be shown that the imaginary part of n_1 satisfies the condition of zero total area [49]:

$$\int_{\mathbb{R}} \text{Im}\, n_1(x;\epsilon)dx = -\left.\frac{\lambda}{k_0^2 n_*}\frac{1}{v(x;\epsilon)}\right|_{-\infty}^{+\infty} = 0, \tag{4.30}$$

so the total optical power is conserved. Equation (4.30) implies a balanced interplay between gain and loss that does not depend on any symmetry of either Im $n_1(x;\epsilon)$ or Re $n_1(x;\epsilon)$. In contraposition to conventional supersymmetric approaches, the factorization energy ϵ can be positioned at any place in the spectrum of n_1 [19]. Besides, the missing state (4.18), now written as

$$E_{(1)}^M(x;\epsilon) = \frac{\mathcal{N}_{(\infty)}^{\mathcal{M}}}{\sqrt{v(x;\epsilon)}}\exp\left[i\lambda\int v^{-1}(x;\epsilon)dx\right], \tag{4.31}$$

is such that its real and imaginary parts are even and odd functions, respectively. We would like to emphasize that the non-linear superposition (4.28) marks a distance

with conventional supersymmetric approaches. Indeed, we have already shown [21] that the superpotential (4.27) can be also written in the conventional logarithmic form $\beta(x;\epsilon) = -\frac{d}{dx}\ln w(x;\epsilon)$, where the coefficients of the linear superposition

$$w(x;\epsilon) = a u_{(1),1}(x,\epsilon) + \left(\frac{b}{2} - i\frac{\lambda}{W_0}\right) u_{(1),2}(x,\epsilon), \tag{4.32}$$

are ruled by the constraint (4.26), with a and b complex numbers in general. Clearly, such a concrete combination of coefficients permits n_1 to satisfy the condition of zero total area, which defines it as a balanced gain-and-loss refractive index.

4.2.2 Bi-orthogonality

The solutions of the paraxial Helmholtz equation (4.1), with $n1(x;e)$ given in (4.29), are obtainable from (4.30). However, while $E^M_{(1)}$ and all the TE modes $E_{(1)}$ are normalizable, they form a peculiar set since $E^M_{(1)}$ is orthogonal to all the $E_{(1)}$ but these last are not mutually orthogonal [22] (such property is not a problem in the Hermitian case since all the new functions satisfy the conventional oscillation theorems). Nevertheless, the eigenfunctions of n_1 satisfy some properties of interlacing of zeros that permit the study of the related systems as if they were Hermitian [23]. In this context, the biorthogonal set formed by the eigenstates $E_{(1)}$ of n_1, together with the eigenstates $\tilde{E}_(1)$ of the complex-conjugated refractive index, written n_1^C, provide an extended space of states where all the basis elements are bi-orthonormal [22] [24] [25]. Indeed, the bi-product

$$\left(\tilde{E}_{(1);m}, E_{(1);n}\right) = \int_{\mathbb{R}} \tilde{E}^C_{(1);m}(x;\epsilon) E_{(1);n}(x;\epsilon) dx \tag{4.33}$$

is equal to zero if $n \neq m$ and serves to define the bi-norm $||E_{(1);n}|| = ||\tilde{E}_{(1);n}||$ if $n = m$ [22]. Having two possible normalizations at our disposal, the conventional norm $\frac{E_{(1)}}{||E_{(1)}||}$ and the bi-norm $\frac{E_{(1)}}{||E_{(1)}||_B}$ we have to take into account that the real and imaginary parts of the TE modes $E_{(1)}$, we have to take into account that the real and imaginary parts of the TE modes $E_{(1)}$ behave qualitatively equal in both normalizations, but their bi-normalized values are usually larger than those obtained with the conventional normalization. Such a difference is reduced as the excitation of the mode increases [25]. Besides, note that the notions of bi-product and bi-norm introduced above coincide with the conventional definitions if $\lambda = 0$.

4.2.3 PT−symmetric case

The expression (4.29) represents a wide family of balanced gain−and−loss refractive indices. A very interesting subset of such family is integrated by the so called parity−time

(PT) symmetric refractive indices. Recalling that invariance under parity and time reversal transformations requires $n(x) = n_x^*$ in quantum mechanics [26], we realize that the effective refractive index $n_0(x)$ should be parity-invariant $n_0(x) = n_0(-x)$ to facilitate the construction of PT−symmetric refractive indices $n_1(x;\epsilon)$. On the other hand, assuming real−valued transformation functions $u_{(1);1}$ and $u_{(1);2}$, we may take $b = 0$ in (4.28) to obtain the quadratic form

$$v_{PT}(x;\epsilon) = a u_{(1);1}^2(x;\epsilon) + c u_{(1);2}^2(x;\epsilon). \tag{4.34}$$

The straightforward calculation shows that using this function in (4.29) one gets a complex valued graded index that is PT-symmetric. Note that $b = 0$ implies $ac = \frac{\lambda^2}{|W_0^2|}$ in (4.26), where $|W_0|$ stands for the modulus of W_0. Then (4.29) yields

$$\begin{aligned} n_{PT}(x) \quad = \quad & n_0(x) + \tfrac{1}{2k_0^2 n_*}\tfrac{d^2}{dx^2} ln\left(u_{(1);1}^2(x;\epsilon) + u_{(1);2}^2(x;\epsilon)\right) \\ & -i\tfrac{|W_0|}{k_0^2 n_*}\left(u_{(1);1}^2(x;\epsilon) + u_{(1);2}^2(x;\epsilon)\right)^{-1}. \end{aligned} \tag{4.35}$$

4.2.4 Recovering the real valued case

As indicated above, if $= 0$ the superpotential (4.27) is reduced to its Hermitian configuration, which produces real-valued indices only. Revisiting the constraint (4.26) we see that $= 0$ implies $b^2 = 4ac$, and thus $b = \pm 2\sqrt{ac}$. We obtain the linear superpositions $\alpha_\pm = \sqrt{a}u_{(1);1} \pm \sqrt{c}u_{(1);2}$, so we arrive at the conventional superpotentials

$$\beta_R(x;\epsilon;\pm) = -\frac{d}{dx}\ln\left[\sqrt{a}u_{(1);1}(x;\epsilon) \pm \sqrt{c}u_{(1);2}(x;\epsilon)\right], \tag{4.36}$$

where a and c are such that β is free of singularities in Dom n_0. Therefore, from (4.13) one has the two-parametric family of real-valued graded indices

$$n_R(x;\epsilon;\pm) = n_0(x) + \frac{1}{k_0^2 n_*}\frac{d^2}{dx^2}\ln\left[\sqrt{a}u_{(1);1}(x;\epsilon) \pm \sqrt{c}u_{(1);2}(x;\epsilon)\right]. \tag{4.37}$$

4.2.5 Applications

4.2.5.1 Adding guided modes one at a time

The fundamental solutions of the paraxial Helmholtz equation for $n_0 = 0$ are well known (From now on, for the sake of simplicity, the expressions of the refractive index profiles are considered up to the additive constant n_*). For positive factorization constants $\epsilon = k^2 > 0$ we write $u_1 = e^{ik(x-x_0)}$ with $W_0 = -i2k$. However the above expressions yield sinusoidal

refractive indices n_1 [22],which are out of the scope of this work. Here we make $k = i\kappa$ to get negative factorization constants $\epsilon = -\kappa^2$, therefore

$$v(x;\kappa) = ae^{2\kappa(x-x_0)} + ce^{-2\kappa(x-x_0)} + b, \quad b^2 - 4ac = -\lambda^2/\kappa^2. \tag{4.38}$$

To simplify our example let us make $a = c$. Then $v(x;k) = 2a\cosh[2\kappa(x-x_0)]$, with $b^2 = 4a^2 - \frac{\lambda^2}{\kappa^2}$. The superpotential (4.27) takes the form

$$\beta_1(x;\kappa) = -\left[\frac{\kappa\sinh\left[2\kappa\left(x-x_0\right)\right] - i\frac{\lambda}{2a}}{\cosh\left[2\kappa\left(x-x_0\right)\right] + \frac{b}{2a}}\right], \quad b^2 = 4a^2 - \frac{\lambda^2}{\kappa^2}, \tag{4.39}$$

so the refractive-index (4.29) is in this case

$$n_1(x;\kappa) = \frac{(2\kappa)^2\left(1 + \frac{b}{2a}\cosh\left[2\kappa\left(x-x_0\right)\right]\right) + i\frac{\lambda}{a}(2\kappa)\sinh\left[2\kappa\left(x-x_0\right)\right]}{2k_0^2 n_*\left(\cosh\left[2\kappa\left(x-x_0\right)\right] + \frac{b}{2a}\right)^2}. \tag{4.40}$$

The complex-valued graded refractive index (4.39) allows the presence of only one guided TE mode, obtained from (4.18) in the form

$$E^M_{(1)}(x;\kappa) = \frac{\mathcal{N}^M_{(1)}}{\sqrt{\cosh\left[2\kappa\left(x-x_0\right)\right] + \frac{b}{2a}}}\exp\left\{-\frac{i}{4a}\arctan\left(\left(\frac{b}{2a} - 1\right)\tanh\left[\kappa\left(x-x_0\right)\right]\right)\right\}. \tag{4.41}$$

Following the indications of the previous section, let us make $\lambda = 0$ and $b = 2a$ in (4.38) and (4.39) to get

$$\beta_R(x;\kappa) = -\kappa\tanh\left[\kappa\left(x-x_0\right)\right], \quad n_R(x;\kappa) = \frac{2\kappa^2}{2k_0^2 n_*\cosh^2\left[\kappa\left(x-x_0\right)\right]}, \tag{4.42}$$

which are the well known expressions for the cosh-like refractive index. The function $n_r(x;k))$ is depicted in figure (4.1a) for a representative propagation constant ϵ, which may be located at any position $\epsilon_1 = -\kappa_1^2$ since it is the only one eigenvalue.

For $b = 0$ and $a = \frac{\lambda}{2\kappa}$ the formulae (4.38) and (4.39) give rise to the PT-symmetric expressions

$$\beta_{PT}(x;\kappa) = -\left(\frac{\kappa\sinh\left[2\kappa\left(x-x_0\right)\right] - i\kappa}{\cosh\left[2\kappa\left(x-x_0\right)\right]}\right), \quad n_{PT}(x;\kappa) = \frac{(2\kappa)^2\left(1 + i\sinh\left[2\kappa\left(x-x_0\right)\right]\right)}{2k_0^2 n_*\cosh^2\left[2\kappa\left(x-x_0\right)\right]} \tag{4.43}$$

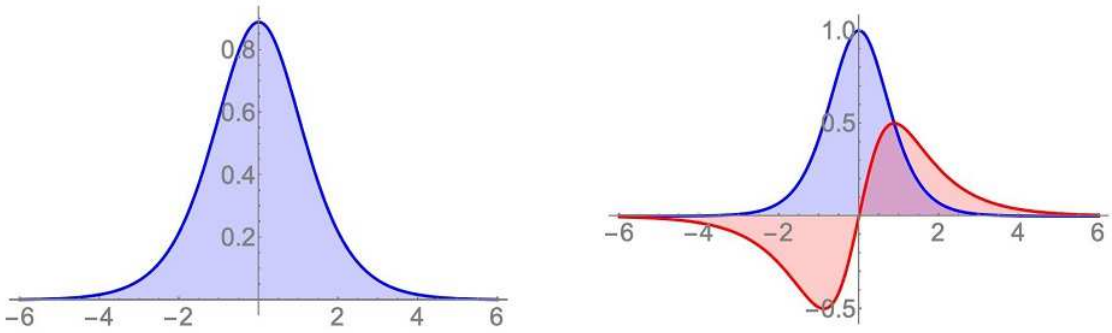

(a) (b)

Figure 4.1: (a) Cosh-like refractive index (4.42) for $\kappa = 2/3$. (b) Parity-time symmetric refractive index (4.43) for $\kappa = 1/2$. In both cases $x_0 = 0, k_0 = \frac{1}{\sqrt{2n_*}}$, and the horizontal axis is mounted on n_*. These graded refractive indices admit the presence of only one guide TE mode of propagation constant $\epsilon = -4/9$ and $\epsilon = -1/4$. In both cases the real part is in blue while the imaginary part is in red.

The PT-symmetric refractive index (4.42) is shown in figure (4.1b) for a representative propagation constant ϵ. As in the previous case, this eigenvalue can be positioned at will in the negative part of the real axis.

If we repeat the procedure, assuming now that $n_1(x;\kappa_1)$ has already been fixed, the finite difference algorithm provides an immediate potential

$$\beta_2\left(x;\kappa_1,\kappa\right) = -\beta_1\left(x;\kappa_1\right) + \frac{2k_0^2 n_*\left(\kappa_1^2-\kappa^2\right)}{\beta_1\left(x;\kappa_1\right)-\beta_1(x;\kappa)}, \tag{4.44}$$

where κ_1 and $\beta_1(x;\kappa_1)$ have been fixed in the previous step. Deciding the concrete value of κ, as well as the analytical form of $\beta_1(x;\kappa)$ in (4.38), the above equation provides the new refractive index

$$n_2\left(x;\kappa_1,\kappa\right) = n_1\left(x;\kappa_1\right) - \frac{1}{k_0^2 n_*}\beta_2'\left(x;\kappa_1,\kappa\right) = -\frac{d}{dx}\left[\frac{2\left(\kappa_1^2-\kappa^2\right)}{\beta_1\left(x;\kappa_1\right)-\beta_1(x;\kappa)}\right], \tag{4.45}$$

where we have used (4.13) with $n_0(x) = 0$.

At the present stage, we have incorporated two propagation constants, so the point-spectrum of $n_2(x;_1,\kappa_)$ is composited by the eigevalues $\varepsilon_1 = \kappa_1^2$, and $\varepsilon = -\kappa$. However, some caution is necessary if the first step was addressed to produce $n_R(x;\kappa_1)$ and we are looking for a second real-valued refractive index $n_R(x;\kappa_1,\kappa)$. In such a case, the inequality

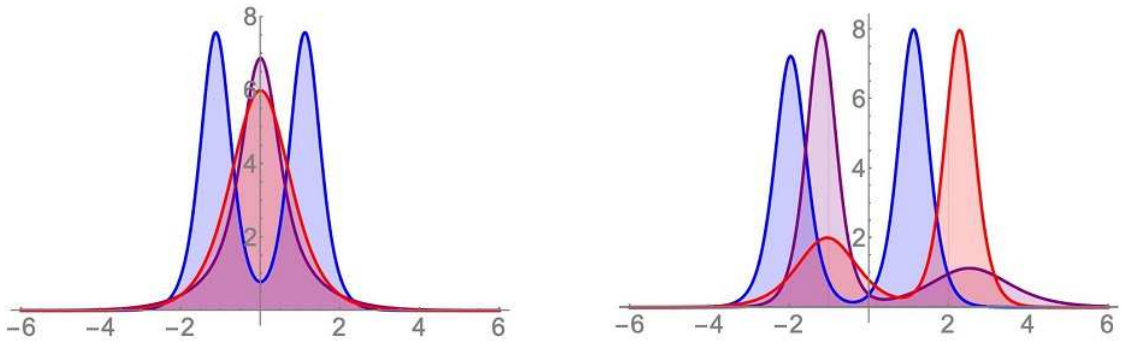

(a) (b)

Figure 4.2: Real-valued refractive index $n_R(x;\kappa_1;\kappa)$ with symmetric (a) and non-symmetric (b) profile, see eq. (4.46). The point-spectrum is composited by only two propagation constants $\{\epsilon,\epsilon_1\}$, explicitly $\{-(1.9)^2,-4\},\{-\frac{9}{16},-4\},\{-1,-4\}$, for curves in blue, purple and red, respectively. In (b) the points (x_0,x_1) are $(0.2,-1),(-1,2),(2,-0.5)$, following the color code indicated above.

$\varepsilon<\varepsilon_1$ must be satisfied in order to obtain regular functions $n_R(x;\kappa_1,\kappa)$. Besides, in such caes, it may be shown [16] that it is better to combine the two different real-valued superpotentials $\beta_R(x;\kappa;\pm)$. The case "+" is reported in equation (4.41), the case "−" corresponds to the complementary expression $\beta_R(x;\kappa;-)=-\kappa\coth[\kappa(x-x_0)]$. We, therefore, arrive at the real-valued graded index

$$n_R\left(x;\kappa_1,\kappa\right)=\frac{2\left(\kappa_1^2-\kappa^2\right)\left(\kappa_1^2\operatorname{csch}^2\left[\kappa_1\left(x-x_1\right)\right]+\kappa^2\operatorname{sech}^2\left[\kappa\left(x-x_0\right)\right]\right)}{\left(-\kappa_1\coth\left[\kappa_1\left(x-x_1\right)\right]+\kappa\tanh\left[\kappa\left(x-x_0\right)\right]\right)^2}. \tag{4.46}$$

The behavior of $n_R(x;\kappa_1;\kappa)$ is shown in figure (4.2) for different spectra $\{\varepsilon,\varepsilon_1\}$ and constants x_0 and x_1.

Remarkably, ε and ε_1 characterize the global profile of the function (4.45). Indeed, for $\kappa_1\gg\kappa_1$ and $x_0=x_1=0$, the refractive index $n_R(x;\kappa_1;\kappa)$ acquires a bell-shaped form. However, a valley arrises at the top of such curve if $\kappa=\kappa_1-\rho$ with $0\leqslant\rho\ll 1$.The dent is more pronounced as $\rho\to 0$, separating the initial bell-like curve into a pair of bell-shaped ones. At the very limit, the new curves have moved in opposite directions toward the domain edges $\pm\infty$. Quite interestingly, actual waveguides are manufactured by including such dent, sometimes for reducing the internal mechanical stress due to the gradient of dopant concentration, and sometimes for reducing the multimode dispersion [27], pp 83.

Having this in mind, figure (4.3) shows the exploration of the parameters that characterize $n_R(x;\kappa_1;\kappa)$ addressed to produce different dent configurations in the

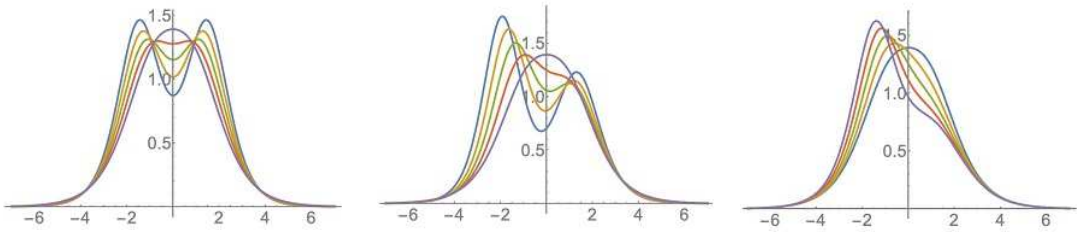

(a) (b) (c)

Figure 4.3: The real-valued refractive index $n_R(x;\kappa_1;\kappa)$ may be produced with a dent if $\kappa = \kappa_1 - \rho$, with $0 \leqslant 1$, in eq. (4.46). This may be symmetrical (a) or asymmetrical (b). Both cases correspond to the point-spectra $\{-\kappa_1^2, -\kappa^2\}$, where κ_1 and $\kappa = 0.55, 0.6, 0.65, 0.7, 0.75$, top to bottom curves as they are viewed at $x = 0$, respectively. In (b), the same curves are evaluated with $x_1 = 0, -0.2, -0.4, -0.6, -0.8$. In (c) the spectrum is fixed, with $\kappa_1 = 1$ and $\kappa = 0.55$. The displacement x_1 takes the values indicated in (b). The dents in (a)-(b), as well as the deformations (c), are deliberately produced in the manufacture of actual refractive indices, see for instance [27].

refractive index. These may be completely symmetrical like in figure (4.3a) or asymmetrical, as it is shown in fig. (4.3b). For $_1 > \kappa$, local deformations may be produced by tuning the displacement parameters x_0 and x_1 see figure (4.3c).

The ordering problem suffered by the propagation constants in the construction of $n_R(x;\kappa_1;\kappa)$ is easily avoided by considering any superpotential (4.38) with $\lambda \neq 0$ in either of the two steps. For instance, like in the previous example, assume that $n_R(x;\kappa_1$ has been fixed in the first step. To include the second eigenvalue ε this time we use the complex-valued superpotential $\beta_{PT}(x;\kappa)$ introduced in (4.42). The new refractive index (4.44) is now complex-valued, given by

$$n_2\left(x;\kappa_1,\kappa\right) = \frac{2\left(\kappa_1^2-\kappa^2\right) f\left(x;\kappa_1,\kappa\right)}{g^2\left(x;\kappa_1,\kappa\right)}, \tag{4.47}$$

where

$$f\left(x;\kappa_1,\kappa\right) = -\kappa_1^2\,\mathrm{sech}^2\left(\kappa_1 x\right) + 2\kappa^2\,\mathrm{sech}^2(2\kappa x) + i2\kappa^2\tanh(2\kappa x)\,\mathrm{sech}(2\kappa x) \tag{4.48}$$

and

$$g\left(x;\kappa_1,\kappa\right) = -\kappa_1\tanh\left(\kappa_1 x\right) + \kappa\tanh(2\kappa x) - i\kappa\,\mathrm{sech}(2\kappa x). \tag{4.49}$$

In (4.47) and (4.48) we have omitted the displacement constants x_0 and x_1 for the sake of simplicity. As $n_R(x;\kappa_1)$ is parity-invariant $n_R(x;\kappa_1) = n_R(-x;\kappa_1)$, the parameters of $n_2(x;\kappa_1,\kappa)$ in (4.46) can be managed to obtain a PT-symmetric refractive index

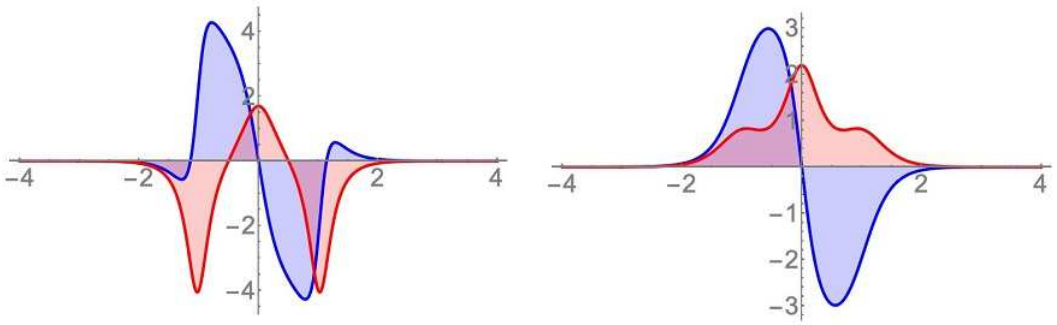

(a) (b)

Figure 4.4: PT-symmetric version of the complex-valued refractive index $n_1(x, \kappa_1, \kappa)$ introduced in eq, (4.47). In contrast with the real-valued case $n_R(x, \kappa_1, \kappa)$, the propagation constants can be added in arbitrary order to the point-spectrum $\{\varepsilon, \varepsilon_1\}$. Nevertheless, although the PT-symmetry is preserved, the profile of $n_1(x; \kappa_1, \kappa)$ is affected by the change $\varepsilon_1 \leftrightarrow \varepsilon$. The point-spectrum is $\{-(1.9)^2, -4\}$. In both cases $x_0 = x_1 = 0$, with the real and imaginary parts in blue and red, respectively.

$n_{PT}(x; \kappa_1; \kappa)$. The result is shown in figure (4.4a) for the process in which we add first ε_1 and then ε with $\varepsilon_1 > \varepsilon$. The reversed process is shown in figure (4.4b). Note that, although the profile of $n_{PT}(x; \kappa_1; \kappa)$ changes, the PT-symmetry is preserved under the change $\varepsilon_1 \leftrightarrow \varepsilon$. The same expression (4.46) gives rise to refractive indices that are not invariant under parity-time transformations, as it is exhibited in figure (4.5).

We have already mentioned that the procedure may be repeated at will. At the k-*th* step, the method provides a set of superpotentials β_k that are available for the finite-difference algorithm, addressed to elaborate the step $k + 1$. The case considered in this section takes the null function $n_0(x) = 0$ as the initial refractive index. The propagation constants are added one at a time in order to arrive at the point-spectrum $\{\varepsilon_1, \varepsilon_2, ..., \varepsilon_{k-1}, \varepsilon_k\}$, which may be decided under prescription. The refractive indices constructed in this form admit k guided TE modes, generated from the initial missing state $E^M_{(1)}(x; \varepsilon)$, via the rule (4.18). These modes obey the bi-product introduced above, which also defines a proper bi-norm that coincides with the conventional norm if $\lambda = 0$.

4.2.5.2 Manipulating a set of guided modes at once

To complete the revision of immediate applications, consider the cosh-like refractive index.

$$n_0(x, m) = \frac{m(m+1)\kappa^2}{\cosh^2(\kappa x)}, \quad m = 1, 2, \ldots \tag{4.50}$$

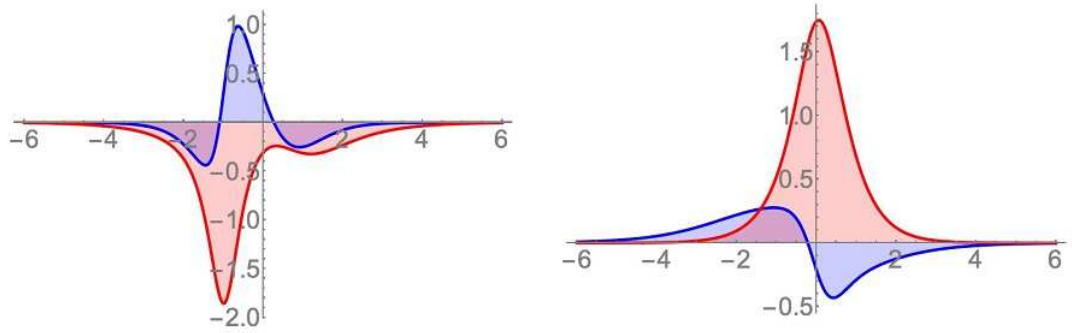

(a) (b)

Figure 4.5: Same as in Figure (4.4), with $x_0 = -0.5$ and $x_1 = 0$. In this case, the complex-valued refractive index $n_1(x;\kappa_1,\kappa)$ is not invariant under PT-transformations.

Potentials $V(x) = -n_0(x,m)$ form the subset of transparent Pöschl-Teller potentials in quantum mechanics. The solutions of the Schrödinger equation for the entire family are well known [28] [29] [33], including resonances and anti-bound states [30] [31]. Our interest in $n_0(x,m)$ obeys the fact that this refractive index admits exactly m guided TE modes, defined by the quadratic rule [28] [29] [33].

$$\varepsilon_{m,\ell} = -\kappa^2(m-\ell)^2, \quad \ell = 0,1,\ldots,m-1, \quad m = \text{ fixed} \tag{4.51}$$

The finite-difference algorithm will provide k additional eigenvalues at the kth iteration, so the spectrum of $n_k(x,m;k)$ is composited by two finite subsets $\{\varepsilon_i\} \cup \{\varepsilon_{m,l}\}$, with $i = 1,2,...,k$. As we have shown in the previous section, depending on the 1-step superpotentials $\beta_l(x,m;\varepsilon)$ and the factorization constants ε, the new eigenvalues ε_i may be positioned at arbitrary places of the initial spectrum $\{\varepsilon_{m,l}\}$.

The fundamental basis of solutions is in this case provided by the functions [28] [29]

$$\begin{aligned} u_1(x;\kappa) &= (\cosh\kappa x)^{m+1}{}_2F_1\left(a,b,\tfrac{1}{2};-\sinh^2\kappa x\right), \\ u_2(x;\kappa) &= (\sinh\kappa x)(\cosh\kappa x)^{m+1}{}_2F_1\left(a+\tfrac{1}{2},b+\tfrac{1}{2},\tfrac{3}{2};-\sinh^2\kappa x\right), \end{aligned} \tag{4.52}$$

where

$$a = \frac{m+1}{2} - \frac{\sqrt{|\varepsilon|}}{2\kappa}, \quad b = \frac{m+1}{2} + \frac{\sqrt{|\varepsilon|}}{2\kappa}. \tag{4.53}$$

To construct the complex-valued superpotential [32], a first function $v(x;\kappa)$ is easily achieved by noticing that the hypergeometric function ${}_2F_1$ is reduced to the identity if $a = 0$. From (4.53) we immediately realize that $|\varepsilon| = \kappa^2(m+1)^2$ produces such a result. Remarkably, the latter value is in correspondence with the spectral rule (4.51) $l = -1$.

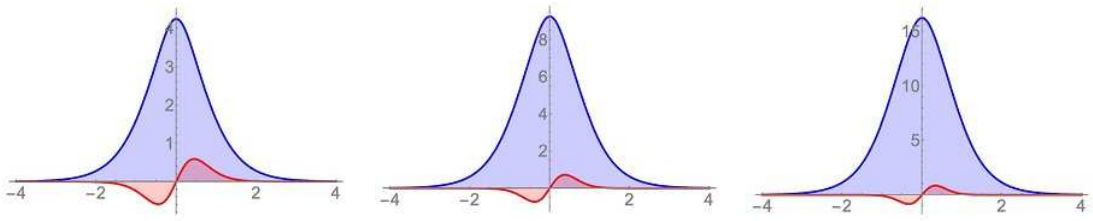

(a) (b) (c)

Figure 4.6: Complex-valued cosh-like refractive indices $n_1(x, m; \kappa)$ exhibiting PT-symmetry. The point-spectrum is finite, including the eigenvalues indicated in captions. The spectral distribution is given by $\epsilon_{m,l} = -\kappa^2(m-l)^2$ with $\ell = 0, 1, ..., m-1$ and $m \geqslant 1$ denoting the number of eigenvalues in the initial spectrum. In all cases ε_M is located at $-\kappa^2(m+1)^2$.

Thus, we are in position of adding the eigenvalue $\varepsilon = \varepsilon_{m,-1}$ to the initial spectrum $\{\varepsilon_{m,l}\}$. The resulting refractive index $n_1(x; m; \kappa)$, obtained from Eq. (4.29), may be chosen to be either real, complex-valued or PT-symmetric. In figure (4.6) we have depicted the case in which $n_1(x, m; \kappa)$ exhibits PT-symmetry. In fig. (4.6a) we started with $n_0(x, 1)$, which admits only one guided TE mode, the one associated with $\varepsilon_{1,0}$. The spectrum of the resulting refractive index$n_1(x, 1; \kappa)$ is therefore integrated by $\varepsilon_M = -(2\kappa)^2$ and $\varepsilon_{1,0} = -\kappa^2$. fig. (4.6b) considers the initial spectrum $\varepsilon_{2,0} = -(2\kappa)^2$,$\varepsilon_{2,1} = -\kappa^2$, and includes the missing state $\varepsilon_M = -(3\kappa)^2$. Similarly for fig. (4.6a). The configuration where the new refractive index is not PT-symmetric is shown in fig. (4.7).

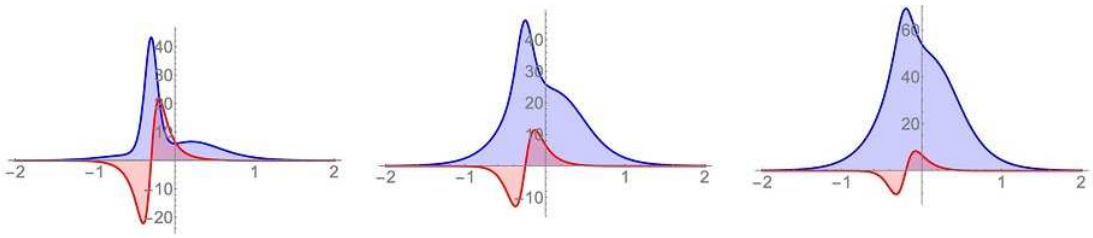

(a) (b) (c)

Figure 4.7: Same as in figure (4.6), with non-PT symmetry.

Chapter 5

Conclusions and Perspectives

We studied deeply the short-range version of the Quantum Harmonic Oscillator in one and two dimensions. In both cases, the fact that the potential "stops" after a cutoff value continued by a free particle potential in the rest of the domain gives rise to the appearance of a kinetic parameter (the wave number) k that encodes the difference of the energy value with respect to the constant potential height. It also let us derive general results that apply to any scatterer of the short-range kind:

- In one dimension, the behavior of the system is completely defined by $m_{2,2}$, the 2-2 entry of the matrix that relates the input with the output, independently of $V(x)$.
- The transmission coefficient is inversely proportionate to $m_{2,2}$ independently of $V(x)$.
- For the one dimensional case, bound states, scattering states and resonant states arise from spanning k around the Complex plane, letting it be pure imaginary, pure real or a mix of both respectively.
- In two dimensions, the behavior of the system is completely defined by the quotient $\frac{C_2}{C_1}$ of the coefficients that accompany the solutions outside the well, independently of $V(r)$.
- In a two dimensional radially symmetric potential the probability density current has an angular component proportional to the angular quantum number l and a radial component proportional to the imaginary part of $\frac{R'}{R}$.
- For bound states and scattering states, $R(r) \in \mathbb{R}$. By the previous conclusion, $\vec{j}_\psi$ only "spins" around, but it does not flow radially.

- For resonant states $\vec{j}_\psi$ has a non-zero radial component. Furthermore, at $r \to \infty$, $\vec{j}_\psi$ tends to be only radial and proportional to the real part of k.

- Analogue to the one dimensional case, bound states, scattering states and resonant states arise from spanning k around the Complex plane, letting it be pure imaginary, pure real or a mix of both respectively.

The actual form of $V(r)$ within the well comes into play when one desires to obtain the specific energies for a determined scatterer. For our case $V(r)$ has a squared dependence on the position while the position doesn't exceed the cut-off value a. Through the continuity and boundary conditions the values of $R(a)$ are useful to determine the specific energies in each phenomena explored.

For the bound states we found that the energy values are practically the same that in the conventional system ($V(r) = r^2$ for all r). We also found that the profile of the solutions for our system are practically identical to those of the conventional system. This happens both in the one and two dimensional cases. This shows that the predictions of the conventional system and its solutions are good enough approximations.

For scattering states we found that there are quantities that quantify the amount of scattering that takes place. For the one dimensional case this is the transmission coefficient T, while for the two dimensional case it is the total scattering section σ. In both cases there are particular energy values that guarantee the most scattering possible.

For resonant states we found that there could be a physical situation of purely outgoing waves, the one which would be related to non-trivial complex values of the energy. However, these states do not conserve probability since they have a time decay, which means that the probability density of finding the particle in any position decreases with time.

The study of this short-range potential has proven useful to put to the test how accurate ideal potential models are compared to a more earth-grounded potential. Several general results came out of it due to having a short range, which would be unknown to us from the study of only ideal potentials. Although a short-range potential implies solving the Schrödinger equations in more regions, and with a bit more difficulty, they have their own richness and the future study of these is not only complementary to others but interesting and of great applicability too.

We parted from Maxwell equations for a inhomogeneous non-magnetic dielectric medium and through reasonable approximations we managed to find a Schrödinger-like equation for the amplitude of the components of the electric field. In particular, for a cylindrical waveguide with a squared dependence of the refractive index the paraxial Helmholtz equation takes the exact form of the stationary Shcrödinger equation for a 2-dimensional oscillator. This mathematical resemblance allowed us to establish a classical-

quantum analogy that allowed us to study a classical system in terms of a quantum one. This analogy was crucial for us to get the propagation constants of the waveguide. Previously, in our study of the 2-dimensional oscillator we found out that short-range potentials' bounded states are practically identical as their whole range counterpart. This knowledge benefited greatly the analogous problem of a cladded waveguide, since it allowed us to find the propagation constants with no need of dealing with any boundary conditions at the core/clad boundary.

A quantum-classical analogy was established between the paraxial Helmholtz equation for a squared profile refractive index and the 2-dimensional oscillator stationary Shcrödinger equation. However, this analogy is not exclusive of squared law indices/wells, indeed it can be established for other refractive indices and potentials but care should be taken that the refractive indices and potentials share the same functional form. In our case, both of them had a radial squared dependence and one cutoff point. For instance, an 1-dimensional analogy between resonant states of a quantum well and leaky modes of a graded index slab has been analyzed in [13].

We have provided new exactly solvable models for optical waveguiding. Applying the supersymmetric finite-difference algorithm, we have generated a wide family of refractive indices whose point-spectrum can be designed under prescription. The family includes refractive indices in both, the real- and complex-valued configurations, the latter admitting all-real eigenvalues (propagation constants) in their point-spectrum. We have shown that the spectral distribution may be organized in arbitrary form if it is constructed adding one at a time the eigenvalues such that complex-valued superpotentials are included. The result is relevant since such a property seems to be unnoticed in optical supersymmetry until the present work, although we have already reported this possibility in quantum mechanics.

One of the main results presented in this work shows that the index-profile strongly depends on the factorization constants that are incorporated. In particular, adding two of them, either in a single step or in a twice iterated movement, one may produce a dent over the top of the profile that is in complete agreement with actual manufacture of refractive indices. The phenomenon is not exclusive of the real-valued indices so produced since it is also admissible in the complex-valued case for the real part of the PT-symmetric refractive indices, see Fig 2. Considering that in the manufacture and evaluation of optical fibers, the measurement of the index profile is one of the most important steps , our results may be useful to analyze the data obtained from such measurements.

Another global result shows that refractive indices admitting a given number of guided TE modes, like the sech-like ones, can be deformed to admit an additional guided mode, the propagation of which can be positioned anywhere in the point-spectrum of the initial refractive index. In addition, the new indices are not required to be PT-symmetric to

allow all-real eigenvalues in their point-spectrum. The transition from these results to the time-dependent case is straightforward, where PT-symmetric structures find interesting applications.

We have addressed the investigation to obtain guided TE modes in the new waveguiding-structures. This is the reason for which we started from initial refractive indices admitting no leaky modes. In previous works we have studied such possibility by analyzing the resonances of the initial structure. It is viable to construct the supersymmetric partners by using resonances of the initial system , a technique implemented also in the cosh-like case and for soliton-like models . However, the transformation of resonances and/or using resonances is elaborated, so it will be analyzed elsewhere. An important point to notice is that, although generated from transparent refractive indices, the new structures presented here lack this property as a consequence of the non-Hermiticity (the clear exception is the real-valued case, since it is well known that supersymmetry leaves transparency invariant for such systems). Insights on the matter have been presented by the PT-symmetry community and will be considered for future progress of our model.

In the present work two lines of study were explored through a quantum-classical analogy. On one hand, we studied a concrete 2-dimensional piece-wise refractive index and found its solution; on the other hand we parted from a 1-dimensional smooth refractive index and found new indexes which are exactly solvable. A natural step to move forward would be to join the insights gained from these and apply them in a hybrid problem. We pose the following question: How can we generalize the SUSY Darboux-deformation method to 2-dimensional systems? Even more, how should the method be adjusted to be applicable not only to smooth refractive indexes, but to abruptly varying indices as well?

A first step into the subject could be a 1-dimensional step-index potential. In chapter 4 we showed what we can do parting from the general solution of a constant refractive index; this solution being associated to a single parameter κ. In a step-index though, there would be two parameters κ_1, κ_2 (one for each step). Therefore, the Darboux-transformation starts with two parameters already in the first iteration...

As a second step, we would try and adjust the method previously developed to varying short-range potentials, like the short-range 1-dimensional oscillator analyzed in the first chapter of this work. Even better weould be to be able to solve the 1-dimensional Coulombian potential (r^{-2}). This would be of great use in a third step...

As a third step, a cylindrical step-index waveguide could follow. Since a cylindrical system can be reduced to solving the radial aspect of the problem only, we would have at hand another 1-dimensional system, with the additional challenge of dealing with the effective potential that comes as a result of the separability of the radial and angular variables. As a result the effective potential would include a centrifugal barrier that depends of a term proportional to r^{-2}, but, of course, this would pose no problem since

that is a problem that would have already been solved.

There is plenty to be done as a follow up of this work. Following this line of research, our understanding of the quantum-classical analogy will go deeper. If we are capable of distinguishing the scope of it, then transitioning smoothly from quantum phenomena to electrical phenomena will provide a great tool for future research in both areas of the physical studies.

Appendix A

A note on the differences of vectorial and scalar Laplacian operators.

The operator ∇^2 that appears on the right hand side of (3.3) is a vectorial operator, therefore different by nature from its scalar "brother". In fact, identity (3.3) is sometimes taken as the definition of the vectorial operator ∇^2. Now, if these operators are naturally different, why are they denoted by the same symbol? The answer is most probably because it turns out that in the case that a vector $\vec{A}$ is expanded in the Cartesian basis as $\vec{A} = A_x\hat{i} + A_y\hat{j} + A_z\hat{k}$ then it is true that

$$\nabla^2\vec{A} = \nabla^2 A_x\hat{i} + \nabla^2 A_y\hat{j} + \nabla^2 A_z\hat{k}, \tag{A.1}$$

which would not be so trivial in the case of cylindrical or spherical basis. Here, the ∇^2 appearing on the right hand side is the scalar operator which appears in the Schrödinger equation, for example. When expressed in Cartesian coordinates (x, y, z), this operator reads

$$\nabla^2\psi = \frac{\partial^2\psi}{\partial x^2} + \frac{\partial^2\psi}{\partial y^2} + \frac{\partial^2\psi}{\partial z^2}. \tag{A.2}$$

On the other hand, when it is expressed in cylindrical coordinates (r, ϕ, z), it reads

$$\nabla^2\psi = \frac{1}{r}\frac{\partial}{\partial r}\left(r\frac{\partial\psi}{\partial r}\right) + \frac{1}{r^2}\frac{\partial^2\psi}{\partial^2\phi} + \frac{\partial^2\psi}{\partial z^2}. \tag{A.3}$$

We will use expression (A.1) for the vectorial operator ∇^2 in (3.5) and, since we are dealing with a cylindrical symmetric problem, we shall use expression (A.3) for the scalar operator ∇^2. We will write the subindexes v and s to distinguish vectorial and scalar operators and *cart.* and *cyl.* to indicate which basis or coordinates are being used.

$$\nabla^2_{v_{cart.}}\vec{E} = \nabla^2_{s_{cyl.}}E_x(r,\phi,z)\hat{i} + \nabla^2_{s_{cyl.}}E_y(r,\phi,z)\hat{j} + \nabla^2_{s_{cyl.}}E_z(r,\phi,z)\hat{z}. \tag{A.4}$$

Bibliography

[1] M. Abramowitz and I. Stegun, *Handbook of Mathematical Functions with Formulas, Graphs, and Mathematical Tables* 10th printing, Department of Commerce, Washington, 1972.

[2] G. Arfken and H. J. Weber, *Mathematical Methods for Physicists* 6th edition, Elsevier Academic Press, Massachusetts, 1972.

[3] R. Courant and D. Hilbert., *Methods of Mathematical Physics Vol. 1* 1st English edition 7th printing, John Wiley and Sons Inc., New York, 1937.

[4] I. Sneddon, *Special Functions of Mathematical Physics and Chemistry* 2nd edition, Interscience Publishers Inc., Edinburgh, 1961.

[5] C. Cohen-Tannoudji, B. Diu and F. Laloë, *Quantum Mechanics Vol. 1*, John Wiley and Sons Inc., New York, 1977.

[6] E. Merzbacher, *Quantum Mechanics*, John Wiley and Sons Inc., New York, 1970.

[7] A. Galindo and P. Pascual, *Quantum Mechanics II*, Springer-Verlag, Berlin, 1991.

[8] I.S. Gradshteyn and I.M. Ryzhik, *Tables of Integrals, Series and Products* 7th edition, Elsevier, Massachusetts, 2007.

[9] M. L. Procopio, Estudio teórico y experimental de la correlación espacial de fotones como un primer paso al cómputo cuántico, Tesis Maestría (Asesores: O. Rosas-Ortiz, V. Velázquez-Aguilar), *Departamento de Física, Cinvestav* (México D.F, 2009).

[10] Y. Ayant and M. Borg, *Funciones Especiales*, Alhambra, Madrid, 1974.

[11] J.D. Jackson, *Classical Electrodynamics* 3rd edition, John Wiley and Sons Inc., New Jersey, 1998.

[12] B. E. A. Saleh and M. C. Teich, *Fundamentals of Photonics* 2nd edition, John Wiley and Sons Inc., New Jersey, 2007.

[13] S. Cruz y Cruz and O. Rosas-Ortiz, Leaky modes of waveguides as a classical optics analogy of quantum resonances, *Adv. Math. Phys.* (2015) 281472

[14] C. Rogers and W.K. Schief, *Bäcklund and Darboux Transformations. Geometry and Modern Applications in Soliton Teory*, Cambridge University Press, Cambridge, 2002.

[15] B. Mielnik and O. Rosas-Ortiz, Factorization: little or great algorithm?, *J. Phys. A: Math. Gen.* **37** (2004) 10007.

[16] B. Mielnik, L.M. Nieto and O. Rosas-Ortiz, The finite difference algorithm for higher order supersymmetry, *Phys. Lett. A* **269** (2000) 70.

[17] O. Rosas-Ortiz, O. Castaños and D. Schuch, New supersymmetry-generated complex potentials with real spectra, *J. Phys. A Math. Theor.* **48** (2015) 445302.

[18] E.L. Ince, *Ordinary Differential Equations*, Dover, New York, 1956.

[19] Z. Blanco-Garcia, O. Rosas-Ortiz and K. Zelaya, Interplay between Riccati, Ermakov and Schrödinger equations to produce complex-valued potentials with real energy spectrum, *Math. Meth. Appl. Sci.* **42** (2019) 4925.

[20] V. Ermakov, Second order differential equations: Conditions of complete integrability *Kiev Univ. Izvestia* **9** (1880), 125. (In Russian). English translation by Harin A.O. in *Appl. Anal. Discret. Math.*, **2** (2008) 123.

[21] K. Zelaya, S. Cruz y Cruz and O. Rosas-Ortiz, On the construction of non-Hermitian hamiltonians with all-real spectra through supersymmetric algorithms, *Geometric Methods in Physics XXXVIII*. Trends in Mathematics. Birkhäuser, Cham, 2020, pp. 283292.

[22] O. Rosas-Ortiz, O. Castaños and D. Schuch, New supersymmetry-generated complex potentials with real spectra. *J. Phys. A Math. Theor.* **48** (2015) 445302.

[23] A. Jaimes-Najera and O. Rosas-Ortiz, Interlace properties for the real and imaginary parts of the wave functions of complex-valued potentials with real spectrum, *Ann. Phys.* **376** (2017) 126144.

[24] O. Rosas-Ortiz and K. Zelaya, Bi-Orthogonal Approach to Non-Hermitian hamiltonians with the oscillator spectrum: Generalized coherent states for nonlinear algebras, *Ann. Phys.* **388** (2018) 2653.

[25] K. Zelaya, S. Dey, V. Hussin and O. Rosas-Ortiz, Nonclassical states for non-Hermitian hamiltonians with the oscillator spectrum, *Quantum Rep.* **2** (2020) 1238.

[26] C.M. Bender and S. Boettcher, Real spectra in non-Hermitian hamiltonians having PT-symmetry. *Phys. Rev. Lett.* **80** (1998) 5243.

[27] T. Okoshi, *Optical Fibers*, Academic Press, New York, 1982.

[28] J.I. Díaz, J. Negro, L.M. Nieto and O. Rosas-Ortiz, The supersymmetric modified Pöschl-Teller and delta well potentials, *J. Phys. A. Math. Gen.* **32** (1999) 84478460.

[29] S. Flügge, *Practical Quantum Mechanics*, Springer, New York, 1974.

[30] D. Cevik, M. Gadella, S. Kuru and J. Negro, Resonances and antibound states for the Pöschl-Teller potential: Ladder operators and SUSY partners, *Phys. Lett. A* **380** (2016) 1600.

[31] O. Civitarese and M. Gadella, Coherent Gamow states for the hyperbolic Pöschl-Teller potential, *Ann. Phys.* **406** (2019) 222

[32] S.M. Chumakov, K.B. Wolf, Supersymmetry Helmholtz optics, *Phys. Lett. A* **193** (1994) 5153.

[33] S. Cruz y Cruz, S. Kuru, and J. negro, Classical motion and coherent states for Pöschl-Teller potential, *Phys. Lett. A* **378** (2008) 1391